

ABSTRACT

Title of Document: AN INTEGRATED ISOTOPIC AND
BIOMARKER ANALYSIS OF THE
GLACIOGENIC VAZANTE GROUP, BRAZIL

Kristen E. Miller, Ph.D, 2012

Directed By: Professor, Alan J. Kaufman, Department of
Geology

The Vazante Group, a meta-sedimentary succession located in south-central Brazil, contains several intervals of diamictite, interpreted as glacial in origin, bracketed by well-preserved carbonate and shale. This glacial succession was previously associated with the global occurrence of Neoproterozoic low latitude glacial deposits (aka Snowball Earth), and biomarkers (molecular fossils) identified from an organic-rich interval within this succession were used to infer active photosynthesis during the ice age (Olcott et al., 2005). However, new Re-Os and detrital zircon U-Pb ages suggest that the upper Vazante Group is ca. 1.3 to 1.0 billion-years old (Geboy, 2006; Azmy et al., 2008; Rodrigues et al., 2008) and thus may preserve evidence for hitherto unknown Mesoproterozoic ice ages. Within this context, I present biomarker and time-series stable isotope data from a basin-wide distribution of pre- and post-glacial sedimentary units in order to i) evaluate the Mesoproterozoic interpretation of this succession, ii) assess the biologic and environmental conditions present when these sediments were deposited, and iii) to understand the co-evolution of life and ocean chemistry in response to rapidly changing environmental conditions. Biomarker distributions and abundances from the

Serra do Garrote Formation, a pre-glacial shale, and the Serra do Poço Verde and Lapa formations, both post-glacial shales, show evidence of a diverse microbial community that would have only existed in a redox stratified water column. Additionally, the presence of aryl isoprenoids, biomarkers indicative of green sulfur bacteria, in the Serra do Garrote and Serra do Poço Verde formations suggest that reducing, sulfide-rich water was present in the photic zone. These biomarkers however, are absent from the Lapa Formation suggesting that sulfidic conditions either receded to deeper water or collapsed entirely. Carbon and sulfur isotopic signatures support the conclusions drawn from this biomarker study. Carbon and sulfur trends from the Serra do Garrote and Serra do Poço Verde formations show evidence of a large, anoxic, isotopically stable, dissolved organic carbon pool (relative to inorganic carbon) and extensive bacterial sulfate reduction of a small, oceanic sulfate reservoir. The Lapa Formation, on the other hand, displays evidence for a smaller, isotopically responsive, dissolved organic carbon pool. The carbon isotopic compositions of carbonates from these three units are consistent with other Mesoproterozoic successions supporting the geochronological age constraints. Taken together, biomarker and time-series stable isotope data from the upper Vazante Group map a transition from a sulfide-rich, stratified, water column to one that, while still stratified, was no longer sulfidic. This environmental transition occurred in response to consecutive Mesoproterozoic ice ages.

AN INTEGRATED ISOTOPIC AND BIOMARKER ANALYSIS OF THE
GLACIOGENIC VAZANTE GROUP, BRAZIL

By

Kristen E. Miller

Dissertation submitted to the Faculty of the Graduate School of the
University of Maryland, College Park, in partial fulfillment
of the requirements for the degree of
Doctor of Philosophy
2012

Advisory Committee:
Professor Alan J. Kaufman, Chair
Professor James Farquhar
Assistant Professor Sujay Kaushal
Senior Scientist George Cody
Professor Catherine Fenselau

© Copyright by
Kristen E. Miller
2012

Acknowledgements

I would like to acknowledge and thank all the people who helped make this project possible. First and foremost, I would like to thank my advisor Alan J. Kaufman who recognized the potential of this biomarker project and supported me throughout the years despite the many twists and turns. Thanks for always helping me to see the bigger picture. Thank you to James Farquhar and all of the graduate and undergraduate students, past and present, in the Farquhar and Kaufman lab groups for the helpful and informative conversations.

I would also like to thank all of our colleagues from outside the University of Maryland who made this project possible. George Cody of the Carnegie Institution of Washington Geophysical Laboratory has always been a great supporter of my work and allowed me to run a seemingly endless number of GCMS analyses and ASE extractions. I emphatically thank you! Also, thanks to Roger Summons, Julio Sepúlveda, Sharon Newman, Marie Giron, Carolyn Colonero, Christian Illing, and Hary Oduro at the Massachusetts Institute of Technology for welcoming me into their lab, sharing their resources, and helping me to work through the many obstacles associated with biomarker work. I truly appreciate having had the opportunity to visit the Summons laboratory and I cannot emphasize enough how much I learned from each person there.

Thank you to Tolentino Flavio de Oliveira and Aroldo Misi for showing me the beautiful and fascinating geology of the Brazilian countryside. Also, a special thanks to Tolentino Flavio de Oliveira and all the geologists at the Companhia Mineira de Metais for providing access to such an extensive set of drill cores and for helping me collect the many samples analyzed in this study.

Thanks also to those who have funded this project: the Chemical Society of America Petroleum Research Fund, The Society for Organic Petrology Spackman Award, and the University of Maryland Green Fund Award.

Finally, I would like to thank my family and friends for their patience, support and encouragement. Thank you to my parents for continuously pushing me, my sister Jessica for being my personal cheerleader, and my boyfriend Andrew for always being there to listen and offer advice.

Table of Contents

Acknowledgements.....	ii
Table of Contents.....	iv
List of Tables.....	vi
List of Figures.....	vii
Chapter 1: Introduction to Precambrian organic matter and geologic history of the Vazante Group, Brazil.....	1
1.1: Introduction.....	1
1.2: Biomarkers.....	3
1.2.1: <i>Biomarker syngeneity</i>	5
1.2.2: <i>Biomarkers as indicators of biologic source and depositional environment</i> ...	7
1.2.3: <i>Biomarkers as indicators of thermal maturity</i>	8
1.2.4: <i>Compound specific isotope analysis</i>	9
1.3: Geology of the Vazante Group, Brazil.....	10
1.3.1: <i>Stratigraphy of the Vazante Group</i>	11
1.3.2: <i>Age constraints of the Vazante Group</i>	13
1.3.3: <i>Geologic strategy for this study</i>	15
1.4: Working hypotheses.....	16
Chapter 2: Carbon and Sulfur Isotopic Signatures from the Vazante Group, Brazil.....	26
2.1: Introduction.....	26
2.2: Sample strategy.....	28
2.3: Methods.....	30
2.4: Results.....	32
2.4.1: <i>Organic carbon</i>	32
2.4.2: <i>Sulfur</i>	33
2.4.3: <i>Carbonate carbon</i>	33
2.5: Discussion.....	34
2.5.1: <i>Organic Carbon and Sulfur</i>	34
2.1.2: <i>Carbonate carbon</i>	38
2.5: Conclusions.....	39
Chapter 3: Biomarkers from the Vazante Group.....	44
3.1: Introduction.....	44
3.2: Organization.....	46
3.3: Sample selection.....	47
3.4: Study 1 – Sonication vs. ASE extractions.....	52
3.4.1: <i>Methods</i>	52
3.4.2: <i>Results</i>	56
3.4.3: <i>Discussion</i>	58
3.4.4: <i>Conclusions</i>	59
3.4: Study 2 – Biomarker from the Serra do Garrote, Serra do Poço Verde and Lapa formations.....	70
3.4.1: <i>Sample selection</i>	70
3.4.2: <i>Methods</i>	71
3.4.3: <i>Results</i>	72

3.4.4: <i>Discussion: Syngeneity</i>	75
3.4.5: <i>Discussion: Biological and Environmental Source</i>	76
3.4.6: <i>Conclusions</i>	83
3.5: Study 3 – Biomarkers from kerogen and bulk extractions: An alternative test for syngeneity	104
3.5.1: <i>Sample selection</i>	104
3.5.2: <i>Methods</i>	105
3.5.3: <i>Results</i>	107
3.5.4: <i>Discussion</i>	107
3.5.5: <i>Conclusions</i>	109
3.6: Study 4 – A Re-Evaluation of Biomarkers from the Vazante Group	114
3.6.1: <i>Sample selection</i>	114
3.6.2: <i>Methods</i>	116
3.6.3: <i>Results and Interpretations</i>	117
3.6.4: <i>Discussion: Syngeneity</i>	122
3.6.5: <i>Discussion: Environmental and Biological Conditions of the Vazante Group</i>	124
3.6.6: <i>Conclusions</i>	126
Chapter 4: Speculations on Mesoproterozoic (?) biological, environmental, and climatic change	135
4.1: Review of Geologic Interpretations.....	135
4.2: Geobiology of the Serra do Poço Verde Formation	136
4.3: Time-series Comparison of the Vazante Shales	138
4.4: Life and Environment in the Mesoproterozoic	141
Appendix A: Precision of Biomarker Measurements	144
Bibliography	145

List of Tables

Table 1.1: Biologically and environmentally significant biomarkers.....	18
Table 3.1: Biomarker sample lithologies and bulk characteristics	49
Table 3.2: Ions monitored for SIM-GCMS.....	61
Table 3.3: Compound abundances (Study 1).....	62
Table 3.4: Source-related biomarker ratios (Study 2).....	85
Table 3.5: Maturity-related biomarker ratios (Study 2).....	88
Table 3.6: Compound abundances (Study 2).....	90
Table 3.7: CSIA (Study 2)	92
Table 3.8: Compound abundances (Study 3).....	110
Table 3.9: Source- and maturity-related biomarker ratios (Study 3).....	111
Table 3.10: Compound abundances (Study 4).....	127
Table 3.11: Source-related biomarker ratios (Study 4).....	128
Table 3.12: Maturity-related biomarker ratios (Study 4).....	129
Table A-1: Analytical uncertainties	144
Table A-2: Peak integration uncertainties.....	144

List of Figures

Figure 1.1: Geologic time scale	19
Figure 1.2: Biomarker formation	20
Figure 1.3: Biomarker stereochemistry.....	21
Figure 1.4: Geologic map of the Vazante Basin	22
Figure 1.5: Composit stratigraphic column of the Vazante Group.....	23
Figure 1.6: Field photographs of geologic features	24
Figure 1.7: Geologic map of the Vazante Basin with core locations.....	25
Figure 2.1: Geologic map of the Vazante Basin with stable isotope sample locations ...	41
Figure 2.2: TOC, $\delta^{13}\text{C}_{\text{org}}$, and $\delta^{34}\text{S}_{\text{py}}$ time-series results.....	42
Figure 2.3: $\delta^{13}\text{C}_{\text{carb}}$ time-series results	43
Figure 3.1: Chromatogram m/z 85 (Study 1).....	63
Figure 3.2: Chromatogram m/z 191 (Study 1).....	64
Figure 3.3: Chromatogram m/z 191 with siloxanes (Study 1).....	65
Figure 3.4: Chromatogram m/z 217 (Study 1).....	66
Figure 3.5: Cross-plots of n-alkane and isoprenoid ratios (Study 1)	67
Figure 3.6: Cross-plots of hopane ratios (Study 1)	68
Figure 3.7: Cross-plots of sterane ratios (Study 1)	69
Figure 3.8: TIC for Blank 2 (Study 2)	93
Figure 3.9: Chromatograms m/z 85 for the Serra do Garrote (Study 2).....	94
Figure 3.10: Chromatograms m/z 85 for the Mocambo (Study 2)	95
Figure 3.11: Chromatograms m/z 85 for the Lapa (Study 2).....	96
Figure 3.12: Detailed chromatogram m/z 85 (Study 2)	97
Figure 3.13: Detailed chromatogram m/z 191 (Study 2).....	98
Figure 3.14: Detailed chromatogram m/z 217 (Study 2).....	99
Figure 3.15: Chromatograms m/z 85 from Brody (2007).....	100
Figure 3.16: Sterane ternary diagram (Study 2).....	101
Figure 3.17: Maturity ratio equilibrium vs oil generation stages.....	102
Figure 3.18: Cross-plot of $\delta^{13}\text{C}_{\text{org}}$ vs. $\delta^{13}\text{C}$ n-alkanes and Ph.....	103
Figure 3.19: Cross-plots of hopane and sterane ratios (Study 3).....	112
Figure 3.20: Sterane ternary diagram (Study 3).....	113
Figure 3.21: M+ \rightarrow 191 transitions for hopanes (Study 4).....	130
Figure 3.22: M+ \rightarrow 205 transitions for methylhopanes (Study 4).....	131
Figure 3.23: Sterane ternary diagram (Study 4).....	132
Figure 3.24: Sterane ternary diagram (Study 3 and 4).....	133
Figure 3.25: Chromatogram m/z 133 (Study 4).....	134
Figure 4.1: Time-series elemental and isotopic compositions from core MAF-42.88 ..	143

Chapter 1: Introduction to Precambrian organic matter and geologic history of the Vazante Group, Brazil

1.1: Introduction

The Proterozoic Eon (2.5-0.543 Ga) records a transition from the extreme and often inhospitable conditions of the Archean Eon (3.8-2.5 Ga), where the atmosphere and oceans were dominantly anoxic and only the simplest of prokaryotic organisms could survive (Cloud, 1972; Walker et al., 1983), to the dawn of the Phanerozoic Eon (543-0 Ma) where macroscopic animals ruled and atmospheric conditions were similar to today (Figure 1.1). Both geologic and geochemical anomalies mark significant environmental events that occurred over the ~2 billion year stretch of the Proterozoic. These include the Great Oxidation Event at ~2.4 Ga when the oceans and atmosphere became irreversibly oxidized (Holland, 1983; 2003; 2005), as well as repeated and potentially global glaciations (aka Snowball Earth) that marked the beginning and end of the Proterozoic Eon (Hoffman et al., 1998; Hoffman and Schrag, 2002). Paleontological, biogeochemical and phylogenetic studies have also identified major biologic events such as the geologically rapid diversification of eukaryotes at ~1.2 Ga (Knoll, 1992; Knoll et al., 2006) and the earliest fossil appearance of large-bodied animals at ~575 Ma (Bowring et al., 2002; Narbonne et al., 2003).

In recent years, many studies have worked to understand the co-evolution of life and environment, especially focusing on the relationship between redox conditions,

global and regional glaciations, and the rise of animals in the Neoproterozoic Era (1000-543 Ma) including the Ediacarian Period (580-543 Ma; Knoll et al., 2004; Canfield et al., 2007; McFadden et al., 2008). In contrast, our understanding of pre-Neoproterozoic life and environment, and how they co-evolved, is more fragmentary. The lack of information from the Mesoproterozoic Era (1.6-1.0 Ga) is due, in part, to the lower abundance of well-constrained fossiliferous sedimentary successions from this time period.

In the absence of diagnostic microfossils, molecular fossils (biomarkers) hold the greatest potential for elucidating microbial communities, their environment, and/or the thermal maturity of the sedimentary rocks in which they are contained. Organic-rich shale in fresh drill core material is an ideal target for biomarker analysis, assuming that drilling fluids have not permeated the rock or that they have otherwise been contaminated by post-depositional fluid flow.

The Vazante Group, a metasedimentary succession in Minas Geras, Brazil that contains several intervals of diamictite interpreted as glacial in origin, is bracketed by thick carbonate and, most importantly, organic-rich shales. The age of the Vazante Group has long been a matter of contention; carbon and strontium isotope chemostratigraphy has been used to suggest a Neoproterozoic age for the Vazante Group (Azmy et al., 2001; 2006; Olcott et al., 2005), whereas the presence of unusual stromatolite bioherms (*Conophyton*) suggest a possibly older (1350-900 Ma), Mesoproterozoic origin for the succession (Cloud and Dardenne, 1973). Supporting the older age, recent Re-Os and U-Pb detrital zircon studies have suggested an age of 1.3 to 1.0 Ga for the upper Vazante Group (Geboy, 2006, Azmy et al., 2008; Rodrigues et al.,

2008). If the Mesoproterozoic age is true, then the Vazante Group represents one of two potential glaciogenic successions known from the Mesoproterozoic; the second comes from a new Re-Os shale age of ca. 1.1 Ga for the glaciogenic Atar Group in Mauritania (Rooney et al., 2010).

The purpose of this study is to use biomarkers in conjunction with carbon and sulfur time-series studies of core material from the Vazante Group to chart the course of biological diversity in the face of rapid environmental and climatic change. Biomarkers, which are the fossilized chemical remains of cell components, can provide direct information about the metabolisms, physiologies, and identities of organisms (including, but not limited to Ourisson et al., 1979; Tissot and Welte, 1984; Moldowan et al., 1985; Peters and Moldowan, 1991; Summons et al., 1999; Brocks et al., 2003). On the other hand, carbon and sulfur isotopic signatures are known proxies for biogeochemical processes functioning at the time of deposition, although secondary effects, such as diagenetic alteration, can complicate interpretations. An evaluation of biomarkers and carbon and sulfur isotopic signatures from organic-rich shales both above and below glacial diamictites can provide important information about the composition of biologic communities before global cooling and during glacial meltdown. Additionally, comparison of carbon and sulfur isotopic trends from the Vazante Group with both Neoproterozoic and Mesoproterozoic successions worldwide will help evaluate whether the Vazante Group could be Mesoproterozoic in age. If true, then biomarkers identified within the Vazante Group can provide important information regarding the environmental and biologic conditions during the late Mesoproterozoic.

1.2: Biomarkers

Biomarkers are fossilized organic molecules from once-living organisms that are preserved through burial and diagenesis and are unique to a particular organism, group of organisms, or an environment. Most biomarkers are the diagenetic products of functionalized lipids that originate in cell membranes (Figure 1.2). The robust hydrocarbon structure of lipids is responsible for their preferential preservation with respect to other biomolecules, such as proteins (Eglinton et al., 1964; Summons et al., 1988; Brocks and Summons, 2003; Summons et al., 2008; Eigenbrode, 2008).

Biomarkers are preserved in sediment much the same way that oil is preserved. High rates of primary production and sedimentation result in the burial and lithification of organic matter. This organic matter is thus isolated from the short-term carbon cycle and can be preserved for millions or even billions of years (Eglinton et al., 1964; Brocks et al., 1999; Brocks et al., 2003; Waldbauer et al., 2009). Biomarkers are preserved as either free, solvent extractable organic matter (hereafter called bitumen) or insoluble organic matter, which is bound in the mineral matrix of the host rock (hereafter called kerogen). Typically, more than 99.99% of the total organic matter is present as non-extractable kerogen (Waldbauer et al., 2009), but its bulk composition rarely provides specific information about biological sources. In contrast, bitumen hosts a suite of paleobiologically and paleoenvironmentally important biomarkers, including *n*-alkanes, isoprenoids, steranes, hopanes, and polycyclic aromatic hydrocarbons (Ourisson et al., 1979; Tissot and Welte, 1984; Moldowan et al., 1985; Peters and Moldowan, 1991; Summons and Powell, 1987), which are the focus of this integrated study (Table 1.1).

The post-depositional thermal history of sedimentary successions also affects the degree of biomarker preservation. In order for an organic molecule to be useful as a biomarker, its fundamental structure must remain intact so that it can be unambiguously traced back to the organism from which it came (Peters et al., 2005). Although some functional groups (e.g. OH groups) may be lost during diagenesis, the basic hydrocarbon structure of a biomarker remains relatively unaltered (Brocks and Summons, 2004). With increasing temperatures (50-150°C) and pressures biomarker structures may undergo rearrangement or aromatization; this process is called catagenesis and it is the prime oil-generating phase (Tissot and Welte, 1984; Peters et al., 2005). Other structural changes to the biomolecules can be used to identify the extent of thermal alteration experienced by the host rock. At higher temperatures (150-200°C) organic matter will undergo 'cracking' in which large hydrocarbon molecules break into fragments (Lorant and Behar, 2002). This process, called metagenesis, forms hydrocarbon gas and destroys most paleobiologically useful biomarkers (Peters et al., 2005). The potential for preservation of biomarkers at even higher temperatures (> 200°C) is uncertain and has been a matter of much debate, especially in studies of Archean rocks (Brocks et al., 1999; Brocks et al., 2003; Waldbauer et al., 2009; Rasmussen et al., 2008).

1.2.1: Biomarker syngeneity

Determining the syngeneity of extracted organic matter is essential to all biomarker studies. If extracted organic matter is syngenetic then it represents the combined inputs of primary productivity and heterotrophic recycling in the depositional environment. Non-syngenetic organic matter can be the result of hydrocarbons migrating

through hydrologically-linked strata (Brocks et al., 2003; Peters et al., 2005); this mobility is essential to the formation of oil and gas reservoirs, so it is a common occurrence. If the biomarkers are non-syngenetic, then the original source-rock may represent a different depositional age or paleoenvironment than that of the host rock. Non-syngenetic biomarkers can also be the result of human-induced contamination such as contact with drilling fluids and plastics, as well as oils from our skin. Extreme care must be taken when handling biomarker samples in order to minimize laboratory contamination.

Biomarker syngeneity is addressed by analyzing biomarker characteristics in the context of the geologic setting, sedimentary paleoenvironment and geochemical characteristics of the host rock. For example, Brocks et al. (2003) assessed the syngeneity of biomarkers extracted from the 2.78-2.45 Ga Mount Bruce Supergroup in Western Australia. They cited the structural stability of the geologic basin and the absence of Phanerozoic biomarkers as evidence that the biomarkers did not migrate in from younger strata. Additionally, Brocks et al. (2003) showed that certain biomarker ratios indicative of thermal maturity correspond to the metamorphic grade of the host rocks. They concluded that the extracted biomarkers were “probably syngenetic.” A new study, which includes the lead author from the earlier work, questioned the validity of this conclusion (Rasmussen et al., 2008). Rasmussen et al. (2008) analyzed the $\delta^{13}\text{C}$ of the bulk kerogen and indigenous pyrobitumen (solidified oil formed through the thermal maturation of the host rock), which represent the indigenous organic matter and compared it to the $\delta^{13}\text{C}$ of the extracted biomarkers. They found that the biomarkers were enriched in ^{13}C by ~10-20 ‰ compared to the indigenous kerogen and pyrobitumen,

indicating that the extracted biomarkers migrated into the strata sometime after the main phase of oil generation, and are therefore not syngenetic.

1.2.2: Biomarkers as indicators of biologic source and depositional environment

Lipids, the biological precursors of most biomarkers, provide structural integrity to the cell membrane and act as the interface between the cell and the surrounding environment. Additionally, the lipid membrane supports proteins that control which compounds (e.g. metabolites) pass into and out of the cell (Dowham and Bogdanov, 2002; Konings et al., 2002; Vorb'eva, 2004; Eigenbrode, 2008). Therefore, the specific structures and distribution of biomarkers in a geologic sample can be indicative of the environmental setting and dominant metabolisms at the time of deposition. For example, biomarkers formed from the pigment isorenieratene are indicative of green sulfur bacteria, which are obligate anaerobes that use H₂S as the electron donor for photosynthesis (Summons and Powell, 1987). The presence of green sulfur bacteria indicates euxinic conditions that extend into the photic zone of the water column (Brocks et al., 2005; Olcott et al., 2005; Cao et al., 2009). Furthermore, biomolecules such as lipids are formed through specific biosynthetic pathways that can be unique to a particular organism (or group of organisms). 24-Isopropylcholestane (24-IPC), for example, is a biomarker that is primarily synthesized by the Demospongiae (Bergquist et al., 1980), which are hypothesized to be the most basal metazoans (Schütze et al., 1999; Skorokhod et al., 1999; Müller, 2001). Currently, the oldest evidence for 24-IPC, is from an interlude between widespread Neoproterozoic glacial events (>635 Ma < ~713 Ma; Love et al., 2009).

1.2.3: Biomarkers as indicators of thermal maturity

The formation of lipids through specific biosynthetic pathways result in molecular structures with highly constrained stereochemistry (Eigenbrode, 2008). Stereochemistry describes the three-dimensional structure of a molecule. Molecules with the same chemical formula but with mirror-image structures are called stereoisomers or enantiomers. An example of this would be two mirror-image structures of asymmetric carbon atoms. Asymmetric carbon atoms, also called chiral centers, are carbon atoms that have all four bonding sites occupied by different substituents. The mirror-image structures are isomers because they cannot be superimposed without breaking bonds (Figure 1.3A). Isomers are named based on the clockwise (R) or counterclockwise (S) ranking of the substituents (Peters et al., 2005). Likewise, asymmetric carbon atoms in a ring will have a functional group, usually hydrogen, which is attached either above (β) or below (α) the plane of the carbon ring.

The biologically imparted stereochemistry of a molecule is often not the most thermally stable conformation. During thermal maturation, the biological isomer is systematically converted to a more thermodynamically favorable (geological) conformation until the molecule reaches equilibrium (Schoell et al., 1983; Moldowan et al., 1986; Seifert and Moldowan, 1980, 1986, 1978). Therefore, the ratio of the biological conformation relative to the geological conformation can indicate the degree of maturation of the biomarker and the sediment. For example, the biological precursor to hopanes has an R configuration at C₂₂ (the 22nd carbon atom; Figure 1.3B). As temperature increases, the 22R configuration is converted to 22S until it reaches

equilibrium (i.e. 22S is being converted back to 22R at the same rate; Schoell et al., 1983). Therefore, an increasing 22S/(22S+22R) ratio indicates increasing thermal maturity and temperature (Peters et al., 2005).

1.2.4: Compound specific isotope analysis

Compound-specific isotopic analysis (CSIA) is a technique used to determine the carbon isotopic composition of individual molecules and is an important tool for evaluating biomarker sources and syngeneity. Molecules that derive from the same biological source have co-varying isotopic compositions (they should have a 1:1 relationship); therefore, if the carbon isotopic compositions of biomarkers differ then they may represent different biologic sources. For example, Hayes et al. (1990) showed that for each 1‰ change in the $\delta^{13}\text{C}$ isotopic composition of acyclic isoprenoids (e.g. pristane and phytane) in samples from the Greenhorn Formation was accompanied by a 2‰ change in the $\delta^{13}\text{C}$ of the *n*-alkanes. They interpreted this difference to be the result of mixing between two different biologic sources with the acyclic isoprenoids representing photosynthetic organisms and the *n*-alkanes derived from secondary inputs such as heterotrophic organisms. Furthermore, Schoell et al. (1994) measured the carbon isotopic composition of individual biomarkers from the Uinta Basin, Utah and found that the C₃₀ hopanes ($\delta^{13}\text{C} = -51.9\text{‰}$) were strongly depleted in ¹³C compared to C₂₉, C₃₁, and C₃₂ hopanes ($\delta^{13}\text{C} = -40.9$ to -44.3‰). This was interpreted to be the result of derivation from a common biologic source for the C₂₉, C₃₁, and C₃₂ hopanes (midwater bacteria) and a contribution from a different source (methylotrophs) for the C₃₀ hopanes.

1.3: Geology of the Vazante Group, Brazil

The Vazante Basin sits on the Western edge of the São Francisco craton in Minas Gerais, Brazil (Figure 1.4). Archean and Paleoproterozoic basement rocks there are overlain by Mesoproterozoic and Neoproterozoic sedimentary successions that extend more than 300 km N-S parallel to the Brasilia Fold Belt. The sediments in the western region of the Vazante Basin, near the Brasilia Fold Belt, are highly metamorphosed and have reached amphibolite to granulite facies (Dardenne, 1978; Fuck et al., 1994). Sediments in the eastern portion of the basin, however, have experienced little deformation and sub-greenschist facies metamorphism (Azmy et al., 2001; 2006; Geboy, 2006). Fluid inclusion studies suggest that dolomitization of the Vazante carbonates began at temperatures below 50°C but may have reached as high as 120-130°C (Azmy et al., 2001). The Vazante sediments were most likely deposited on a passive margin of the Brasiliano Ocean (Campos-Neto, 1984; Fuck et al., 1994), however, some have argued they were deposited in a foreland basin at the start of the Brasiliano-Pan African Orogeny (Dardenne, 2000). The lack of volcanic ash in the Vazante sediments supports the passive margin setting. Based on paleomagnetic reconstructions, the paleolatitude of the São Francisco craton was between 45-60° when the Vazante sediments were deposited (D'Agrella-Filho et al., 1990; 2004; Tohver et al., 2005). In contrast, the predominance of thick carbonates lead some authors to believe that the Vazante Basin must have been in a more tropical environment and therefore closer to the equator when sediments were deposited (Azmy et al., 2008).

1.3.1: Stratigraphy of the Vazante Group

The Vazante Group consists of seven mapable units, which are (from base to top) the Santo Antônio do Bonito, Rocina, Lagamar, Serra do Garrote, Serra do Poço Verde, Morro do Calcário and Lapa formations (Figure 1.5). The Vazante Group is mainly composed of thick stromatolitic and rhythmic carbonates with intermittent units of organic-rich mudstone and shale, as well as several intervals of poorly sorted diamictite believed to be of glacial origin (Geboy et al., in prep.).

The Santo Antônio do Bonito Formation is a diamictite that contains outsized clasts of quartzite and granite that are both faceted and striated in a fine-grained carbonaceous matrix (Dardenne, 2001).

The Rocinha Formation is a phosphate bearing rhythmic carbonate and slate unit (Azmy et al., 2008).

The Lagamar Formation consists of phosphate bearing siltstone and slate at the base and is topped by a thick unit of grey limestone. *Conophyton metulum* and *Jacutophyton* bioherms are present at the top of the formation (Cloud and Dardenne, 1973; Figure 1.6). Additionally, a fault trace separating the phosphate bearing basal Lagamar from the upper Lagamar is observed in outcrop (Figure 1.6).

The Serra do Garrote Formation is a thick deposit of dark grey slate with interbedded black limestone and fine quartzite layers. *Conophyton metulum* is also prevalent towards the base of this formation. The high-relief columnar morphology of these stromatolites indicates water depths below storm-wave basin (Schopf and Sovietov, 1976).

The Serra do Poço Verde Formation contains stromatolitic carbonates unconformably in contact with glacial diamictite. The stromatolitic carbonate is referred to as the Retiro Member. The diamictite contains angular and rounded clasts of stromatolitic carbonate from the Retiro Member in a fine-grained matrix that grades from carbonate to organic-rich black shale. The abundance of ice-rafted debris decreases up section in the thick organic-rich black shale (henceforth called the Mocambo; Figure 1.6). Petrographic examination of the Mocambo reveals the presence of glendonite, a pseudomorph of ikiate, which is a carbonate mineral that forms in organic-rich sediment at temperatures between -1.9 and 7°C (Olcott et al., 2005; James et al., 2005). The gradation from carbonate to shale facies suggests a transgressive period related to regional sea-level rise as the ice sheet fragmented and melted.

The Morro do Calcário Formation consists of stromatolitic carbonates that are unconformably in contact with glacial diamictite. A broadly recognized unconformity separates the Moro do Calcário from the overlying Lapa Formation and in some locations the Lapa Formation directly overlies the Serra do Poço Verde formation (Azmy et al., 2001; Misi et al., 2007). Some authors have related the Lapa diamictite to the underlying diamictite of the Serra do Poço Verde Formation, thus making the Mocambo a syn-glacial deposit (Olcott et al., 2005). In contrast, we propose (Geboy et al., in prep.) that the Morro do Calcário diamictite is associated with a later Lapa glaciations, which excavated the underlying stromatolitic carbonate and then filled the subglacial valley with debris at the end of the younger ice age.

The Lapa Formation contains a glacial succession at its base topped by a thick marl unit. The glacial succession consists of a thin diamictite and an organic-rich shale

unit hosting ice-rafted debris. The wide-spread cementation of the glacial sediments with iron-oxides and the local accumulation of iron-formation support the glacial origin of this succession (Derry et al., 1992; Brody et al., 2004). Additionally, overlying carbonate and marl near the base of the Lapa Formation preserve a strong negative $\delta^{13}\text{C}$ excursion typical of post-glacial cap carbonates (Brody et al., 2004; Azmy et al., 2006; Chapter 2 of this study).

1.3.2: Age constraints of the Vazante Group

The lack of radiometrically datable ash layers within the Vazante Group make determining the age difficult. Some researchers have argued that the Vazante sediments are Neoproterozoic in age (Azmy et al., 2001, Olcott et al., 2005) and that the glacial diamictites therefore correspond to globally recognized “Snowball Earth” events diagnostic of this time. This argument is mainly based on carbon and strontium isotopic signatures from the Vazante Group that have been tentatively correlated to the Sturtian-aged (750-700 Ma; Knoll and Walter, 1992; Kaufman et al., 1997) glaciogenic sequence of the Bambuí Group to the east in Brazil and of the Otavi Group on the Congo Craton (Azmy et al., 2001; Azmy et al., 2006; Misi et al., 2007). Strontium isotopes from the phosphorites in the Rocinha and the base of the Lagamar formations ($^{87}\text{Sr}/^{86}\text{Sr} \approx 0.7075$; Misi et al., 2007) match those in carbonates throughout much of the Bambuí Group (Misi et al., 2007). One of these, a thick carbonate dominated by seafloor aragonite precipitates in the Sête Lagoas Formation is constrained by Pb-Pb carbonate analysis to be Sturtian (740 ± 22 Ma; $n = 11$; $\text{MSWD} = 0.66$) in age (Babinski et al., 2007). Furthermore, U-Pb SHRIMP dating of detrital zircons from the matrix of the Santo Antônio do Bonito

diamictite and from the Rocinha Formation give maximum depositional ages of 997 ± 29 Ma and 935 ± 14 Ma respectively (Rodrigues et al., 2008), supporting the Neoproterozoic age assignment for the lower Vazante Group.

However, the presence of *Conophyton metula* and *Jacutophyton* bioherms within the overlying Lagamar Formation, as well as other geochemical age constraints from the Serra do Garrote, Serra do Poço Verde and Lapa formations suggests an older age for the upper half of the succession. Recent Re-Os shale dating of the Serra do Garrote and Serra do Poço Verde shales yield depositional ages between 1.3 and 1.0 Ga (Geboy, 2006; Azmy et al., 2008). Similarly, U-Pb SHRIMP ages of detrital zircons indicate a maximum depositional age of ca. 1.5 Ga for the Serra do Garrote and ca. 1.1 Ga for the Serra do Poço Verde and Lapa formations (Rodrigues et al., 2008). The older ages determined by Re-Os and U-Pb detrital zircon analyses, which were conducted in three independent laboratories, as well as stromatolite biostratigraphy, coupled with muted stratigraphic variations in carbon isotopes relative to those in Neoproterozoic successions, all support the claim that the upper Vazante Group was most likely deposited during the Mesoproterozoic Era.

The apparent discrepancy between the ages of the lower and upper Vazante Group can be explained by the presence of a thrust fault near the base of the Lagamar Formation (Figures 1.5; 1.6). Here it appears that the older, Mesoproterozoic sequence was thrust on top of younger Neoproterozoic units. A Mesoproterozoic interpretation for the upper Vazante Group is significant because previously the Mesoproterozoic was believed to be a time that was largely ice-free (Eyles, 2008). Evidence for glaciations in the late

Mesoproterozoic suggests a longer duration for the Cryogenian (ca. 850-635 Ma; an interval of time currently under consideration for period status) than previously thought.

1.3.3: Geologic strategy for this study

Shales and carbonates associated with the Serra do Garrote, Serra do Poço Verde and Lapa formations were chosen as the focus of this biomarker and carbon and sulfur time-series study because they represent pre- and post-glacial depositional cycles. The Serra do Garrote Formation represents normal background sedimentation before the Serra do Poço Verde ice age. The Serra do Poço Verde (Mocambo) shale and Lapa Formation shale, on the other hand, represent sedimentation in the aftermath of two distinct glacial episodes with the Mocambo shale accumulating at the terminus of the first glacial cycle and the Lapa Formation at the terminus of the second.

Samples were collected in 2007 from 11 unmineralized exploratory drill cores (Figure 1.7) from the Companhia Mineira de Metais in Minas Gerais, Brazil with the assistance of head geologist Tolentino Flavio de Oliveira and collaborator Aroldo Misi of the Universidade Federal da Bahia, Instituto de Geociências. The cores are laterally distributed over more than 150 km and represent a N-S transect of the Vazante Basin. Samples were also collected from one core (MAF-011) in the western region of the Vazante Basin, which represents deposition in a distal setting. The strategic sampling of cores spanning the length of the Vazante basin and both proximal and distal basin localities was intended to provide a record of the lateral extent of different environmental facies and biological conditions. Additionally, a basin-wide distribution of cores should

aid in the identification and tracking of non-syngenetic biomarkers introduced through hydrocarbon migration.

Stratigraphic sampling through the Serra do Garrote, Serra do Poço Verde and Lapa formations was performed in order to evaluate how biologic and environmental conditions changed through time and with respect to glaciation. The exploratory drill cores that were sampled for this project were drilled in search of Pb-Zn mineralization that occurs in the Morro do Calcário Formation. Because this zone of mineralization is stratigraphically above the Mocambo, most cores terminate before reaching the Serra do Garrote Formation. Only one core (B4LS-01) contained material from the Serra do Garrote Formation that could be sampled. The Serra do Poço Verde Formation, on the other hand, is represented by samples from eight cores (MAF-009, MAF-011, MAF-42.88, MAF-45, MAF-28, PPF-08, PPF-2A, and PAF-32) that span over 150 km of the continental margin, as well as proximal and distal environments of the Vazante Basin. Samples from the majority of these cores were taken from the Mocambo shale; however, two cores (MAF-011 and MAF-42.88) also sampled the stromatolitic carbonate of the Retiro Member. The Lapa Formation is represented by three cores (B3LF-11, MAF-45, and PPF-04). While the number of cores sampled for the Lapa Formation is not as extensive as from the Serra do Poço Verde Formation, they do represent a basin-wide distribution.

1.4: Working hypotheses

Several hypotheses are address in this study: i) Based on geologic observations and new Re-Os and U-Pb ages, we hypothesize that the upper Vazante Group is late

Mesoproterozoic in age. Biomarker distributions and carbon and sulfur isotopic signatures will therefore have similar characteristics to what is observed in other Mesoproterozoic successions, and these should differ from biomarker and isotopic studies of Neoproterozoic successions; ii) We hypothesize that there are syngenetic biomarkers in the Vazante Group and that these biomarkers reflect the biological conditions that are consistent with both the time and environment in which they were deposited. iii) Changing environmental conditions (e.g. the transition from ice-covered to ice-free environments) will affect both the biologic community and chemical composition of the depositional environment. These changes will be reflected in the biomarker and carbon and sulfur isotopic compositions of organic matter from the Vazante Group.

Table 1.1: Biologically and environmentally significant biomarkers.

Compound	Biologic Origin	Environmental Implication	Reference
High MW <i>n</i> -alkanes	Higher plants	Terrestrial	Tissot and Welte, 1984
Low MW <i>n</i> -alkanes	Algae	Aquatic	Tissot and Welte, 1984
Pristane	Chlorophyll a, bacteriochlorophylla and b, some archaea	Sunlight, oxidizing conditions	Didyk et al., 1978; Ten Haven et al., 1987
Phytane	Chlorophyll a, bacteriochlorophyll a and b, some archaea	Sunlight, reducing conditions	Didyk et al., 1978; Ten Haven et al., 1987
MMAAs	Cyanobacteria	Sunlight	Shiea et al., 1990
Hopanes	Bacteria	---	Ourisson et al., 1979
C ₃₁ -C ₃₅ hopanes	Aerobic bacteria	Oxic conditions	Ourisson et al., 1979
2 α MeH	Cyanobacteria	Sunlight	Summons et al., 1999
3 β MeH	Microaerophylic proteobacteria (Methanotrophic bacteria)	Redox stratified water column	Summons and Jahnke, 1992
γ	Bacteriovores	Redox stratified water column	Moldowan et al., 1985; Sinninghe Damsté et al., 1995
Steranes	Eukaryotes	Oxic conditions	Peters and Moldowan, 1991
24-IPC	Demosponges	Oxic conditions	Bergquist et al., 1980
Aryl Isoprenoids and Isorenieratene	Green Sulfur Bacteria	Sunlight, euxinic conditions	Summons and Powelle, 1987

* MW=molecular weight, MMAAs=monomethylalkanes, 2 α MeH=2 α -methylhopane, 3 β MeH=3 β -methylhopane, γ =gammacerane, 24-IPC=24-isopropylcholesterane

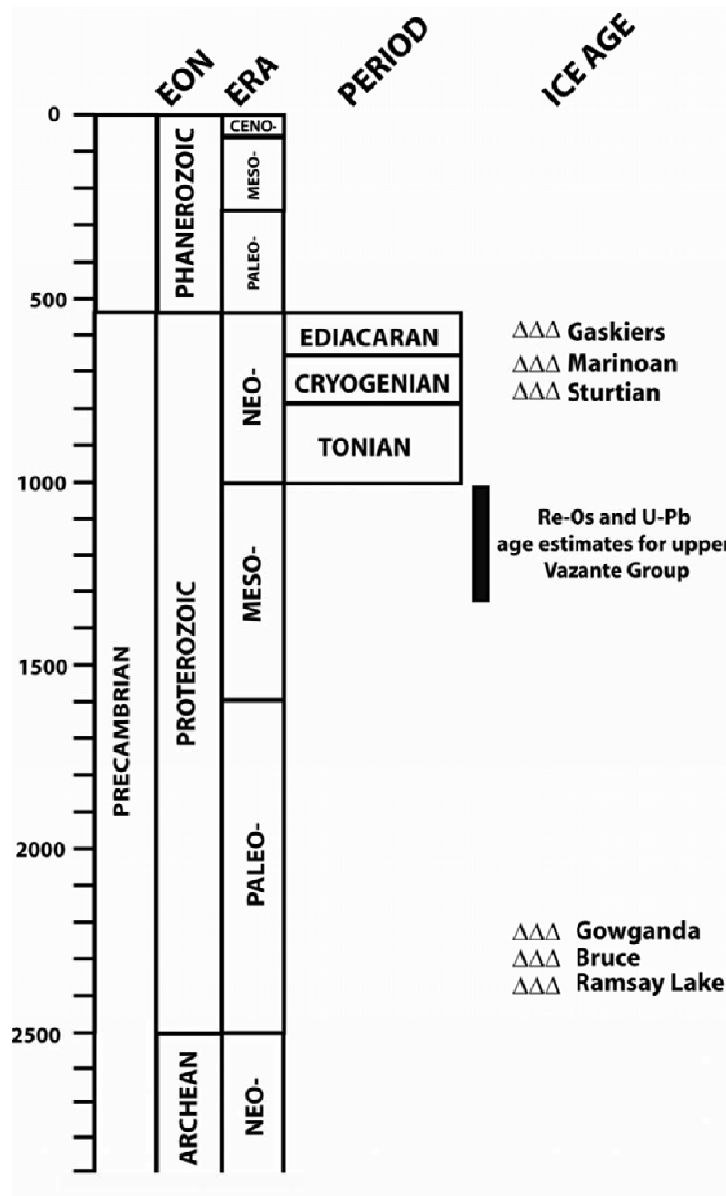


Figure 1.1: Precambrian time scale with internationally recognized subdivisions and general placement of widespread glacial deposits ($\Delta\Delta\Delta$) in the Neoproterozoic and Paleoproterozoic eras. Paleoproterozoic ice ages are named after three key glacial events in southern Ontario. Age ranges for the upper Vazante Group based on Re-Os and U-Pb detrital zircon studies are shown.

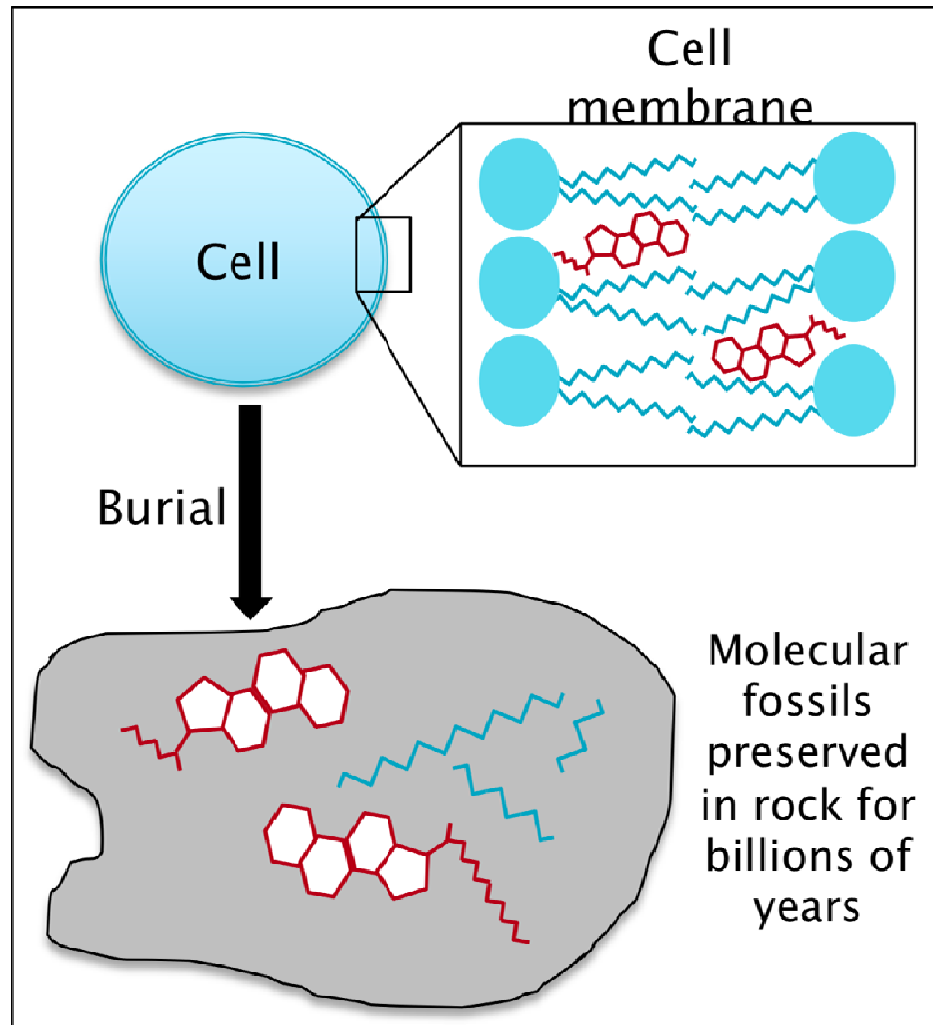


Figure 1.2: Cartoon of biomarker formation. Biomarkers typically originate as lipids that form a cell membrane. When the cell dies the lipids are released and can be preserved in the rock matrix for billions of years.

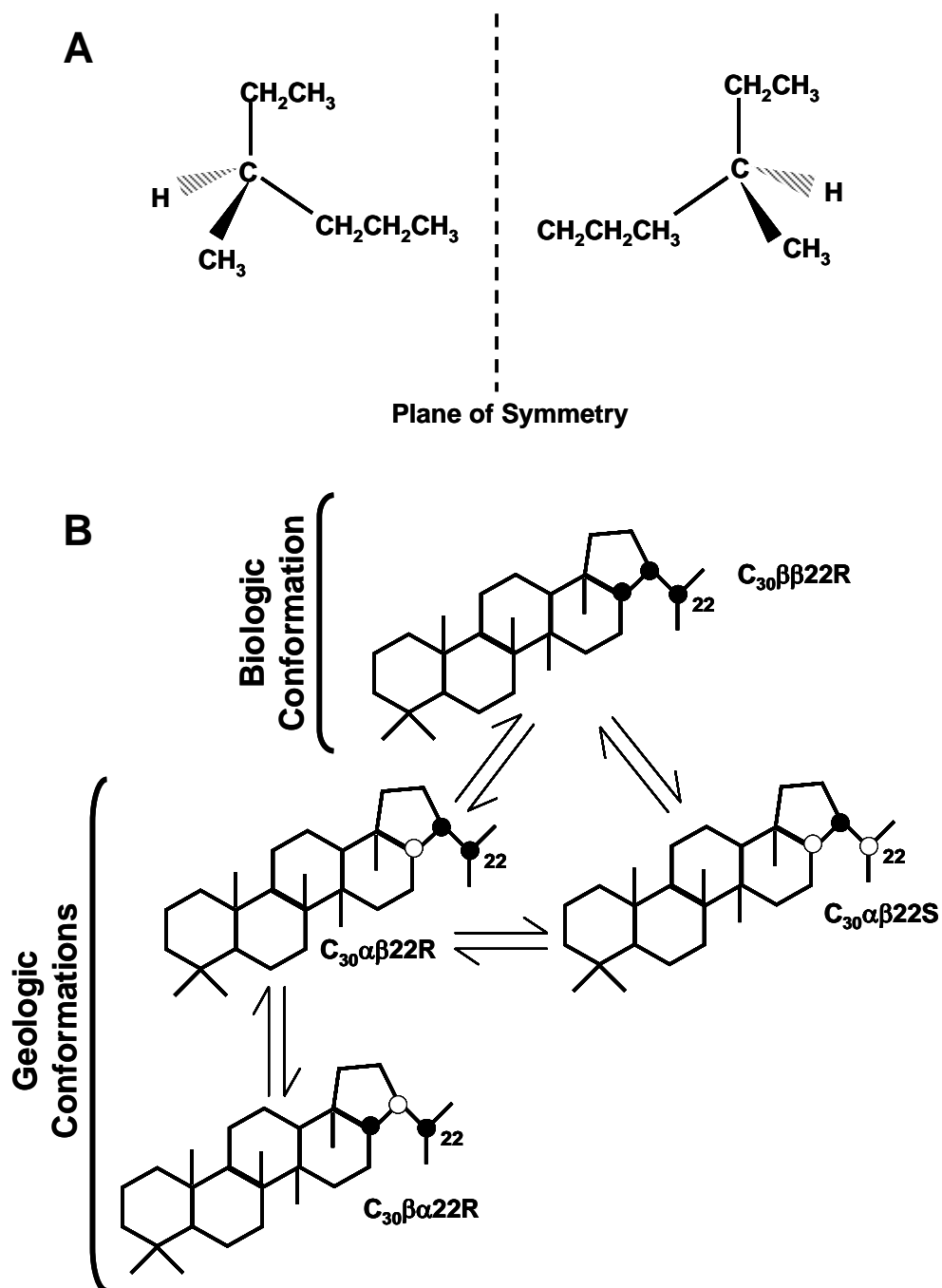


Figure 1.3: A) Schematic of asymmetric carbon atoms. The two molecules are mirror-images of each other but cannot be superimposed without breaking bonds. They are therefore isomers. B) An example of C_{30} hopane isomers. The open circles represent α and the closed circles represent β substituents.

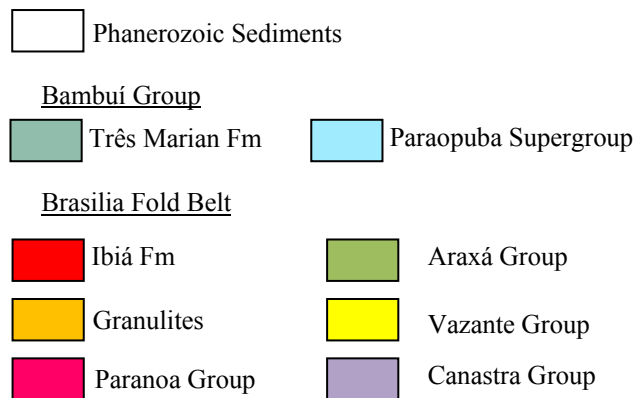
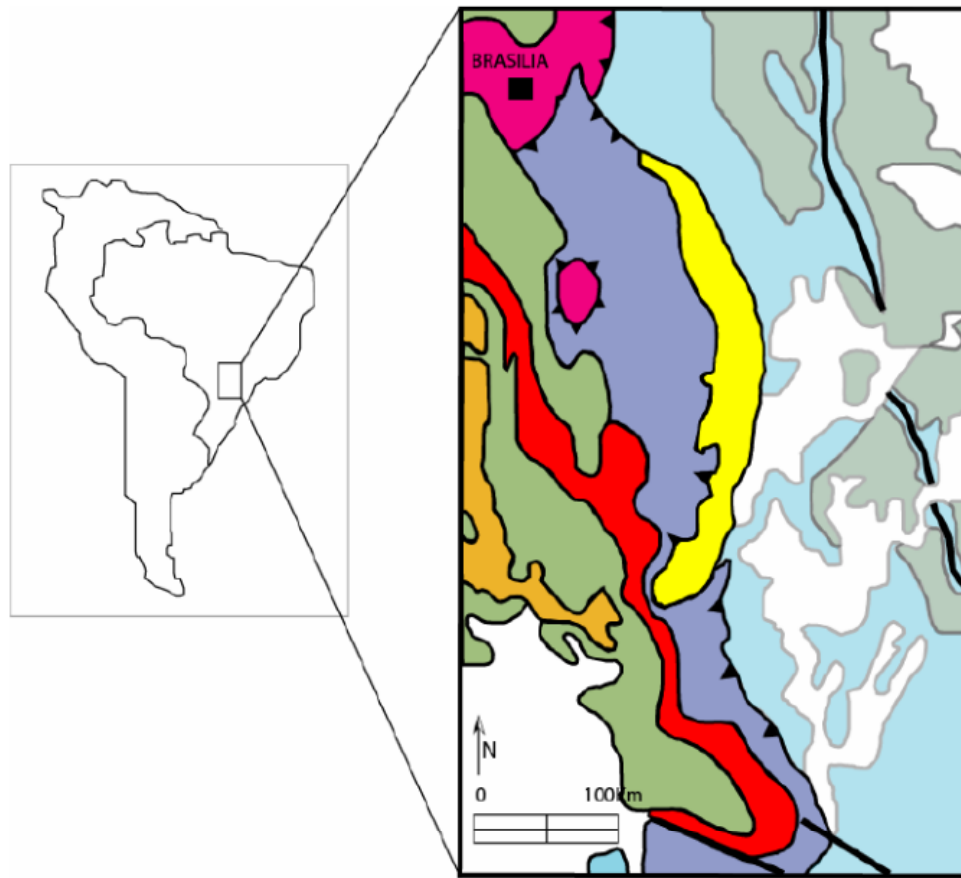


Figure 1.4: Geologic setting of the Vazante Group on the São Francisco Craton in Brazil.

Modified from Babinski et al., 2005.

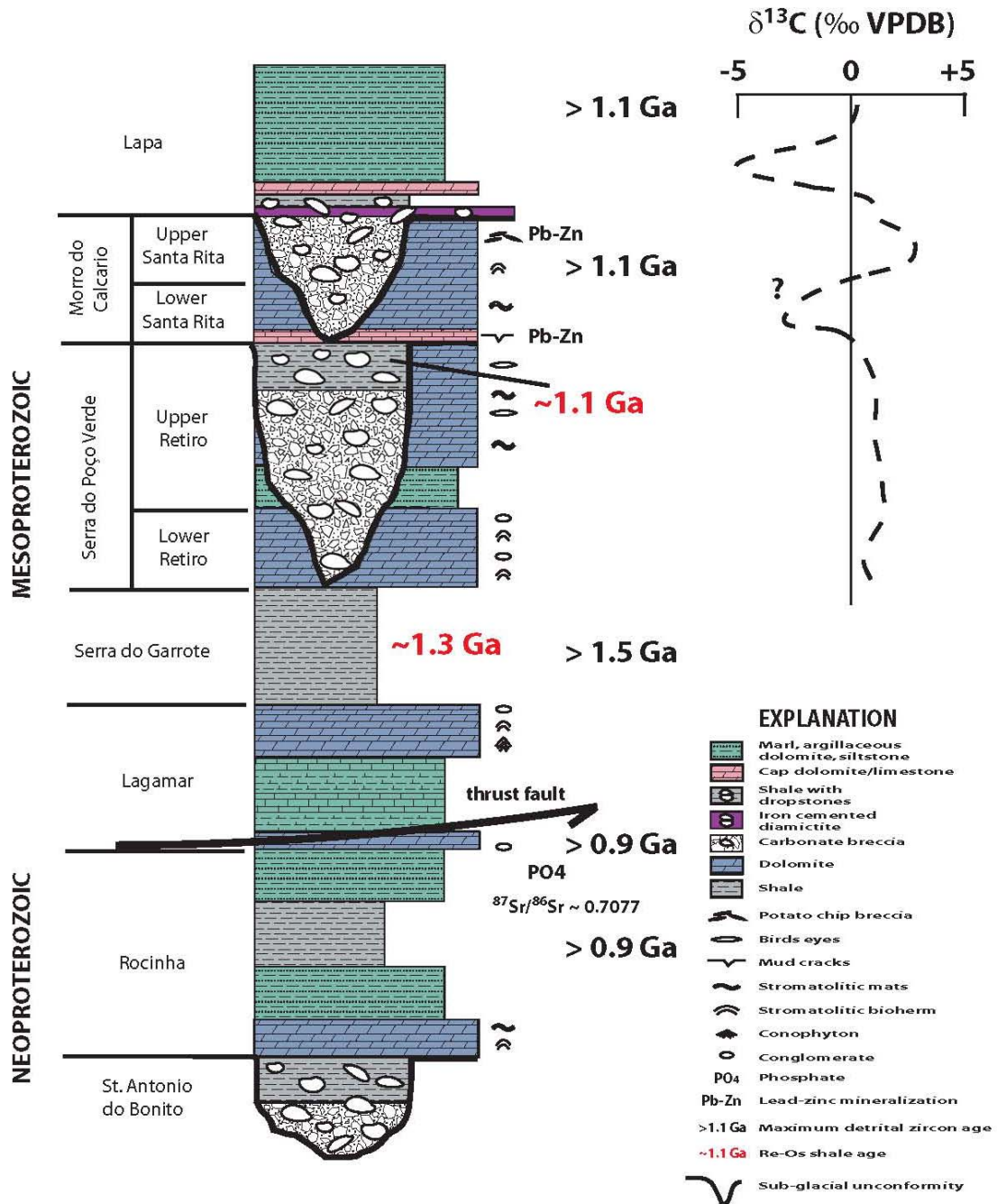


Figure 1.5: A composite of the lithologic and structural stratigraphy of the Vazante Group with Re-Os (Geboy, 2006; Azmy et al., 2008) and detrital zircon U-Pb (Rodrigues et al., 2008) age constraints and a generalized $\delta^{13}\text{C}_{\text{carb}}$ profile.

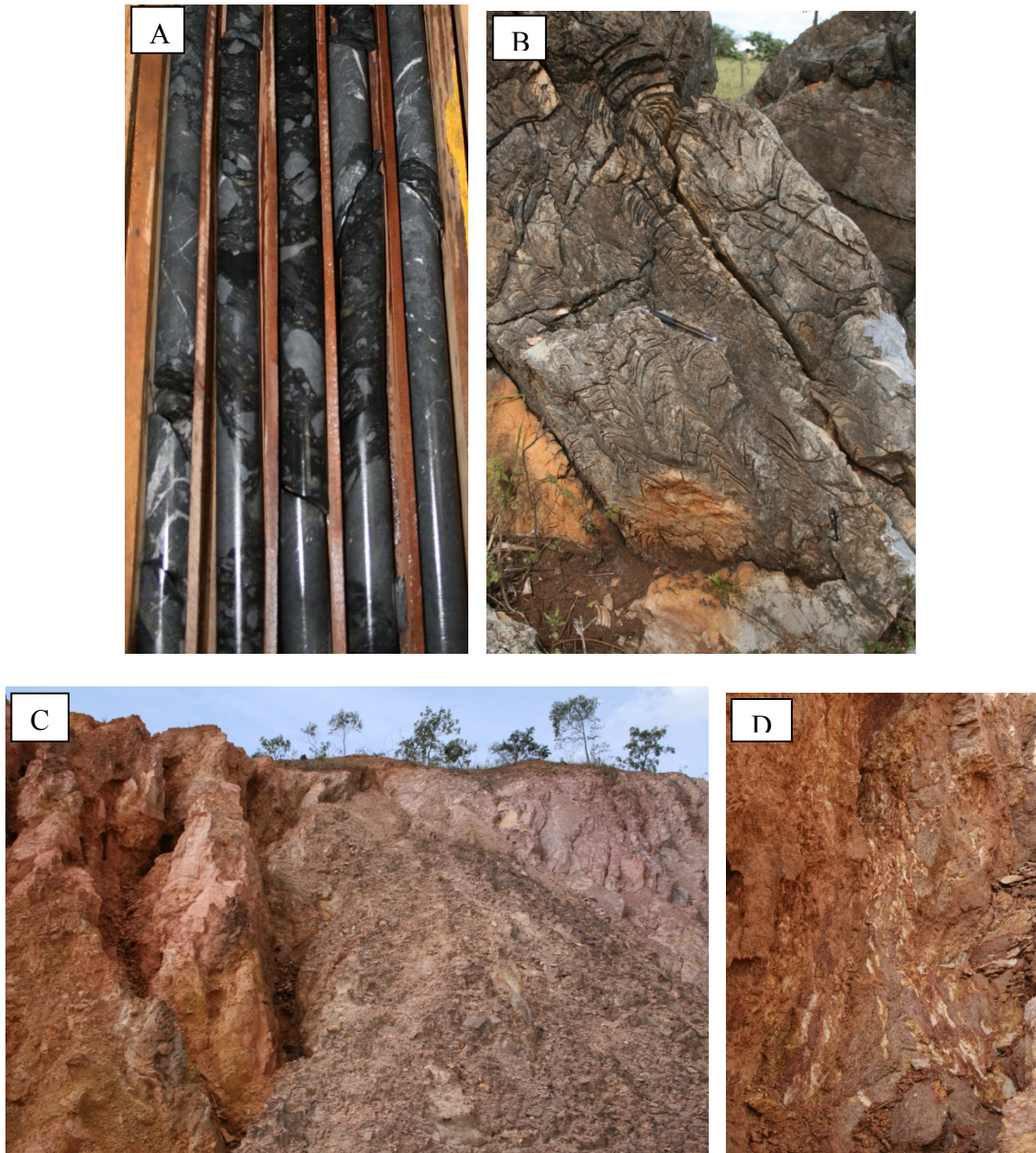


Figure 1.6: Field photographs of A) carbonate ice-rafted debris in the organic-rich Mocambo shale within the Serra do Poço Verde Formation; B) Conophyton stromatolite from the Lagamar Formation; C) Thrust fault trace with brown to mauve sandy mylonite to the left and bedded purple shale and siltstone of the upper Rochina Formation to the right; D) Close up of clay and quartz-rich mylonite at the thrust fault contact.

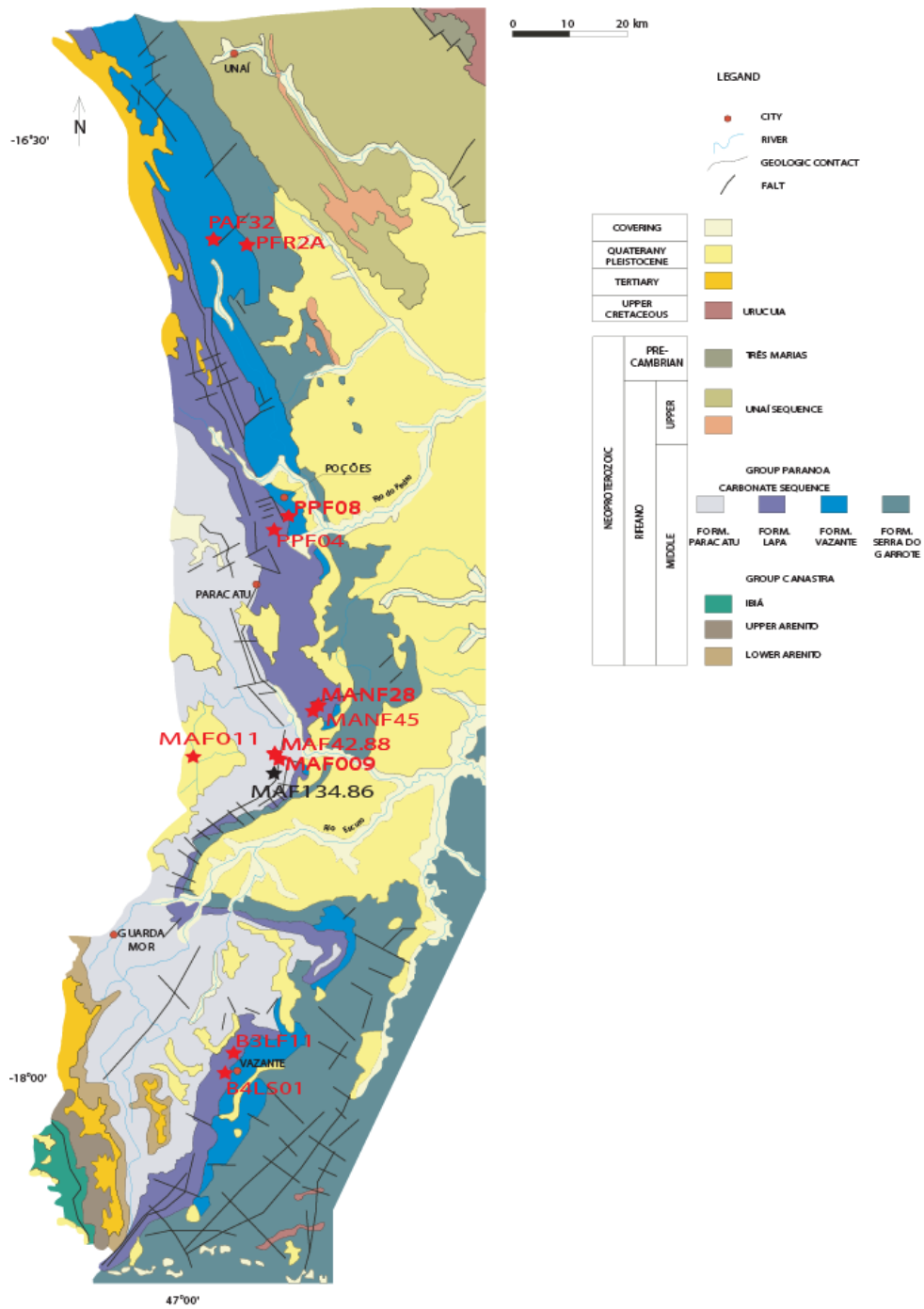


Figure 1.7: Basin-wide distribution of Vazante Group cores. Red stars indicate the location of each core analyzed in this study. The black star (core MAF-134.86) represents the core analyzed by Brody (2006).

Chapter 2: Carbon and Sulfur Isotopic Signatures from the Vazante Group, Brazil

2.1: Introduction

Time-series stable carbon and sulfur isotope abundances recorded in sedimentary rocks from the Vazante Group may provide important information about changing environmental conditions during the Proterozoic, as well as later diagenetic and metamorphic processes that affected the succession. If well preserved, carbon and sulfur isotopic signatures recorded in organic matter and mineral sulfides are useful proxies for microbial-induced cycling of these biologically significant elements. Carbon isotopic signatures of inorganic carbon (i.e. carbonate) however, serve as a proxy for changes in the carbon isotopic composition of seawater. Taken together, an integrated examination of organic carbon and carbonates from the Vazante Group can be used to support inferences of the interaction between life and environment provided by the biomarker results from this study.

A microbial imprint on the cycling of carbon and sulfur may be inferred from isotopic signatures recorded in sedimentary rocks due to the fact that biological processes impart specific isotopic fractionations, the magnitude of which may be modulated by environmental factors. For example, during photosynthesis the lighter carbon isotope ^{12}C is preferentially fixed relative to the heavier carbon isotope ^{13}C ($^{13}\text{CO}_2 + \text{H}_2\text{O} \rightarrow ^{12}\text{CH}_2\text{O} + \text{O}_2$) such that resulting organic carbon is isotopically depleted by 28-32 ‰ (Hayes et al., 1999) relative to input CO_2 . Limitation of CO_2 however, either by low atmospheric

pCO₂ or extreme growth rates of photoautotrophs can result in decreasing magnitude of carbon isotope fractionation (Reeburgh et al. 1991, Coale et al. 1996, Bidigare et al. 1997, Popp et al. 1998). Isotopic compositions of sedimentary carbonates and organic carbon are recorded as the ratio of ¹³C/¹²C in the sample (*s*) relative to a reference material (*ref*). This is usually expressed in delta-notation:

$$\delta^{13}\text{C} = 1000 * \left(\frac{\left(\frac{^{13}\text{C}}{^{12}\text{C}} \right)^s}{\left(\frac{^{13}\text{C}}{^{12}\text{C}} \right)^{ref}} - 1 \right)$$

The reference material used for carbon isotopic analyses is Vienna PeeDee belemnite (V-PDB).

In contrast to carbon buried as the result of primary productivity, carbonate, which precipitate from seawater, do not have large associated fractionations (Emrich and Vogel, 1970). Thus, the carbon isotopic signatures of carbonates largely reflect the carbon isotopic value of seawater at the time of deposition (Emrich and Vogel, 1970), if these have not subsequently been altered (Knauth and Kennedy, 2008). One test for alteration of Proterozoic samples is to compare magnitudes of fractionation between carbonate and co-existing organic matter (Knoll et al., 1986; Hayes et al., 1999), and these will be evaluated in the present study.

Similar to the biological process of photosynthesis, sulfur-utilizing bacteria, including sulfate reducing bacteria (SRB), fractionate sulfur isotopes by preferentially incorporating the light ³²S rather than the heavier ³⁴S isotope (³⁴SO₄²⁻ + CH₂O → H₂³²S + CO₂). The degree of fractionation is indicative of the specific metabolism utilizing the sulfur as well as the availability of sulfate and organic substrates. This again is recorded

in sediments as the ratio of $^{34}\text{S}/^{32}\text{S}$ in the sample (*s*) relative to a reference material (*ref*) and is also expressed in delta notation:

$$\delta^{34}\text{S} = 1000 * \left(\frac{\left(\frac{^{34}\text{S}}{^{32}\text{S}} \right)_s}{\left(\frac{^{34}\text{S}}{^{32}\text{S}} \right)_{ref}} - 1 \right)$$

The reference material used for sulfur isotopic analyses is Vienna Canyon Diablo Triolite (V-CDT).

Although the fractionation of carbon and sulfur isotopes can be unique to specific organisms, it is also dependent on the amount of carbon and sulfur available in the system. For example, the fractionation imparted by SRB ranges from ~-2-46 ‰, depending on sulfate concentrations (Habicht and Canfield 1997, Canfield, 2001). This is because when sulfate is abundant SBR can impart their full fractionation, but when sulfate is limited the fractionation approaches zero because SRB will use any available sulfate ion regardless of whether it is $^{32}\text{SO}_4^{2-}$ or $^{34}\text{SO}_4^{2-}$ (Habicht et al., 2002).

The goal of this study is to construct new time-series isotopic trends through the Serra do Garrote, Serra do Poço Verde and Lapa formations in order provide an assessment of the environmental conditions prior to and immediately after glaciation. This time-series isotopic analysis is independent of the biomarker study, however, it also provides environmental context for interpreting biomarker results. Furthermore, comparison of isotopic trends from the Vazante Group with Neoproterozoic and Mesoproterozoic successions may help to evaluate the possible age of the Vazante Group and its biomarkers.

2.2: Sample strategy

Organic-rich shale samples as well as carbonates were collected from multiple cores throughout the Vazante Basin and sampled from selected intervals of the Serra do Garrote, Serra do Poço Verde, and Lapa formations (Figure 2.1). The samples were collected every 2-5 meters in specific intervals within each core so that changes in the carbon and sulfur isotopic composition could be observed with respect to time. However, lacking knowledge of sedimentation rates, it is not possible to directly assess the rate of change recorded in the isotopic tracers. We can however, make the assumption that the Serra do Garrote Formation, which is a non-glacial shale underlying the Serra do Poço Verde and Lapa diamictites, represents the slow accumulation of sediment prior to glaciation, whereas the Serra do Poço Verde and Lapa formations represent the comparatively rapid deposition of sediment released during post-glacial melting of two distinct ice-ages.

Organic-rich shales and marls, which were collected for organic carbon and sulfur isotopic analysis, were taken from three cores (B3LF-11, MAF-45, and B4LS-01; Figure 2.2). Each of the three cores represents a different Vazante formation; B4L-S01 sampled the continuous grey slate of the Serra do Garrote Formation, the lower 40 m of core MAF-45 sampled organic rich shale of the Mocambo interval within the Serra do Poço Verde Formation, and core B3LF-11 as well as the upper 65 m of core MAF-45 sampled the organic rich shale and marl of the Lapa Formation.

Carbonate samples were also collected from three cores (MAF-28, PPF-08, MAF-009; Figure 2.3). The samples from core MAF-28 were collected from a carbonate directly overlying the Mocambo shale. Samples from PPF-08 were collected from a marl below the Mocambo, as well as stromatolitic carbonate and the carbonaceous matrix from

a carbonate diamictite overlying the Mocambo. Samples from core MAF-009 represent a nearly continuous sampling of carbonates starting below the Mocambo and continuing through the first 20 m of the Lapa Formation. Samples underlying the Mocambo were collected from a dolarenite that grades from a laminated fine-grained to a massive dolarenite and then grades into the diamictite.

2.3: Methods

Shale samples collected for organic carbon and pyrite sulfur isotopic analysis were powdered and homogenized using a ceramic mortar and pestle. The powdered samples were then acidified to remove any carbonate. Carbonate was removed by addition of 6 M HCl until the powders were no longer reactive. The samples were then rinsed twice with ultrapure 18 M Ω Milli-Q water and dried in an oven at 60°C.

Approximately 500 ug aliquots of acid treated residue were weighed into tin cups for carbon and sulfur elemental and isotopic analysis. An additional ~500 ug of V₂O₅ were added to the tin cups designated for sulfur analysis to assist with combustion. The samples were analyzed using a Eurovector Elemental Analyzer (EA) coupled to a GC IsoPrime Continuous Flow (CF) Mass Spectrometer. Samples were loaded into an EA autosample carousel, which individually dropped each sample into a combustion column heated to 1040°C. A timed pulse of O₂ enabled combustion of the samples and a constant flow of He carrier gas (~90 ml/min) transferred the combustion products through a reaction tube packed with chromium and cobalt oxides for quantitative oxidation of O₂ resorption. Samples intended for carbon analysis then proceeded through a reduction column packed with reduced Cu wire heated to 660°C; sulfur analyses did not use this

reduction column. Both carbon and sulfur samples were then carried through a 10-cm magnesium perchlorate water trap before entering a 0.8 m stainless steel GC column for further purification. The GC column was packed with Porapak 50-80 mesh resin and heated to 90°C and was used to isolate CO₂ (in the case of carbon analysis) and SO₂ (in the case of sulfur analysis) gas from other combustion products before entering the mass spectrometer. Detection of sample pulses in the mass spectrometer were preceded by 30 second reference gas injections. Isotopic values were reported in δ notation as parts per mil (‰) relative to the Pee Dee Belemnite (V-PDB) standard for carbon and the Canyon Diablo Troilite (V-CDT) standard for sulfur. Uncertainties were determined by multiple analyses of standards (NIST 912a for carbon and NBS 127 for sulfur) and were typically better than $\pm 0.1\%$ (1σ) for carbon analyses and ± 0.3 (1σ) for sulfur analyses.

Carbon abundance was also measured along with carbon isotopic composition. The measured carbon abundance represents the organic carbon fraction of acidified residues. Therefore, total organic carbon (TOC) was calculated as a weight % of the total carbon, taking into account carbon present in the removed carbonate fraction. Uncertainties based on these measurements were typically better than $\pm 0.6\%$ (1σ).

Carbonate samples were cut and one side was polished so that areas of alteration free carbonate could be selected for analysis. In general the finest-grained portions of the samples, away from any weathering grinds or secondary veins, were identified (Kaufman and Knoll, 1995) and the selected areas were then drilled with a Servo Products diamond-tipped microdrill (1 mm diameter) so that 1-2 mg of carbonate powder was collected. Approximately 100 μg of the carbonate was placed into a Wheaton V-vial and then analyzed using a GV IsoPrime Dual Inlet (DI) Mass Spectrometer. Samples in vials were

placed in a Multi-prep inlet system and reacted with 0.1 ml of 102.5% phosphoric acid for 10 minutes at 90°C. The resulting CO₂ and water vapor were then cryogenically separated and the isotopic abundances of carbon and oxygen were measured from the evolved CO₂. The resulting isotopic values are reported in δ notation as parts per mil (‰) relative to the Pee Dee Belemnite (V-PDB) standard. Uncertainties on these measurements for both C and O isotopes were determined by multiple analyses of a standard (NBS 19) and are typically better than ±0.02‰ (1σ) for both carbon and oxygen isotopes.

2.4: Results

2.4.1: Organic carbon

TOC and the isotopic composition of organic carbon ($\delta^{13}\text{C}_{\text{org}}$) were analyzed from three cores: B4LS-01, MAF-45 and B3LF-11 (Figure 2.2). TOC for the Serra do Garrote Formation (B4LS-01), ranges from 0.0-4.4 wt % with most values falling between 1 and 2 wt %. The $\delta^{13}\text{C}_{\text{org}}$ for the Serra do Garrote Formation ranges from -31.2 to -27.6‰ and displays little variation. Similarly, TOC from the Serra do Poço Verde Formation (lower MAF-45) range from 0.32-1.59 wt % and have largely invariant $\delta^{13}\text{C}_{\text{org}}$ values ranging from -31.0 to -28.5‰. TOC from the Lapa Formation from the same core (upper MAF-45) range from 0.2-1.2 wt %. $\delta^{13}\text{C}_{\text{org}}$ values however range from -28.9 to -24.7‰ and show a slight positive shift (~3‰) towards heavier values with height in the drill core. Lapa TOC recorded in core B3LF-11 ranges from 0.1-3.8 wt % with average values falling between 1 and 2.2 wt %. $\delta^{13}\text{C}_{\text{org}}$ values from these samples are highly variable

and range from -35.3 to -22.0‰. There is a positive shift (~5‰) towards heavier values in the lower 100 m of the core; above this, the high variability of the $\delta^{13}\text{C}_{\text{org}}$ values do not show a clear trend.

2.4.2: Sulfur

High-resolution sulfur isotopic analysis of sedimentary pyrite ($\delta^{34}\text{S}_{\text{py}}$) was performed on the same three cores from the Vazante Group (B4LS-01, MAN-45 and B3LF-11; Figure 2.2). Similar to the $\delta^{13}\text{C}_{\text{org}}$ signal seen in the Serra do Garrote Formation, the $\delta^{34}\text{S}_{\text{py}}$ values from core B4LS-01 are remarkably invariable and range from +1.1 to +5.0‰. $\delta^{34}\text{S}_{\text{py}}$ values from the Serra do Poço Verde Formation (lower MAF-45) however, range from +12.6 to +19.6‰, showing a 7‰ shift towards heavier value with height. Excluding two anomalous values (+7.5 and +29.7‰) at the unconformity, the $\delta^{34}\text{S}_{\text{py}}$ values from the upper, Lapa portion of this core (MAF-45), range from +8.7 to +18.2‰ and show a negative shift towards lighter values with height. Conversely, Lapa samples from core B3LF-11 range from +15.5 to +34.5‰ and display a ~20‰ shift towards heavier values with height.

2.4.3: Carbonate carbon

The carbon isotopic composition of carbonate carbon ($\delta^{13}\text{C}_{\text{carb}}$) was analyzed from three separate cores: MAF-28, PPF-08 and MAF-009 (Figure 2.3). The $\delta^{13}\text{C}_{\text{carb}}$ values from the Serra do Poço Verde, measured in core MAF-28, range from +1.81 to +2.76‰ and display no obvious trend. The values from the Serra do Poço Verde core PPF-08 however range from -0.10 to +2.68‰ and shift from heavier to lighter values

with height. The shift in $\delta^{13}\text{C}_{\text{carb}}$ values within this core occurs at the boundary between the Mocambo and the underlying carbonate unit. The $\delta^{13}\text{C}_{\text{carb}}$ values from core MAF-009, which samples the Serra do Poço Verde and Lapa formations, display the greatest variation compared with the other cores. The values range from -1.19 to +1.93‰ in the Serra do Poço Verde Formation and from -3.30 to -0.29‰ in the Lapa Formation. One laminated dolarenite sample from the Serra do Poço Verde Formation has a negative value of -1.19‰ whereas the rest of the dolarenite samples have values in the narrow range of +0.64 to +0.73‰. The values then shift towards slightly heavier values, up to +1.41‰, as the matrix of the diamictite grades from carbonate to shale. The samples from the Lapa Formation display a negative $\delta^{13}\text{C}_{\text{carb}}$ excursion at the base, down to values as low as -3.30‰, and then a continuous positive trend approaching zero (-0.29‰) with height.

2.5: Discussion

Interpretations of carbon and sulfur isotopes from the organic rich shales and carbonates of the Vazante Group provide an avenue for characterizing the environmental or redox conditions that were present before and after basin-wide (and potentially global) Vazante glaciations. The Serra do Garrote Formation is pre-glacial and, therefore, represents background environmental conditions prior to glaciations. The Serra do Poço Verde and Lapa formations however, were deposited in the wake of two separate ice ages and represent the environmental change that occurred in the glacial aftermath.

2.5.1: Organic Carbon and Sulfur

Organic carbon and sulfur from the Serra do Garrote, Serra do Poço Verde, and Lapa formations display varying isotopic trends indicating evolving redox conditions. The Serra do Garrote Formation shows highly invariable $\delta^{13}\text{C}_{\text{org}}$ and $\delta^{34}\text{S}_{\text{py}}$ signatures over ~80 m of pre-glacial shale indicating an extended period of stasis long before the onset of Vazante glaciations. A similar trend, at least in the $\delta^{13}\text{C}_{\text{org}}$ signature, is seen in the lower Doushantuo Formation, an Ediacaran (635-542 Ma) succession in South China (McFadden et al., 2008). McFadden and colleagues (2008) found that, although $\delta^{13}\text{C}_{\text{carb}}$ fluctuated between positive values and negative excursions, the $\delta^{13}\text{C}_{\text{org}}$ remained stable at about -30‰. They interpreted this decoupling of $\delta^{13}\text{C}_{\text{org}}$ and $\delta^{13}\text{C}_{\text{carb}}$ signatures to be due to the presence of a large dissolved organic carbon (DOC) pool. The large size of the DOC pool they suggest would effectively buffer the $\delta^{13}\text{C}_{\text{org}}$ isotopic signature against fluctuations in the DOC pool (e.g. changes in the flux in/out of oxidized/reduced species). The dissolved inorganic carbon (DIC) pool however would have been comparatively small and therefore perturbations in the DIC reservoir, such as increased oxidation, would be reflected in the $\delta^{13}\text{C}_{\text{carb}}$ signature. A large DOC pool and a small DIC pool could be maintained in a strongly redox stratified water column where a thin layer of oxygenated surface water overlays anoxic, reducing, deeper water (Rothman et al., 2003).

Although the Doushantuo is younger than any age proposed for the Vazante Group, the principle of a large isotopically buffered DOC pool can be applied to explain the invariant $\delta^{13}\text{C}_{\text{org}}$ signature observed in the Serra do Garrote Formation. High TOC concentrations also support the hypothesis of a large DOC pool insofar as the more DOC there is in the water column, the more organic carbon (C_{org}) will be exported to the

seafloor for burial. Decoupling of the DOC and DIC pools however cannot be assessed without a corresponding suite of $\delta^{13}\text{C}_{\text{carb}}$ values.

The $\delta^{34}\text{S}_{\text{py}}$ signature seen in the Serra do Garrote Formation is also highly invariant. A similar invariant signal is observed in the Wollogorang and Reward formations from the McArthur Basin, a well-studied late Paleoproterozoic (ca. 1.73 and 1.64 Ga respectively) succession in northern Australia (Shen et al., 2002). Shen and colleagues (2002) interpreted this to indicate that the water column was strongly stratified with a large euxinic (anoxic and H_2S -rich) pool overlain by a small sulfate reservoir. They based this on the invariance seen in $\delta^{34}\text{S}_{\text{py}}$ values from sulfides from the Black Sea, which is a modern analogue for highly euxinic conditions in the water column. However, $\delta^{34}\text{S}_{\text{py}}$ values of pyrite precipitating from the euxinic portion of the Black Sea are extremely depleted relative to coeval sulfate ($\delta^{34}\text{S}_{\text{py}}$ range from -39 to -34‰; Raiswell and Canfield, 1998) whereas the $\delta^{34}\text{S}_{\text{py}}$ values reported by Shen et al. (2002; ca. +4‰ and +18‰, respectively, from the two formations), like those reported from the Serra do Garrote Formation (ca. +4‰), are enriched relative to the sulfides from the Black Sea. The enrichment in the Proterozoic units may be the result of extensive BSR acting on a small sulfate pool in a closed system (i.e. the rate of sulfate consumption is \geq the rate of sulfate supply; Jorgensen, 1979; Zaback et al., 1993). The lighter ^{32}S would be preferentially removed from the sulfate pool via BSR and sequestered in pyrite (Jones and Starkey, 1957; Harrison and Thode, 1958; Kaplan and Rittenberg, 1964). This would lead to progressive isotopic enrichment in the sulfate pool, which in turn would lead to isotopic enrichment in the sulfide pool.

Unlike the Serra do Garrote Formation, the Serra do Poço Verde and Lapa formations display greater variability in $\delta^{13}\text{C}_{\text{org}}$ and $\delta^{34}\text{S}_{\text{py}}$ signatures. While the $\delta^{13}\text{C}_{\text{org}}$ in the Serra do Poço Verde Formation appears to be invariant, possibly indicating the presence of a large DOC pool (Rothman et al., 2003; McFadden et al., 2008), the $\delta^{34}\text{S}_{\text{py}}$ signature displays a positive shift ($\sim 7\text{‰}$) towards heavier values. Again this suggests a stratified water column where intense BSR is acting upon a small sulfate pool (Habicht et al., 2002). However, Azmy et al. (2001) reported $\delta^{34}\text{S}$ of two carbonate-associated sulfate (CAS) samples from the Serra do Poço Verde Formation, ranging from +10.8 to +16.9‰. If true, then the sulfides reported here (+12.6 to +19.6‰) display no fractionation or possibly even an inverse fractionation ($\delta^{34}\text{S}_{\text{cas}} < \delta^{34}\text{S}_{\text{py}}$) relative to seawater sulfate. If complete reduction of the sulfate pool occurred then the $\delta^{34}\text{S}_{\text{py}}$ would reflect the starting isotopic composition of sulfate. Therefore, conservatively, this is consistent with extensive, or even complete, reduction of the sulfate pool (Shen et al., 2002).

Opposing trends in the $\delta^{13}\text{C}_{\text{org}}$ and $\delta^{34}\text{S}_{\text{py}}$ signatures in the Lapa marl (core MAF-45) are consistent with what has been observed in other studies of the Vazante group (Geboy, 2006; Brody, 2007). A shift towards heavier carbon isotopes may be the result of carbon limitation due to high rates of primary production (Hollander and McKenzie, 1991). The primary producers, which produce oxygen as waste, would at least partially oxidize the water column and potentially increase the sulfate pool. The re-oxidation of bacterially reduced H_2S would result in sulfate with lighter $\delta^{34}\text{S}$ values (Canfield and Teske, 1996). Additionally, with more sulfate available bacterial sulfate reducers would

be able to express a larger fractionation, thus resulting in a shift towards lighter ^{34}S isotopes.

Conversely, the $\delta^{13}\text{C}_{\text{org}}$ and $\delta^{34}\text{S}_{\text{py}}$ signatures in core B3LF-11 from the Lapa Formation display corresponding positive trends. This suggests that the amount of available sulfate was decreasing while the rates of primary production were increasing. Furthermore, Azmy et al. (2001) reported $\delta^{34}\text{S}_{\text{CAS}}$ from the Lapa Formation to be ca. +22‰. If true then the shift in $\delta^{34}\text{S}_{\text{py}}$ in the upper portion of the core to values up to +34.5‰ suggest an inverse fractionation between seawater sulfate and sedimentary pyrite. Shen and colleagues (2010) record inverse sulfur fractionation in the Neoproterozoic Quanji Group in northwest China and interpreted it to be the result of deposition from a stratified water column with isotopically distinct sulfur pools. They suggest that the $\delta^{34}\text{S}_{\text{CAS}}$ values reflect the isotopic composition of surface water sulfate (an open system) whereas the $\delta^{34}\text{S}_{\text{py}}$ values reflect sulfate limitation in a closed system (e.g. sulfate and the resulting sulfide trapped in pore space in the sediment would become progressively enriched as BSR distilled out the lighter ^{32}S isotope).

2.1.2: Carbonate carbon

Carbonate carbon from the Serra do Poço Verde and Lapa formations can be used as a tool to correlate the upper Vazante Group with other Meso- or Neoproterozoic successions. The slightly positive $\delta^{13}\text{C}_{\text{carb}}$ values (ca. +1 to +2‰) from cores PPF-08 and MAF-28 and the lower section of core MAF-009 as well as the negative excursion in the Lapa carbonate have been observed in multiple cores throughout the Vazante basin (Azmy et al., 2001; Azmy et al., 2006; Brody, 2007) and are typical of Mesoproterozoic

carbonates (Kah et al., 1999; Kah et al., 2001; Frank et al., 2003). Azmy et al (2001) observed that pre-Lapa $\delta^{13}\text{C}_{\text{carb}}$ values are about +2‰ and then drop to values of about -2‰ at the top of the Lower Santa Rita (previously called the Middle Pamplona). The values briefly return positive and then drop again to negative values as low as -8‰ at the base of the Lapa. The observation of negative carbon isotope excursions in carbonates overlying glacial diamictite is similar to what is observed in the cap carbonates associated with Neoproterozoic glaciation.

Azmy et al. (2001) originally assigned a Neoproterozoic age to the Vazante Group based on the time-series carbonate carbon isotopic signature. However, the observed carbonate isotopic trend is strikingly similar to what has been observed in Mesoproterozoic carbonates. Observed Mesoproterozoic carbonate isotopic trends are typically between +2 and +4 ‰ with episodic negative shifts to values around -1 to -2 ‰ (Kah et al., 1999; Kah et al., 2001; Frank et al., 2003). The positive values are most often explained in terms of increased burial of isotopically light organic carbon. Frank et al. (2003) suggests that eukaryotic diversification allowed for a more efficient packaging of organic material, which could be transported to deep anoxic water where it is easier to preserve and sequester. Thus the removal of organic carbon from the short-term carbon cycle drove isotopic compositions to more positive $\delta^{13}\text{C}$ values. The negative excursions were explained as short-term perturbations in the carbon cycle acting on a small DIC pool.

2.5: Conclusions

The carbon and sulfur isotopic composition of pre- and post-glacial shales and carbonates provides important information regarding the interaction between life and environment during Proterozoic glacial events. The pre-glacial Serra do Garrote Formation displays invariable $\delta^{13}\text{C}_{\text{org}}$ and $\delta^{34}\text{S}_{\text{py}}$ signatures suggesting deposition from a largely anoxic water column with large, isotopically buffered DOC pool overlain by a thin oxic layer. The post-glacial Serra do Poço Verde and Lapa formations differ in that they display varying $\delta^{13}\text{C}_{\text{org}}$ and $\delta^{34}\text{S}_{\text{py}}$ isotopic trends. The Serra do Poço Verde Formation may reflect complete depletion of the sulfate pool. The Lapa Formation however, may reflect increased oxidation of the bacterially reduced sulfate, possibly due to increased primary production. While these conditions are recorded in both Neo- and Mesoproterozoic sedimentary successions (e.g. Shen et al., 2002; Johnston et al., 2008, McFadden et al., 2008; Shen et al., 2010), the $\delta^{13}\text{C}_{\text{carb}}$ of the upper Vazante formations is most consistent with other Mesoproterozoic successions (Kah et al., 1999; Kah et al., 2001; Frank et al., 2003).

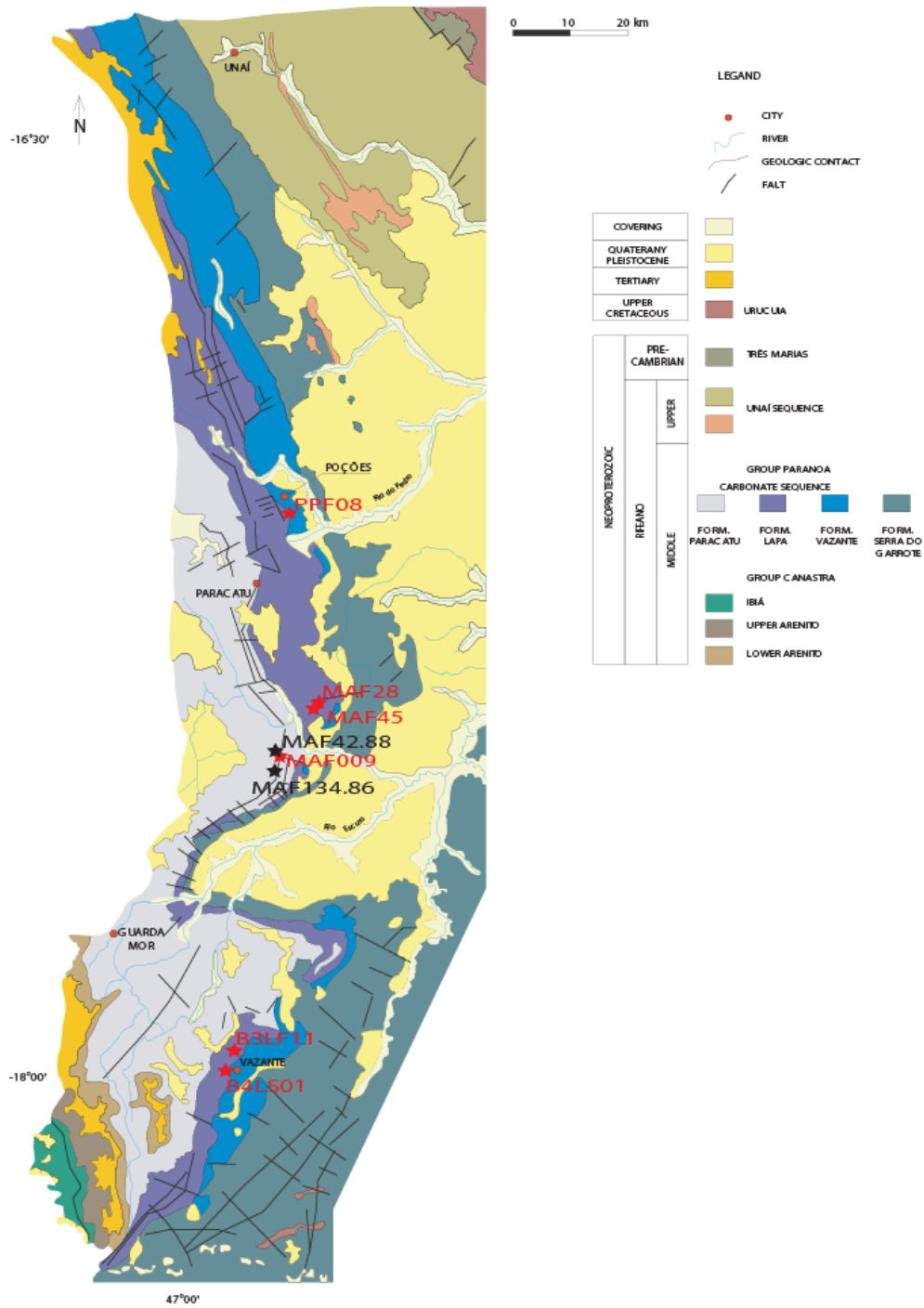


Figure 2.1: Geologic map showing the location of cores sampled for time-series carbon and sulfur isotopic analysis. The red stars show the location of a core sampled in this study. The black stars show the location of a core sampled in previous studies (MAF-134.86 from Brody, 2007 and MAF-42.88 from Olcott et al., 2005).

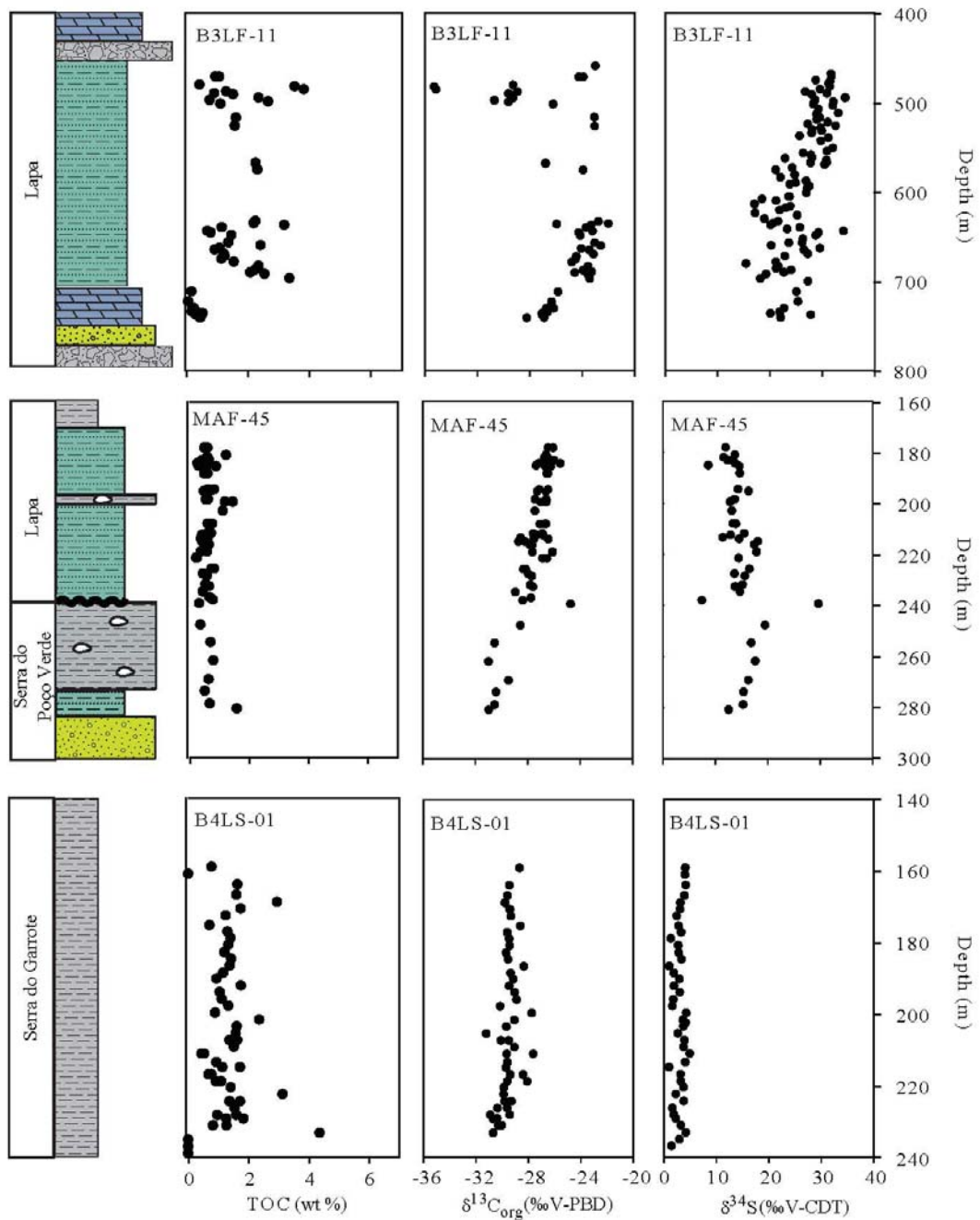


Figure 2.2: TOC, $\delta^{13}\text{C}_{\text{org}}$, and $\delta^{34}\text{S}$ signatures for the Vazante Group. Core B3LF-11 and the marl unit of core MAF-45 represent the Lapa Formation, the shale diamictite unit of core MAF-45 represents the Mocambo and core B4LF-01 represents the grey slate from the Serra do Garrote Formation. TOC is shown as a weight % and $\delta^{13}\text{C}_{\text{org}}$ and $\delta^{34}\text{S}$ are in ‰. Legend shown in Figure 2.3.

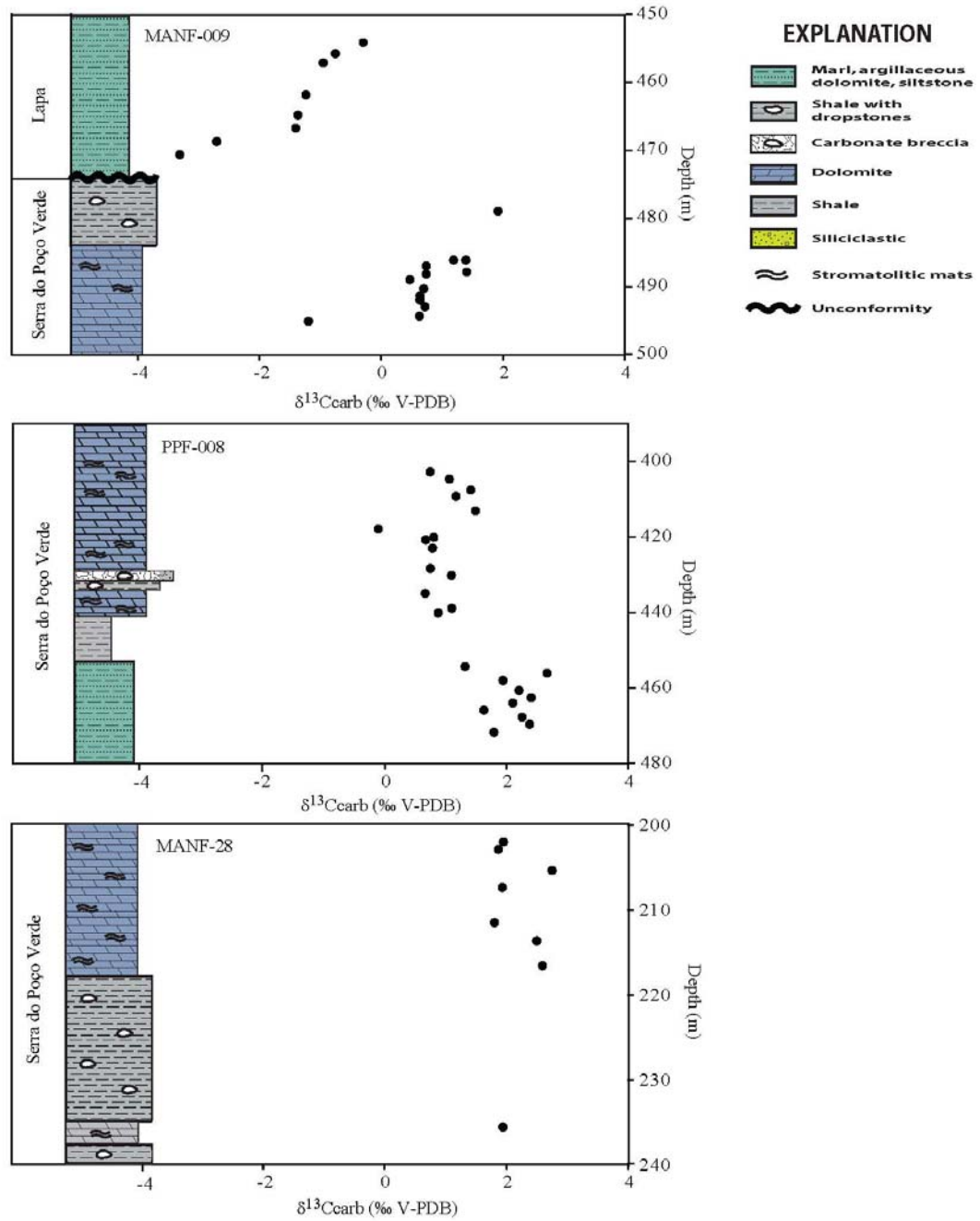


Figure 2.3: Carbonate isotopic trends of the Vazante Group. Core MAF-009 shows the $\delta^{13}\text{C}_{\text{carb}}$ signature for carbonate units below the Mocambo as well as the basal portion of the Lapa Formation. Cores PPF-08 and MAF-28 show the $\delta^{13}\text{C}_{\text{carb}}$ signature for carbonate units bracketing the Mocambo unit.

Chapter 3: Biomarkers from the Vazante Group

3.1: Introduction

Understanding the nature of life and its relationship to changing environments from molecular and isotopic clues preserved in ancient rocks is a difficult and oftentimes daunting task. In Phanerozoic strata, paleontological studies have pieced together a discontinuous history of the rise and radiation of the major taxa of plant and animals (e.g. Braiser et al., 1997; Grotzinger et al., 2000), but these organisms generally have large morphologically distinct bodies and hard (i.e. mineralized) parts that are readily preserved. In contrast, the microscopic life that dominated the seas in the Archean and Proterozoic eons are only occasionally preserved in older strata that has endured repeated tectonic, diagenetic, and metamorphic processes. While bacteria display great variance in their metabolic activities and, therefore, have significant effects on biogeochemical processes in an array of environments (e.g. Jones and Starkey, 1957; Harrison and Thode, 1958; Kaplan and Rittenberg, 1964), they show remarkably little variation in cell morphology. Thus, even in the few cases of excellent preservation where fossilization on the cellular level has occurred (Xiao et al., 1998), it is difficult to unambiguously match microbial fossils with species and thus, metabolisms. The study of organic biomarkers however, offers a unique opportunity to identify the presence of specific microorganisms that were dominant contributors to organic matter preserved in Proterozoic rocks.

An examination of biomarkers from the Proterozoic Vazante Group, which contains several intervals of organic-rich black shale (interleaved with likely glacial

deposits) ideal for biomarker extraction and analysis, provides for systematic stratigraphic tests of the co-evolution of life and environment. A previous study of the Mocambo, an organic-rich shale containing dropstones in the Serra do Poço Verde Formation, identified biomarkers indicative of a complex microbial community consisting of photoautotrophs and heterotrophs, anaerobic and aerobic bacteria, and eukaryotes (Olcott et al., 2005). The specific microorganisms identified in this study would have thrived in a redox stratified water column where euxinic conditions extend into the photic zone, and ice-cover, if it was present at all, was thin enough to allow sunlight to penetrate into the underlying water column. However, another study, which analyzed biomarkers from the Lapa Formation, found inconsistencies in biomarker ratios as well as bimodal *n*-alkane distributions that may indicate input from non-syngenetic hydrocarbon sources (Brody, 2007). This finding is significant because in order for biomarkers to provide any information regarding life and environment in the Proterozoic, they must be shown to be derived from authigenic organic matter (i.e. they must be syngenetic to the host rock). Neither of the aforementioned studies however, have sufficient sample density or distribution to fully address the possibility of non-syngenetic biomarker contaminants; these reports each focused on only a single shale interval preserved in a single core (MAF-42.88 for the Olcott study and MAF-134.86 for the Brody study; Figure 1.6).

In contrast, the present study is the first to sample all three organic-rich shale intervals from a basin-wide distribution of cores (Figure 1.6). This extensive data set not only permits an assessment of variations in biomarker distributions through time associated with the wax and wane of ice ages, but it also allows for comparison of

biomarker distributions in contemporaneous near shore and offshore settings from the Vazante Basin. Furthermore, through the course of this study multiple sample handling and extraction techniques were evaluated and used to isolate biomarkers from the Vazante Group (Brody, 2007; Sherman et al., 2007; Waldbauer et al., 2009; Hallmann et al., 2010). The close comparison of techniques allows for the assessment of possible non-syngenetic biomarkers contaminants, either introduced to the Vazante rocks prior to sampling or by laboratory procedures. If the biomarkers are shown to be syngenetic then they can provide information about the specific organisms and environmental conditions before and after widespread glaciation. However, if the biomarkers are determined to contain non-syngenetic inputs, such as those introduced by migrating hydrocarbon-bearing fluids, then this would have major implications for any conclusions drawn from previous biomarker studies of the Vazante Group.

3.2: Organization

In this chapter, I present the results of four discrete biomarker studies of the Vazante Group. The purpose of each is the same: i) to identify the samples most likely to contain syngenetic organic matter, ii) to use biomarker analysis to describe the biologic and environmental conditions that were present when Vazante Group sediments were deposited, and iii) to compare biomarker distributions from the Serra do Garrote, Serra do Poço Verde and Lapa formations in order to assess how biologic conditions and water column chemistry evolved through time, and with respect to large-scale environmental changes. However, the techniques used to differ with each study. This is due to the fact that questions that arise from the results of one study were used to inform the procedure

used for the next. Therefore, the studies are presented and discussed in chronological order.

3.3: Sample selection

Samples were collected from 11 unmineralized exploratory drill cores in 2007 from the Companhia Mineira de Metais in Minas Gerais, Brazil with the assistance of head geologist Tolentino Flavio de Oliveira and collaborator Aroldo Misi. The cores are laterally distributed over more than 150 km of the Vazante basin and represent a N-S of transect of the basin margin (Figure 1.6). A total of 50 samples were collected for biomarker analysis from the Serra do Garrote, Serra do Poço Verde and Lapa formations. The specific samples were chosen based on the absence of obvious mineralization, veining, and obvious sulfide oxidation on the surface of the sample. Samples collected for biomarker analysis were wrapped in annealed aluminum foil before being placed in plastic bags to limit contamination. Sample lithologies and bulk characteristics are listed in Table 3.1.

Of the original group of 50 samples collected for this biomarker study only those thought to contain enough extractable organic matter (EOM) for biomarker analyses were initially chosen for further study. Extractable organic matter consists of bitumen and any soluble organic matter that can be freed from kerogen with organic solvents. An estimate of the EOM abundance for each sample was based on a comparison of TOC contents and ROCK EVAL pyrolysis results. TOC was determined for each sample using the methods described in Chapter 2, while ROCK EVAL analyses were performed at the Institute of Geology and Geochemistry of Petroleum and Coal, Aachen University, Germany.

ROCK EVAL pyrolysis is believed to show the hydrocarbon potential of samples. In these measurements one gram of powdered sample was heated from 250°C to 550°C under a controlled temperature program. As the sample is heated to 300°C, unbound hydrocarbons are volatilized and the resulting CO₂ is measured on a flame ionization detector (FID). This peak, called S1, represents the free bitumen present in the sample. As the sample is heated to 550°C the kerogen is thermally cracked and volatilized. CO₂ released from the thermal cracking of kerogen is also measured on the FID; this is the S2 peak. The S2 peak indicates the hydrocarbon generative potential or the amount of organic material indigenous to the sample. The S3 peak is a measurement of the CO₂ that is produced from oxygen-containing functional groups. This is measured on a thermal conductivity detector (TCD). The resulting S1, S2 and S3 peaks for all samples were generally low, which suggests that the amount of EOM per sample was also low. Any sample with low TOC (<0.5 %) and no measurable S1 peak was removed from the sample set and archived, reducing the original sample set to a total of 41.

Table 3.1: Sample descriptions and bulk characteristics of all samples collected for this biomarker study. *Samples that were initially removed from the study due to low estimated EOM. †Low EOM samples which were included in Study 4.

Formation or Member	Core	Depth	Sample Description	TOC (%)	Sulfur (%)	$\delta^{13}\text{C}_{\text{org}}$	$\delta^{34}\text{S}$	S1 (mg/g rock)	S2 (mg/g rock)	S3 (mg/g rock)
Lapa	PPF-04	257.62	Fissile black shale, sphalerite	1.7	2.1	-25.5	23.7	0.260	0.000	0.460
Lapa	PPF-04	258.78	Fissile black shale	1.4	2.1	-24.8	23.7	0.140	0.010	0.270
Lapa	PPF-04	263.75	Fissile black shale, sphalerite	1.8	1.7	-25.0	22.2	0.255	0.000	0.400
Lapa	PPF-04	273.65	Massive black shale	2.6	1.2	-27.1	22.4	0.130	0.000	0.285
Lapa	PPF-04	277.84	Finely laminated dark grey marl	1.8	1.1	-27.7	22.2	0.180	0.010	0.390
Lapa	PPF-04	283.27	Finely laminated dark grey marl	0.9	1.4	-26.1	24.4	0.175	0.000	0.470
Lapa	*†MAF-45	191.1	Pyritic black shale	0.6	0.6	-26.1	18.4	0.000	0.000	0.000
Lapa	*†MAF-45	197.4	Massive black shale	0.5	0.2	-26.7	17.0	0.000	0.000	0.410
Lapa	MAF-45	204.57	Finely laminated dark grey marl	0.7	0.6	-26.4	17.8	0.015	0.000	0.060
Lapa	B3LF-11	459.7	Finely laminated dark grey marl, iron oxides	0.6	0.5	-22.9	26.8	0.010	0.000	0.045
Lapa	B3LF-11	517.1	Black mudstone, recrystallized	1.9	1.8	-23.0	26.1	0.055	0.000	0.110
Lapa	B3LF-11	527.24	Finely laminated dark grey marl	2.0	1.7	-23.0	26.0	0.025	0.000	0.105
Lapa	B3LF-11	536.76	Massive black mudstone	0.0	3.0	---	25.0	0.090	0.000	0.000
Lapa	B3LF-11	568.82	Finely laminated dark grey marl	2.6	1.3	-26.8	24.0	0.140	0.000	0.150
Lapa	B3LF-11	636.62	Fissile black shale	2.9	1.7	-25.9	20.1	0.120	0.000	0.140
Lapa	B3LF-11	690.14	Finely laminated dark grey marl	2.2	1.6	-23.2	21.2	0.140	0.000	0.175

Formation or Member	Core	Depth	Sample Description	TOC (%)	Sulfur (%)	$\delta^{13}\text{C}_{\text{org}}$	$\delta^{34}\text{S}$	S1 (mg/g rock)	S2 (mg/g rock)	S3 (mg/g rock)
Lapa	B3LF-11	730.15	Finely laminated medium grey marl, pyrobitumen	0.2	0.0	-26.5	---	0.010	0.000	0.020
Mocambo	PAF-32	66.4	Fissile black shale	1.8	0.9	-30.2	15.8	0.295	0.000	0.555
Mocambo	PAF-32	70.7	Fissile black shale	0.5	1.2	-28.3	11.8	0.120	0.010	0.230
Mocambo	PAF-32	76.35	Fissile black shale	0.6	1.1	-29.3	17.3	0.020	0.000	0.000
Mocambo	*PAF-32	89.65	Weathered fissile grey shale	0.5	0.9	-27.0	16.6	0.000	0.000	0.640
Mocambo	PAF-32	100.8	Fissile black shale	1.5	0.7	-27.5	13.2	0.080	0.000	0.000
Mocambo	PPF-2A	216.2	Massive black mudstone	1.0	0.6	-28.6	20.1	0.050	0.000	0.205
Mocambo	PPF-2A	226.4	Massive black mudstone	1.2	0.5	-20.5	22.4	0.010	0.000	0.425
Mocambo	†PPF-2A	227.25	Massive black mudstone	1.2	1.2	-26.2	21.4	0.115	0.000	0.170
Mocambo	PPF-08	432.05	Black shale	1.2	1.1	-26.2	22.9	0.040	0.000	0.325
Mocambo	PPF-08	432.7	Fissile black shale	1.1	1.6	-24.6	23.5	0.095	0.000	0.120
Mocambo	PPF-08	443.45	Fissile black shale	1.3	1.5	-25.0	24.6	0.055	0.000	0.000
Mocambo	PPF-08	450.99	Fissile black shale	1.0	1.4	-24.2	24.5	0.330	0.010	0.720
Mocambo	MAF-28	219.05	Massive black mudstone	1.6	1.9	-25.7	21.8	0.010	0.000	0.125
Mocambo	MAF-28	225.5	Massive black mudstone	2.4	3.0	-25.9	19.5	0.020	0.000	0.150
Mocambo	MAF-28	231.55	Black shale	1.3	2.9	-25.7	21.6	0.015	0.000	0.000
Mocambo	†MAF-45	239.12	Massive, pyritic black mudstone	0.7	0.1	-27.8	---	0.000	0.000	0.280
Mocambo	MAF-42.88	802.32	Black shale	0.7	1.7	-25.5	24.8	0.010	0.000	0.135
Mocambo	MAF-42.88	802.86	Black shale	1.5	2.0	-25.3	25.4	0.160	0.005	0.450
Mocambo	MAF-42.88	808.32	Black shale	1.9	0.4	-25.7	22.3	0.030	0.000	0.435
Mocambo	†MAF-42.88	811.75	Pyritic black shale	3.2	0.8	-26.2	20.5	0.090	0.000	0.430
Mocambo	†MAF-42.88	818	Massive dark grey carbonate	---	---	---	---	---	---	---

Formation or Member	Core	Depth	Sample Description	TOC (%)	Sulfur (%)	$\delta^{13}\text{C}_{\text{org}}$	$\delta^{34}\text{S}$	S1 (mg/g rock)	S2 (mg/g rock)	S3 (mg/g rock)
Mocambo	*†MAF-009	474.75	Pyritic black shale	0.5	1.0	-25.8	23.5	0.000	0.000	0.000
Mocambo	MAF-009	475.5	Black shale	2.0	1.6	-24.5	22.6	0.010	0.000	0.130
Mocambo	*†MAF-009	476.85	Black shale	0.6	2.6	-25.5	23.8	0.000	0.000	0.000
Mocambo	MAF-009	479	Black shale	3.2	1.1	-22.1	19.6	0.005	0.000	0.265
Mocambo	MAF-011	847.85	Massive black mudstone	1.3	1.4	-23.5	25.1	0.020	0.000	0.165
Mocambo	MAF-011	850.9	Massive black mudstone	1.2	1.8	-24.6	---	0.030	0.000	0.570
Retiro	*MAF-42.88	868.85	Massive light grey carbonate	0.0	0.1	-24.2	---	0.020	0.000	0.225
Retiro	*†MAF-011	844.1	Massive dark grey carbonate, stromatolitic	0.5	0.3	-25.5	17.1	0.000	0.000	0.160
Retiro	*†MAF-011	845.45	Finely laminated dark grey carbonate, stromatiolitic	0.8	0.0	-24.9	18.4	0.020	0.000	0.345
Garrote	†B4L.S01	138.2	Massive dark grey mudstone	1.4	3.1	-29.8	7.7	0.030	0.000	0.345
Garrote	†B4L.S01	164.1	Massive black mudstone	3.4	2.0	-29.6	12.3	0.125	0.000	0.470
Garrote	†B4L.S01	207.8	Massive dark grey mudstone	1.5	0.8	-29.0	12.4	0.160	0.000	0.300
Garrote	B4L.S01	225.4	Massive dark grey mudstone	1.4	0.4	-29.4	11.9	0.075	0.000	0.200
Garrote	B4L.S01	237.1	Massive dark grey mudstone	1.4	1.2	-30.2	11.6	0.035	0.000	0.195

3.4: Study 1 – Sonication vs. ASE extractions

This study compares biomarker distributions from two different methods of organic matter extraction in order to determine the benefits and drawbacks of each. Eleven samples from the Mocambo shale and one procedural blank were manually extracted using a sonication method and then the same samples were re-extracted using an automated Accelerated Solvent Extractor (ASE). These samples were chosen because they have the highest TOC compositions of the Mocambo samples and were therefore thought to be the most promising samples for biomarker analysis.

3.4.1: Methods

To avoid laboratory contamination, all solvents used during sample processing and extraction were of the highest grade possible (HPLC grade). Glassware was washed with soap and water, annealed at 450°C for 6-8 hrs, and then rinsed three times with dichloromethane (DCM) immediately prior to use. Quartz sand was annealed at 850°C for 8 hours. All other materials such as Al foil and glass wool were annealed at 450°C for 6-8 hours prior to use. Immediately prior to use, all laboratory equipment was rinsed three times with DCM. One procedural blank, consisting of ~100 g of Si gel (63-200 mesh), was processed for every 10 samples. The Si gel was cleaned three times by sonication in organic solvents DCM:Methanol (DCM:MeOH; 9:1) for 20 minutes each and then annealed at 200°C for 8 hours.

Between 63-184 g of sample were prepared for biomarker extraction in the Stable Isotope Laboratory at the University of Maryland. The samples were first rinsed with DI water to remove any obvious dirt. Then the outer ¼ cm of each sample was ground off

using a Struers grinding apparatus in order to remove surface contaminants. Large core samples were then cut into smaller pieces using a diamond edged rock saw and these were broken into ½ cm sized pieces using a stainless steel mortar and pestle that was extensively cleaned with soap and water, DCM and annealed sand prior to use. The sample chips were then cleaned three times by sonication in ultrapure Milli-Q water for 15 minutes followed by a Milli-Q rinse under vacuum. After cleaning, the samples were loosely covered and left in the fume hood overnight to dry. Once dry the sample chips were rinsed 3x with DCM, dried, and then powdered using a shatterbox equipped with an alumina lined mill and puck. The mill and puck were cleaned with soap and water, DCM and annealed sand between each sample run, however, it is important to note that separation between the base and side wall of the mill left a gap that could not be thoroughly cleaned.

Once the samples were cleaned and powdered, they were ready for the bitumen extraction process. Two different bulk rock extraction techniques were used including in-house sonication and use of a Dionex 200 ASE housed at either the College of William and Mary's Virginia Institute of Marine Science (VIMS) and the Carnegie Institution of Washington Geophysical Laboratory (CIW).

Sonication extraction – Sample powders were divided into ~25 g aliquots and loaded into 60 ml pyrex beakers. Twenty ml of DCM:MeOH (9:1) were added to each 60 ml beaker and then sonicated in a Branson 2510 sonicator for 30 minutes. The solvent was then decanted into a collection beaker; solvents from each aliquot of the same sample were combined. This process was then repeated two additional times. The extracts were subsequently passed through a wide bore glass column packed with ~3 cm of Si gel in

order to remove any particles that may have been decanted into the collection beaker along with the solvent extract. This step was repeated, using new Si gel, until all particles were removed. The extract was then loosely covered with Al foil and allowed to evaporate under the fume hood to a volume of ~1 ml; special care was taken to make sure that the extracts did not evaporate to complete dryness.

ASE extraction – ASE extraction was performed in two different laboratories under the supervision of Dr. Elizabeth Canuel (VIMS) and Dr. George Cody (CIW). The methods used in each laboratory however, were the same. Pre-extracted sample powders were loaded into stainless steel Dionex extraction cells and loaded onto a Dionex ASE 200. The ASE was programmed to extract the samples at 1000 psi and 100°C. A DCM:MeOH mixture (9:1 ratio) was flushed through the sample to solvate the EOM. Each sample cell was extracted twice to maximize the amount of organic material extracted. The effluent was collected after extraction and concentrated to ~1 ml under a gentle stream of ultra pure N₂ gas or by allowing the solvent to evaporate in a fume hood.

The extracts, both from the sonication and ASE extractions, were purified prior to GCMS analysis in order to facilitate compound identification. DCM-rinsed reduced Cu wires were added to each extract and allowed to react for 2-6 hours in order to remove elemental sulfur. If the Cu wires turned black, indicating the presence of elemental sulfur, then more Cu was added. When a reaction could no longer be observed, the extract was dried down to ~70 µl under a gentle stream of ultra pure N₂ gas. The extract was then transferred, using a 10 µl Hamilton syringe, to an Al dish prepped with ~0.2 g of Si gel. The tray was then loosely covered with Al foil and left overnight in the fume hood to allow the extract to dry onto the Si gel. Once the extract was set, it was

transferred to a glass pipette column packed with 0.6 g of Si gel. Then 1.5 ml of hexane (Hex), 4 ml of DCM:Hex (4:1), and 4 ml of DCM:MeOH (7:3) were sequentially eluted through the column to separate the saturate, aromatic, and polar fractions respectively. The solvent from each fraction was then dried down and replaced with DCM. The internal standard 3-methylheneicosane (100 ng) was added to the saturate fraction to aid in the quantification of the *n*-alkane and isoprenoid compounds and *p*-terphenyl-d₁₄ (100 ng) was added to the aromatic fraction to help quantify aromatic compounds.

Gas Chromatography Mass Spectrometry (GCMS) was performed on the saturate and aromatic fractions of the Vazante sample extracts using an Agilent 6890N gas chromatograph coupled to an Agilent 5973 Mass Selective detector located in Dr. George Cody's laboratory at CIW. The samples were injected in splitless mode with He as the carrier gas. The GC oven was programmed to hold at 60°C for 2 minutes, heat to 140°C at 10°/min and then heat from 140° to 300°C at 3°C/min with a final hold time of 24 minutes resulting in a total run time of 87 minutes per sample. The GC was fitted with a 60 m HP-5ms fused silica capillary column. The source was operated in EI-mode with an ionization energy of 70 eV. Samples were run in both full scan and selected ion monitoring (SIM) modes. The full scan analyses scanned a mass range of 50-600 m/z whereas SIM analyses scanned only the masses identified in Table 3.2. The resulting chromatograms were processed using HP Chemstation software. Compound peaks were identified based on comparison of retention times with a *n*-alkane standard and published mass spectra. Peak areas of each compound were manually integrated and quantified using the following equation:

$$\text{amount compound} = \frac{(\text{area compound})(\text{amount std})(\text{response factor})}{\text{area std}}$$

where std is an internal standard and response factor is defined as:

$$response\ factor = \frac{(area\ std)/(amount\ compound)}{(area\ compound)/(amount\ std)}$$

where std is an internal standard in a *n*-alkane mixture with known compound quantities.

Calculation of analytical and peak integration uncertainties were used to assess the precision of the biomarker measurements reported in this dissertation. Analytical uncertainties, which describe the reproducibility of compound peak intensities resulting from GC-MS analyses, were determined by running a sample or standard multiple times and calculating the standard deviation for each resulting compound peak. Peak integration uncertainties, on the other hand, reflect the precision with which peak areas were determined, either by manual integration or automated software integration. Peak areas measured by SIM-GC-MS analyses were manually integrated multiple times and a standard deviation for each compound peak was calculated. Typical analytical and peak integration uncertainties are summarized in Appendix A (Tables A-1 and A-2).

3.4.2: Results

A complex mixture of compounds including normal and branched alkanes, acyclic isoprenoids, hopanes, and steranes were identified in all sample extracts. Normal alkanes and the isoprenoids, pristane (Pr) and phytane (Ph), were the most abundant compounds in both the sonication and ASE extracts (Table 3.3). The total abundance of the *n*-alkanes from the sonication extracts range from 0.01-0.35 ng/g normalized to extracted sample. Additionally, the extracts display either unimodal or bimodal distributions and range in carbon length from C₁₄ to C₃₁ (Figure 3.1). The *n*-alkanes from

the ASE extract similarly display both unimodal and bimodal distributions (Figure 3.1). However, the *n*-alkanes in the ASE extracts are more abundant (0.12-4.9 ng/g) than in the sonication extracts and range in carbon length from C₁₄ to C₃₆. Pr and Ph concentrations in the ASE extracts are also greater than those measured in the sonication extracts (Table 3.3).

Hopanes were detected in both the sonication and ASE extracts; however, due to differences in biomarker yields, the abundance and range of hopanes varied between the two techniques. While absolute abundances of hopanes and steranes could not be calculated (due to a lack of a structurally comparable internal standard) the hopane peak areas in the ASE extracts are at least 20x larger than hopane peak areas measured from the sonication extracts from the same samples (Figure 3.2). Hopanes identified in the ASE extracts represent the full range of C₂₇-C₃₅ regular and rearranged varieties. Hopanes identified in the sonication extracts, on the other hand, do not display the full range of hopanes in all samples; the extended hopanes could not be discerned in five samples (PPF-2A-216.2, PPF-08-432.4, MAF-28-219.05, MAF-009-479, and MAF-011-847.85). Additionally, one sample (PAF-32-66.4) displayed no measurable hopanes.

The ASE extracts however, also contained a homologous series of non-hydrocarbon peaks, identified as polysiloxanes (henceforth called siloxanes), which co-eluted with several key hopanes on the m/z 191 SIM trace (Figure 3.3). Siloxanes are chains of alternating Si and O atoms that are common additives in plastics, synthetic rubber, cosmetics, lotions, adhesives, and more (Tomanek, 1990). They also make up the stationary phase of the GC column and could be the result of column degradation (Cody, pers. Comm.). These siloxanes were not detected in m/z 191 SIM trace from the

sonication extracts. In order to test if the siloxanes were introduced via the ASE, annealed sand blanks were also ASE extracted. These sand extracts, as well as several solvent rinses of the materials involved in both the ASE and sonication extractions, were analyzed using GCMS. However, no siloxanes or other biomarker compounds were identified in any of these runs.

Similar to the hopanes, sterane peak areas measured from ASE extracts were at least 20x larger than sterane peak areas measured from the sonication extracts (Figure 3.4). Additionally, steranes were not detected in the sonication extract for sample PAF-32-66.4. However, where present, the sonication and ASE extracts have the same range of C₂₇-C₂₉ regular and rearranged steranes.

3.4.3: Discussion

A comparison of *n*-alkane distributions and biomarker ratios calculated from the sonication and ASE extracts show that, while there are some differences, the biomarker distributions that result from these two extraction techniques are similar. Normal alkane distributions are alike, in that samples with bimodal distributions in the sonication extracts also have bimodal distributions in the ASE extracts; the same is true for samples with unimodal distributions (Figure 3.1). Additionally, the ratio Pr/Ph from the sonication extracts have nearly a 1:1 correlation ($m=0.87$) with the Pr/Ph ratio calculated from the ASE extracts (Figure 3.5a). The ratios of Pr/*n*-C₁₇ and Ph/*n*-C₁₈ from the two extraction techniques however, show a higher amount of the isoprenoids relative to *n*-alkanes in the sonication extract than in the ASE extract ($m=0.41$ and 0.67 respectively; Figure 3.5b,c). This may suggest that the sonication and ASE extractions have different

efficiencies for extracting isoprenoids vs. *n*-alkanes. However, it is more likely that the ratios are affected by a measurement error introduced when integrating the low yields from the sonication extracts.

Hopane and sterane ratios calculated from the ASE and sonication extracts also appear to correlate. A comparison of 17 hopane ratios from the ASE extracts with hopane ratios from the sonication extracts show a positive correlation ($m=1.15$; Figure 3.6a). However, some hopanes involved in calculating these ratios are affected by the co-elution of siloxanes. To correct for this, the ASE extracts were re-analyzed using a modified GC temperature regime (60°C for 2 minutes, heat to 140°C at 10°/min, heat from 140° to 300°C at 4°C/min, and hold for 10 minutes for a total run time of 60 minutes) that shifted the residence time of the siloxanes with respect to the hopanes. The resulting corrected hopane ratios (*) from the ASE extracts have a 1:1 correlation ($m=0.95$) with the hopane ratios from the sonication extracts (Figure 3.6b). A comparison of 22 sterane ratios on the other hand, shows higher values from the ASE extracts than from the sonication extracts ($m=0.73$; Figure 3.7). Again, this could be interpreted to mean differential extraction efficiencies for select steranes within each extract; however, it is more likely due to bias in integrating the low yields of the sonication extract.

3.4.4: Conclusions

The question of which extraction technique should be used for the remaining samples from the Vazante Group comes down to which extracts results in measurable biomarker yields without introducing non-syngenetic compounds. ASE extraction

resulted in at least 20x higher biomarker yields, however, non-syngenetic siloxanes were also present on the m/z 191 SIM trace. ASE extracts of sand blanks however, do not contain detectable siloxanes, thus suggesting that the ASE is not the source of the siloxanes. Additionally, the lack of siloxanes in the sonication extracts could be because they are below detection in these low yield extracts rather than that they are indeed absent. Therefore, although the source of the siloxanes cannot be determined at this time, it appears that it is not related to the extraction process. This, along with the higher yields and the fact that biomarker ratios can be calculated despite the presence of siloxanes lead me to decide that ASE extraction is the superior method to use for the remaining Vazante Group samples. The biological and environmental interpretations of the ASE extracted samples will therefore be discussed in the next study.

Table 3.2: Ions monitored in SIM (selected ion monitoring) mode for the saturate and aromatic fractions.

	m/z	Compounds monitored
Saturates	85	<i>n</i> -alkanes
	191	Hopanes, A and B rings
	205	Hopanes, D and E rings
	217	Steranes
	218	Steranes, $\beta\beta$ conformation
	259	Diasteranes
	Aromatics	133
231		Triaromatic steranes
253		Monoaromatic steranes

Table 3.3: Abundances of total *n*-alkanes and pristine (Pr) and phytane (Ph) from sonication extracted and ASE extracted samples.

Abundances are reported as ng/g of extracted sample.

Formation or Member	Core	Depth (m)	Sonication Extraction				ASE Extraction			
			Mass (g)	Total <i>n</i> -Alkanes (ng/g)	Pr (ng/g)	Ph (ng/g)	Mass (g)	<i>n</i> -Alkanes (ng/g)	Pr (ng/g)	Ph (ng/g)
Mocambo	PAF-32	66.4	110.61	0.03	0.001	0.002	107.00	0.12	0.001	0.002
Mocambo	PAF-32	70.7	91.95	0.35	0.027	0.040	90.82	2.6	0.160	0.276
Mocambo	PPF-2A	216.2	120.88	0.01	0.000	0.000	116.60	0.32	0.001	0.004
Mocambo	PPF-08	432.05	123.55	0.02	0.000	0.000	121.80	0.35	0.002	0.007
Mocambo	MAF-28	219.05	167.35	0.02	0.001	0.001	163.57	0.28	0.004	0.009
Mocambo	MAF-28	225.5	156.15	0.12	0.001	0.001	151.98	0.35	0.004	0.009
Mocambo	MAF-42.88	802.32	184.95	0.11	0.003	0.003	166.33	1.2	0.016	0.022
Mocambo	MAF-42.88	811.75	162.47	0.11	0.012	0.012	150.65	4.9	0.157	0.203
Mocambo	MAF-009	475.5	164.71	0.06	0.001	0.001	149.77	0.32	0.016	0.013
Mocambo	MAF-009	479	186.55	0.01	0.001	0.001	168.09	0.61	0.020	0.018
Mocambo	MAF-011	847.85	92.43	0.01	0.001	0.001	87.63	0.17	0.006	0.008
Mocambo	MAF-011	850.9	116.13	0.04	0.003	0.005	106.90	0.40	0.033	0.076

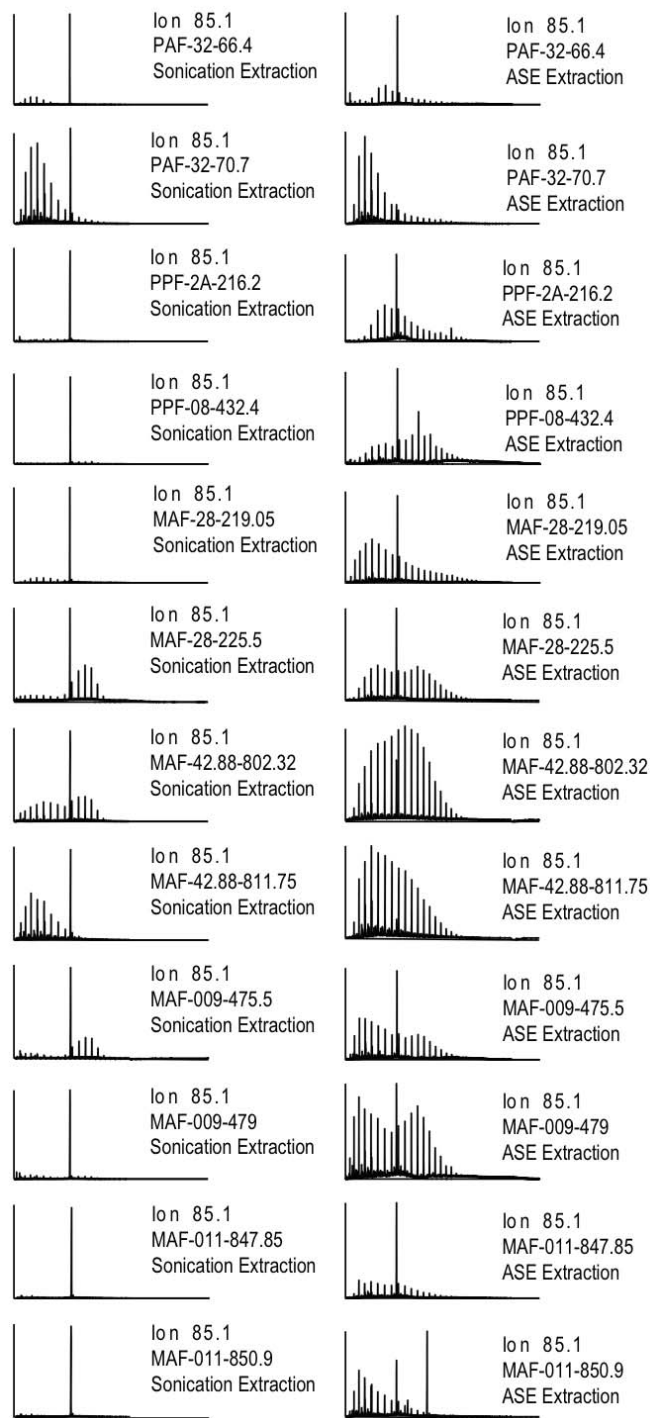


Figure 3.1: Selected ion chromatograms (m/z 85) showing the n -alkane distributions for samples extracted by sonication and ASE. The large peak central in each trace is a 3-methylhenicosane internal standard (100 ng). The x-axis is residence time and the y-axis is peak intensity.

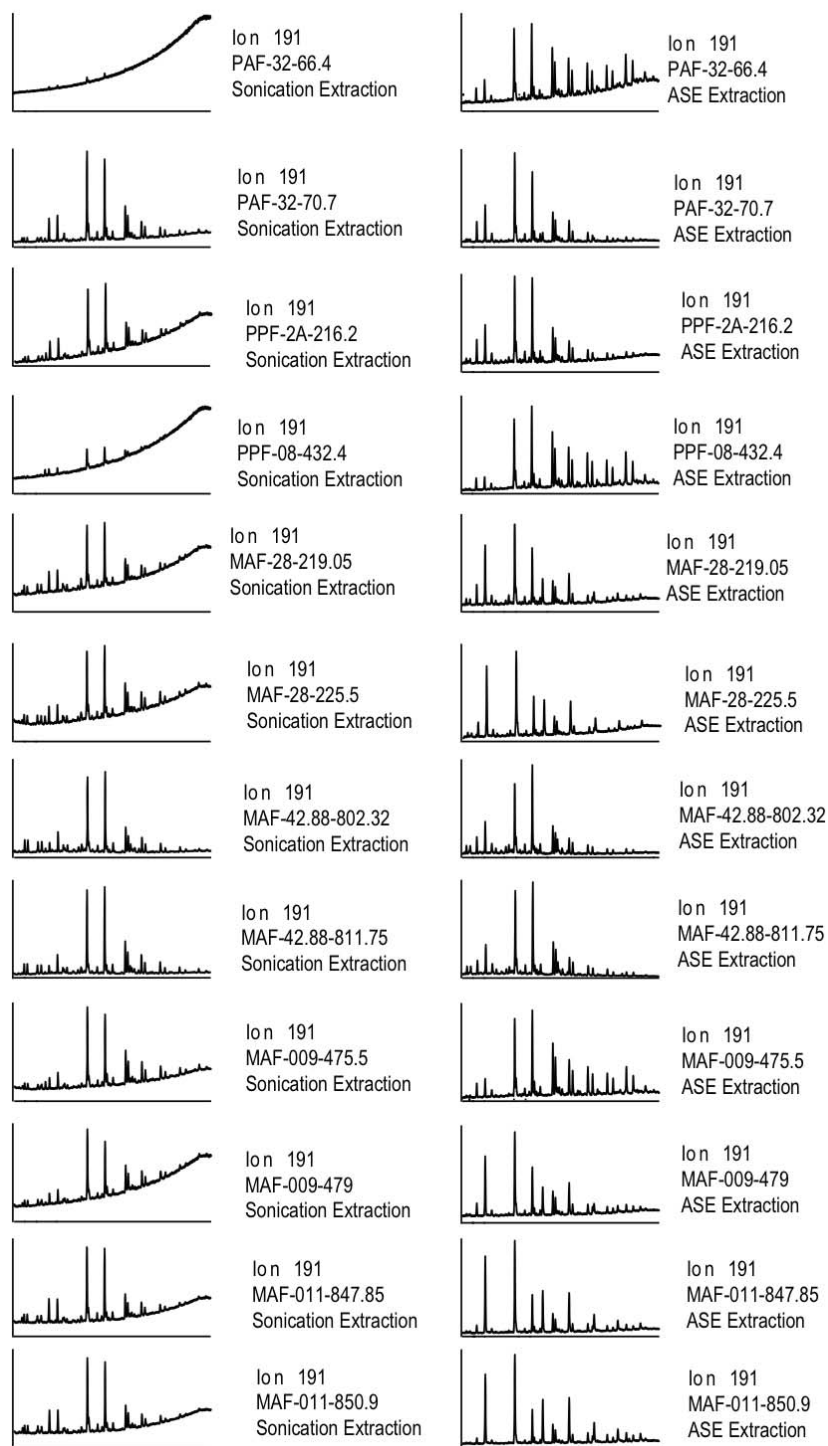


Figure 3.2: Selected ion chromatograms (m/z 191) showing the hopane distributions for samples extracted by sonication and ASE. The x-axis is residence time and the y-axis is peak intensity.

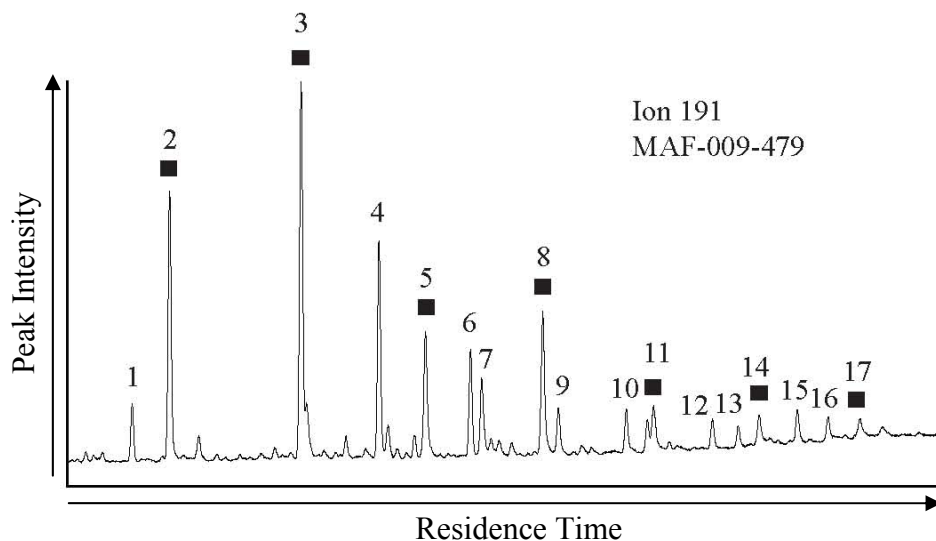


Figure 3.3: Selected ion chromatogram (m/z 191) showing hopane and siloxanes in the ASE extract. The black boxes identify a siloxane peak. 1=Ts, 2=Tm+Siloxane, 3= $\alpha\beta$ C₂₉H+Siloxane, 4= $\alpha\beta$ C₃₀H, 5=Siloxane, 6= $\alpha\beta$ C₃₁S, 7= $\alpha\beta$ C₃₁R, 8= $\alpha\beta$ C₃₂S+Siloxane, 9= $\alpha\beta$ C₃₂R, 10= $\alpha\beta$ C₃₃S, 11= $\alpha\beta$ C₃₃R+Siloxane, 12= $\alpha\beta$ C₃₄S, 13= $\alpha\beta$ C₃₄R, 14=Siloxane, 15= $\alpha\beta$ C₃₅S, 16= $\alpha\beta$ C₃₅R, and 17=Siloxane.

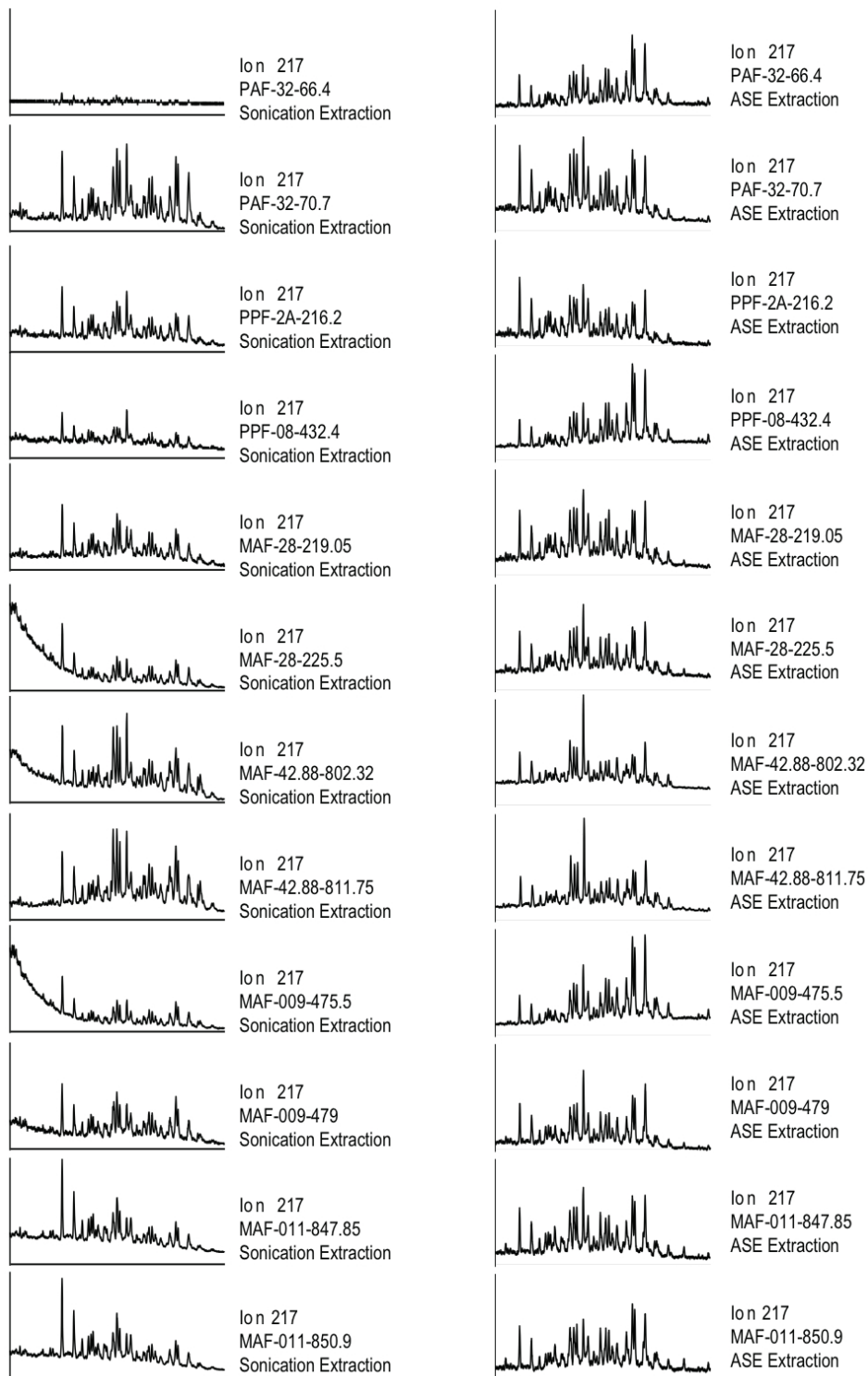


Figure 3.4: Selected ion chromatogram (m/z 217) showing steranes from the sonication and ASE extracts. The x-axis is residence time and the y-axis is peak intensity.

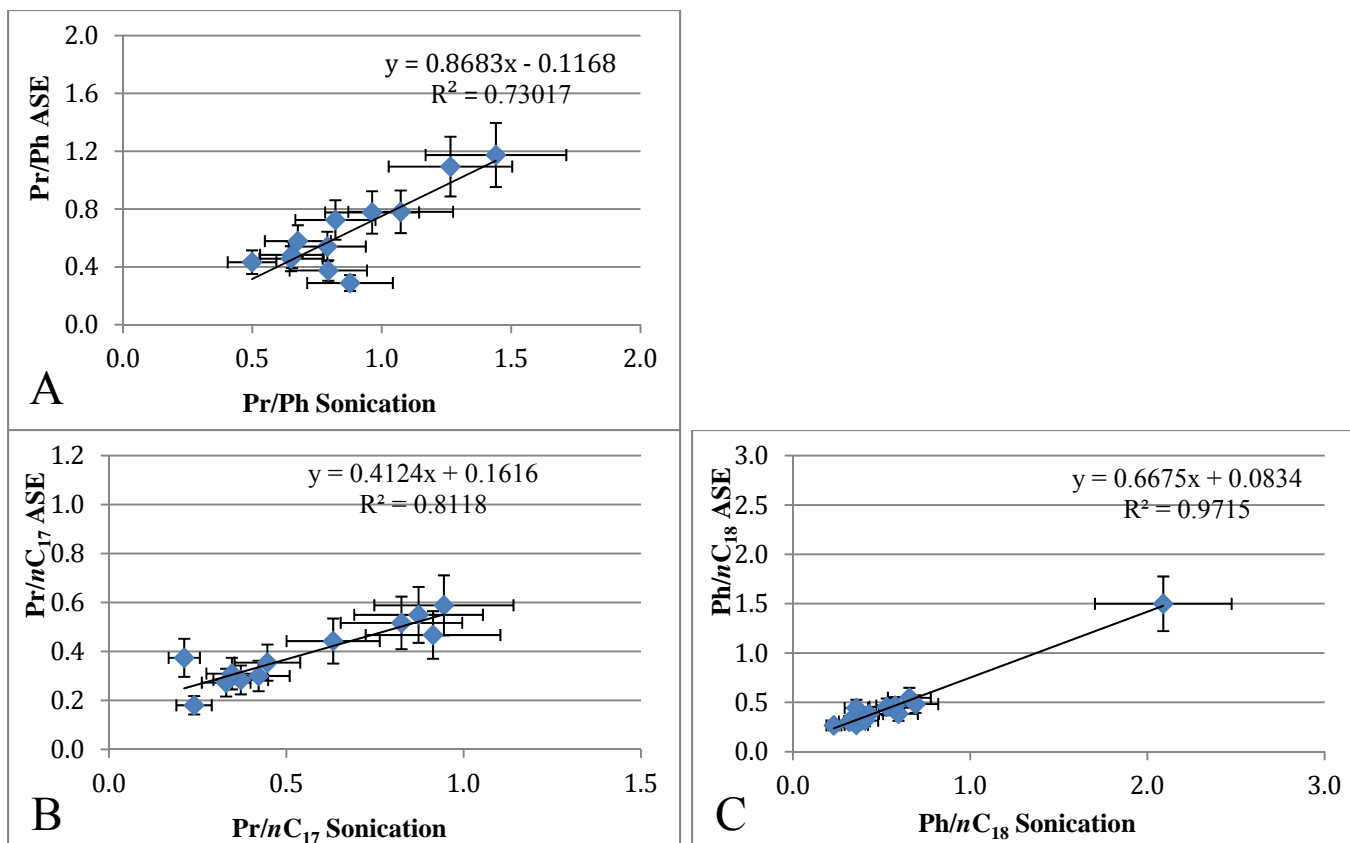


Figure 3.5: Cross-plots of *n*-alkane and Pr and Ph ratios show the relationship between sonication and ASE extracts. A) A plot of Pr/Ph calculated from the sonication and ASE extracts have close to a 1:1 relationship. Plots of Pr/*n*C₁₇ (B) and Ph/*n*C₁₈ show preferential extraction of Pr and Ph relative to *n*-alkanes in the sonication extract. Uncertainties are 1 σ .

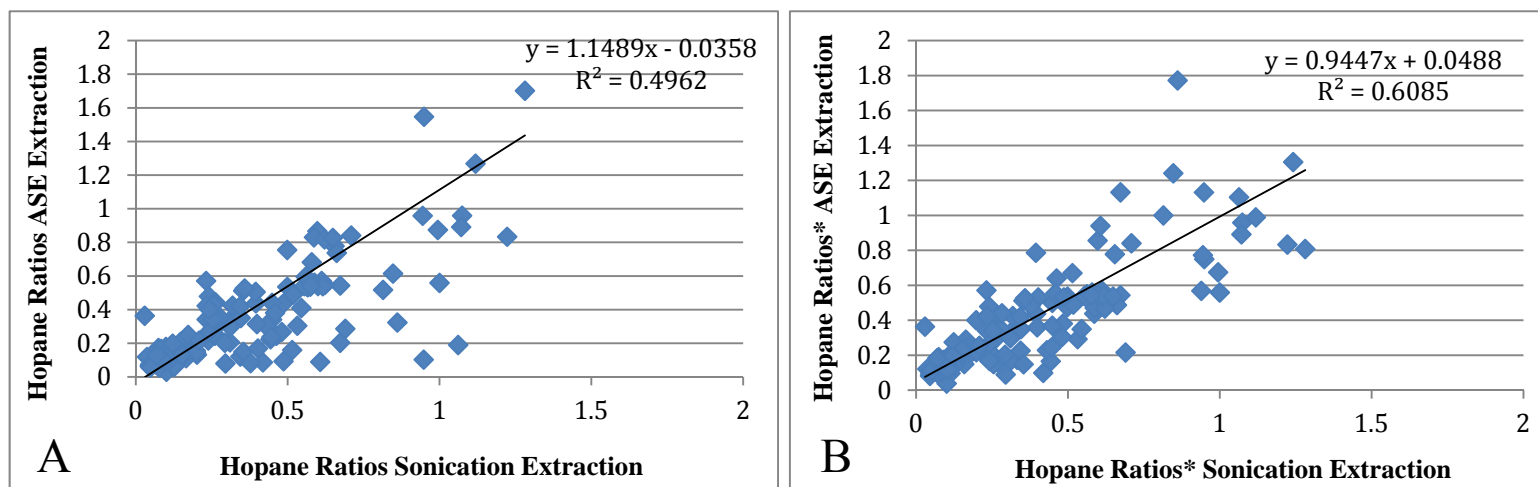


Figure 3.6: A) Cross-plots of all hopane ratios calculated from the sonication extract vs ASE extract. B) Cross-plot of all hopane ratios corrected for siloxanes from the sonication and ASE extracts. Hopane ratios corrected for siloxanes in the ASE extract have a 1:1 relationship with the hopane ratios calculated from the sonication extract.

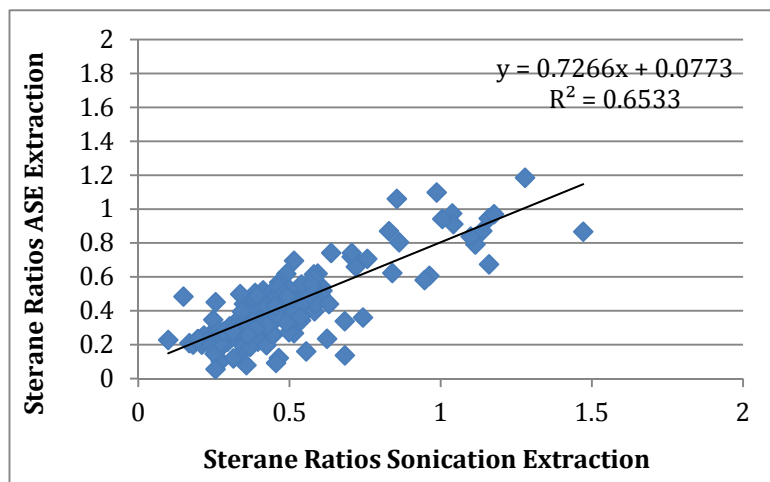


Figure 3.7: Cross-plot of all sterane ratios calculated from the sonication and ASE extracts.

3.4: Study 2 – Biomarker from the Serra do Garrote, Serra do Poço Verde and Lapa formations

This study examines biomarker distributions from the Serra do Garrote, Serra do Poço Verde and Lapa formations. The purpose of this work is to use biomarkers, analyzed by GCMS and Compound Specific Isotopic Analysis (CSIA) to characterize the biological conditions and environmental setting that contributed to the preservation of organic matter in the Vazante Group. However, GCMS analysis, which is not capable of fully resolving all biomarkers, is used as a powerful but survey method of the biomarkers within the Vazante samples. Therefore, another aim of this study is to use this initial assessment of biomarkers to identify samples most likely to contain only syngenetic organic matter, so that these samples can be subjected to higher-resolution quantitative biomarker analyses (i.e. metastable reaction monitoring GC-MS).

3.4.1: Sample selection

The samples chosen for this study consist of the 41 samples that were previously identified as acceptable candidates for biomarker analysis based on TOC composition and ROCK EVAL pyrolysis results. These samples include five Serra do Garrote samples from one core (B3LS-01), 21 Serra do Poço Verde samples from seven cores (PAF-32, PPF-2A, PPF-08, MAF-28, MAF-42.88, MAF-009, and MAF-011), and 15 Lapa samples from three cores (PPF-04, MAF-45, and B3LF-11). The Serra do Garrote was sampled in only one core. The Serra do Poço Verde Formation represents the most comprehensive sample set, although, all the samples are from the Mocambo shale; no samples from the Retiro Member were included in this study because they have low TOC

(<0.5 %) and no measurable S1 peak determined by ROCK EVAL pyrolysis. It is important to note that the samples from core MAF-42.88 were taken from the same core and the same depth interval as the samples in the Olcott et al. (2005) study. Additionally, core MAF-011 is the only core sampled that was drilled in the western region of the Vazante Basin. The western region represents the distal portion of the basin and, therefore, deeper water conditions; however, the western edge of the basin has also experienced higher temperatures (amphibolite-granulite facies; Dardenne, 1978; Fuck et al., 1994) associated with Brasiliano orogenesis. The Lapa Formation samples were collected from three cores. One sample from core B3LF-11, at a depth of 730.15 m, was collected from a zone that contained pyrobitumen-filled fractures. This sample was included in the data set as a baseline to see if there was vertical migration of the pyrobitumen (solidified oil) up the core.

3.4.2: Methods

All samples and procedural blanks were processed using the methods described for Study 1. Samples were ASE extracted and analyzed using GCMS in Dr. George Cody's laboratory at CIW. The GCMS runs were conducted under the same conditions described in Study 1 along with a second SIM analysis of m/z 191 using the modified GC oven conditions (60°C for 2 minutes, heat to 140°C at 10°/min, heat from 140° to 300°C at 4°C/min, and hold for 10 minutes for a total run time of 60 minutes) to correct for co-elution with siloxanes.

Additionally, compound specific isotope analysis (CSIA) was performed on the saturate fraction of the extracts in order to measure the carbon isotopic composition of

individual compounds. CSIA was performed using a HP 6890 gas chromatograph interfaced with a combustion furnace coupled to a GV IsoPrime continuous flow mass spectrometer located in the Stable Isotope Laboratory at UMD. The samples were manually injected in splitless mode with He as the carrier gas. The GC oven was programmed to hold at 50°C for 2 minutes, then heat to 300°C at 5°C /min and hold at 300°C for 25 minutes resulting in a total run time of 77 minutes per sample. The GC was fitted with a 60 m HP-5ms fused silica capillary column. The combustion furnace, which interfaces with the GC and MS, consists of a quartz furnace tube packed with Ag wool and oxidized Cu wires that is held at 850°C. The MS was operated in EI-mode with an ionization energy of 70 eV and a 600 mV trap current. The data were processed using IonVantage software and the resulting isotopic values were reported in δ notation as parts per mil (‰) relative to the Pee Dee Belemnite (V-PDB) standard. Analytical uncertainties were determined by multiple analyses of an *n*-alkane standard and were typically better than $\pm 0.4\text{‰}$ (1σ). Uncertainties of sample replicates were typically better than $\pm 0.5\text{‰}$ (1σ).

3.4.3: Results

Normal and branched alkanes, isoprenoids, hopanes, and steranes were identified in samples from the three studied Vazante Group shales. Structural identifications as well as CSIA results for each formation are presented here.

Procedural blanks – A total of four procedural blanks were analyzed along with these samples. The procedural blanks contain an abundance non-biomarker compounds consisting mainly of siloxanes and branched alkanes (Figure 3.8). Furthermore, while Pr

and Ph were not identified in the procedural blanks, trace amounts of hopanes and steranes were present. These were only slightly less abundant than found in the samples (sample peaks were on average ~1.5x larger). Additionally, the hopanes and steranes identified in these blanks have similar biomarker ratios (Tables 3.4; 3.5) as seen in the samples and therefore have similar biomarker distributions. DCM rinses of materials used during sample processing and extraction showed no trace of these contaminants.

Alkanes and Isoprenoids – Normal alkanes, measured on $m/z=85$ SIM

chromatograms, were the most abundant compounds found in the study collection. Total abundances for the *n*-alkanes range from 0.10-0.58, 0.04-4.9, and 0.15-6.3 ng/g for the Serra do Garrote, Mocambo, and Lapa samples, respectively (Table 3.6). The *n*-alkanes from the Serra do Garrote Formation range in carbon number from C_{15} to C_{34} and display unimodal distributions centering on the C_{17} - C_{20} *n*-alkanes (Figure 3.9). Similarly, the majority of the Mocambo samples ($n=16$), which range in carbon length from C_{13} to C_{39} , have unimodal distributions centering on the C_{16} - C_{20} *n*-alkanes (Figure 3.10). In contrast, five of the Mocambo shales (PPF-08-432.05, MAF-28-225.5, MAF-42.88-802.32 and MAF-009-474.5 and 479.0) display bimodal *n*-alkane distributions. These samples have one *n*-alkane ‘hump’ centering on the C_{16} - C_{20} *n*-alkanes and a second ‘hump’ centering on the C_{25} *n*-alkanes. This bimodal distribution of *n*-alkanes is also observed for six samples from the Lapa Formation (MAF-45-204.57, PPF-04-257.62, 258.78, and 283.27, and B3LF-11-459.7 and 730.15; Figure 3.11). The remaining Lapa samples ($n=9$) have unimodal distributions centering on the C_{15} - C_{18} *n*-alkanes.

In addition to *n*-alkanes, branched alkanes (aka monomethylalkanes or MMAs), and the isoprenoids Pr and Ph were identified on $m/z=85$ SIM chromatograms (Figure

3.12). MMAs elute between *n*-alkanes and are present in the same carbon number range as the most abundant *n*-alkanes. Pr and Ph, which elute just after the C₁₇ and C₁₈ *n*-alkanes, were present in all samples (Table 3.6).

Hopanes – Hopanes, measured on m/z=191 SIM chromatograms, are also present in the Vazante samples. These include both the regular and thermally rearranged forms of the C₂₇ and C₂₉-C₃₅ hopanes (Figure 3.13). The C₂₉ and C₃₀ regular hopanes ($\alpha\beta$ C₂₉H and $\alpha\beta$ C₃₀H) dominate the m/z=191 traces in all samples. In the Serra do Garrote samples $\alpha\beta$ C₃₀H is consistently more prevalent than $\alpha\beta$ C₂₉H (Table 3.4). The same is true for the majority of the Mocambo samples (n=18) with the exception of samples MAF-42.88-802.32 and MAF-011-847.85 and 850.9 where $\alpha\beta$ C₂₉H is more abundant. Unlike the Serra do Garrote and the majority of the Mocambo samples, the Lapa samples do not exhibit a clear predominance of $\alpha\beta$ C₃₀H relative to $\alpha\beta$ C₂₉H; instead, the $\alpha\beta$ C₂₉H and $\alpha\beta$ C₃₀H peak intensities are either equal or there is a slight predominance of the $\alpha\beta$ C₂₉H.

Other hopanes such as the C₃₁-C₃₅ extended hopanes (R and S conformations) and gammeracerane (γ) were also present in the Vazante Group samples. A full range of C₃₁-C₃₅ extended hopanes, which progressively decrease with increasing carbon number, were identified in all of the Serra do Garrote and Mocambo samples and in the majority of the Lapa samples (n=12). The three Lapa samples that do not contain all C₃₁-C₃₅ extended hopanes are all from the same core, including B3LF-11-536.76, 568.82, and 690.14. Gammeracerane, which elutes after the C₃₁ extended hopanes, was identified in all Vazante samples except for two from the Lapa formation, again in the same core (B3LF-11-568.82 and 690.14).

Steranes – Similar to the hopanes, the sterane SIM chromatograms ($m/z=217$) display a range of C_{27} - C_{29} regular and thermally rearranged steranes and diasteranes as is expected for geologic samples (Figure 3.14). The C_{27} and C_{29} steranes dominate the $m/z=217$ trace. Four out of the five samples from the Serra do Garrote Formation and half of the Mocambo ($n=10$) samples show a slight predominance of the C_{29} steranes relative to the C_{27} hopanes (Table 3.4). On the other hand, the remaining Serra do Garrote, Mocambo and Lapa samples show a predominance of the C_{27} steranes relative to the C_{29} steranes.

Compound Specific Isotope Analysis – CSIA was used to measure the $\delta^{13}C$ isotopic composition of individual n -alkanes and Pr and Ph from the Vazante Group samples. Due to weak peak intensities (< 2 nA) each analysis was repeated three times. Even with such replication, only 11 Mocambo samples yielded measurable results (Table 3.7). Precision of sample replicates was typically better than $\pm 0.5\%$ (1σ). The average n -alkane $\delta^{13}C$ composition of these samples ranged from -30.1 to -28.3 ‰. The $\delta^{13}C$ of Ph was detected in six samples and ranged from -36.7 to -33.6 ‰. The $\delta^{13}C$ of Pr, on the other hand, was only detected in one sample (MAF-42.88-808.32); its value was -30.7 ‰.

3.4.4: Discussion: Syngeneity

All procedural blanks contained n -alkanes, hopanes, and steranes that were, on average had only 1.5x lower in abundance than the samples. The presence of these compounds within the procedural blanks could have resulted from one or more of the following possibilities: i) The Si gel used as the procedural blank contained trace oils, ii) non-sample related oil was introduced into the blanks sometime during sample

processing and/or extraction (i.e. laboratory contamination), iii) sample material was introduced into the blanks sometime during sample processing and/or extraction (i.e. cross-contamination). The first two options are possible but seem less likely because DCM rinses of the Si gel and all other materials used during sample processing and extraction were devoid of such compounds. The third option however, is more likely, especially since we know that some crossover was inevitable due to the poor condition of the shatterbox mill and puck. Additionally, comparison of biomarker ratios calculated from the blanks with ratios calculated from samples show that they fall within the same range (Table 3.4; 3.5). This suggests a relationship between the biomarkers in the blanks and the samples. It is however, uncertain if the biomarkers in the samples are syngenetic to the rock they were extracted from or if they too represent contamination. These questions will be addressed further in Studies 3 and 4.

3.4.5: Discussion: Biological and Environmental Source

Compound distributions and biomarker ratios calculated from these samples can be used to characterize biological, depositional, and diagenetic processes affecting the composition of organic matter deposited in the Vazante Group only if non-syngenetic organic material is insignificant. However, the possibility that the biomarkers presented here are the result of non-syngenetic contamination means that any interpretations of biological and environmental sources must be considered tentative.

Alkanes and Isoprenoids – Normal alkanes, isoprenoids and MMAs are not considered to be true biomarkers because they are not specific to organisms and can be formed by non-biologic processes (Hoering 1980; Klomp, 1986; Kissin, 1993). Despite

these complications, the distribution of these compounds may still reflect biological and environmental sources of organic matter, as well as estimates of thermal maturity, as long as they are used in conjunction with other source- and maturity-related biomarker ratios.

The distributions of *n*-alkanes, which are ubiquitous in sedimentary organic matter, can vary depending on biologic source and thermal maturity. For example, higher plants preferentially synthesize high molecular weight *n*-alkanes ($>n\text{-C}_{25}$) whereas bacteria and algae tend to produce low molecular weight *n*-alkanes ($<n\text{-C}_{25}$; Tissot and Welte, 1984). Therefore, the dominance of low molecular weight *n*-alkanes in the samples with unimodal distributions may indicate a lack of terrigenous input (Bourbonniere and Meyers, 1996). However, a rapidly decreasing abundance of *n*-alkanes with increasing carbon number, as observed in these samples, is characteristic of condensate-like distributions. The presence of these may be related to the thermal maturity of the sample insofar as they form by either thermal cracking of larger compounds or by condensation from a gas phase (Thompson, 1987, 1988).

The bimodal distributions, on the other hand, most likely reflect multiple source inputs rather than thermal maturity. The higher molecular weight ‘hump’ observed in these samples is distinct in abundance and distribution from the lower molecular weight ‘hump’ and therefore, probably represents a different source of organic matter. A similar bimodal distribution was observed in the six samples from the Lapa Formation previously analyzed by Brody (2007; Figure 3.15). Insofar as all samples have experienced the same level of thermal maturity, the bimodal distributions most likely represent migration of non-syngenetic hydrocarbons into specific samples. This is certainly the case with the samples from the Lapa Formation in core, B3LF-11, which has a strongly bimodal *n*-

alkane distribution in the pyrobitumen-bearing sample (B3LF-11-730.15) and unimodal *n*-alkane distributions in the remaining seven samples (except at depth 459.7 m).

The isoprenoids Pr and Ph can also be used to make inferences about organic matter sources and syngeneity. While the precursors of Pr and Ph can be made by a number of different organisms, their most common source are from phototrophic organisms (Powell and McKirdy, 1973). Therefore, the presence of Pr and Ph suggests phototrophic organisms were an important source of the organic matter extracted from the Vazante samples. Additionally, the ratio Pr/Ph can provide information about the redox conditions of the depositional environment. This is because phytol, the side chain of chlorophyll, preferentially converts to Pr under oxic conditions and Ph under reducing conditions. Pr/Ph values less than one are hence typically associated with anoxic deposition whereas values greater than one are typical of oxic environments (Didyk et al., 1978). All of the samples from the Serra do Garrote and Lapa formations and the majority of samples from the Mocambo (n=19) have Pr/Ph values <1 (Table 3.4) suggesting an anoxic depositional environment. Notably, only two Mocambo samples, both from core MAF-009, have Pr/Ph values >1 (Table 3.4). Coincidentally, these samples also have strongly bimodal *n*-alkane distributions. If the bimodal *n*-alkane distributions in these samples are the result of the introduction of non-syngentic hydrocarbons then Pr and Ph could similarly represent a non-syngenic component.

Similar to Pr and Ph, MMAs are commonly associated with phototrophic organisms, specifically, cyanobacteria. This is based on the observation that MMAs are produced in higher concentration by cyanobacteria than by most other organisms (Shiea et al., 1990). Additionally, MMAs are present in higher abundance in Precambrian

sedimentary rocks relative to those from the Phanerozoic (Fowler and Douglas, 1987; Summons, 1987; Summons et al., 1999). The ubiquitous presence of MMAs in the Vazante samples suggests that cyanobacteria contributed significantly to the organic matter and support the Proterozoic age of the succession.

Hopanes – Although some hopanoids, the precursor of hopanes, are synthesized by a select group of higher plants, the main source of sedimentary hopanes is from prokaryotes (Ourisson et al., 1979). Additionally, specific hopanes and hopane ratios can be used to make inferences about the environment, especially related to redox conditions present during deposition and early diagenesis of the organic matter. For example, although the precursor compound for γ is uncertain, it is thought to originate from tetrahymanol (Venkatesan, 1989; ten Haven et al., 1989), a compound mainly produced by a bacteriovorus living at the anoxic/oxic interface in the water column (Sinninghe Damsté et al., 1995). Therefore, the presence of γ is typically used to suggest a redox-stratified water column. The identification of γ in samples from the Serra do Garrote, Mocambo and all but two samples from the Lapa Formation supports the view of an extended period of redox stratification in the Vazante Basin.

The C₃₁-C₃₅ extended hopanes can also provide important information regarding the redox conditions in the depositional setting. Bacteriohopanetetrol, the precursor of the C₃₁-C₃₅ extended hopanes, is synthesized by aerobic bacteria (Ourisson et al., 1979), which suggests oxic conditions. However, the relative abundance of the C₃₅ extended hopanes suggests a highly reducing depositional environment for much of the Vazante Group. This parameter, recorded as % of the total extended hopanes (%C₃₅H), is based on the observation that the C₃₄ and C₃₅ extended hopanes are typically only preserved

under highly reducing conditions (Peters and Moldowan, 1991). Additionally, the diagenetic formation of the extended hopanes stops after the C₃₂ hopanes if oxygen is present (Demaison et al., 1983). Typically, the % C₃₅H is $\geq 5\%$ when deposited under highly reducing conditions (Cao et al., 2009). Except for the three Lapa samples that did not contain the full range of C₃₁-C₃₅ extended hopanes, all of the % C₃₅H values for the Vazante samples were within error of 5% or greater (Table 3.4), suggesting highly reducing conditions. Furthermore, two of the three Lapa samples that do not contain the C₃₁-C₃₅ extended hopanes also do not host any γ . The %C₃₅H values and the γ results are therefore consistent with one another and suggest a redox stratified water column with both oxic and highly reducing conditions.

Steranes – Steranes are the diagenetic products of sterols, which originate in eukaryotes (Kerr and Baker, 1991). Therefore, the presence of steranes in Vazante Group samples suggests that eukaryotes contributed to the organic pool preserved in these rocks. However, a qualitative assessment of the relative inputs from eukaryotic and prokaryotic organisms, represented by the ratio of steranes:hopanes (S/H), shows that, while eukaryotes were present, prokaryotes were dominant (Table 3.4).

The presence of steranes, however, has implications for the source of organic matter and environmental conditions within the Vazante Group. For example, the ubiquitous presence of steranes in all samples suggests either oxic or suboxic conditions. This interpretation is based on the assumption that sterol synthesis requires oxygen to proceed; the lower limit of oxygen necessary for sterol synthesis is in the nanomolar range (~ 7 nM; Waldbauer et al., 2011).

Additionally, the relative abundances of the C₂₇, C₂₈, and C₂₉ steranes, plotted on a ternary diagram (Figure 3.16), not only provide information about their biologic sources, but can also be used to evaluate whether the samples are closely related. Extracts with a close genetic relationship should plot near to each other on the ternary diagram, whereas samples with different organic sources will plot separately (cf. Grantham et al., 1988). Samples from the Serra do Garrote, which are all from a single core, plot together; samples from the Mocambo and Lapa however, display a greater spread. Five samples from the Mocambo appear to plot away from the other Mocambo samples. Interestingly, three of these samples also have bimodal *n*-alkane distributions. In general, the samples from the Serra do Garrote and the majority of the Mocambo samples (n=16) plot together, whereas samples from the Lapa Formation are shifted towards the C₂₇ sterane corner of the diagram. This suggests that the Serra do Garrote and Mocambo samples may have a similar source of organic matter whereas the Lapa had a different source.

Thermal Maturity Ratios – As discussed in Chapter 1, comparison of certain hopanes and steranes with their thermodynamically rearranged counterparts can indicate the thermal maturity of the samples. Additionally, a comparison of these biomarker ratios with each other should serve as a test for the syngeneity of the biomarkers.

The maturity biomarker ratios from each of the three formations show conflicting results (Table 3.5). Two hopane rearrangement ratios, C₃₂S/(S+R) and β α C₃₀H/(β α + α β), reach equilibrium in the early stage of oil production, whereas sterane rearrangement ratios, Σ C₂₇-C₂₉S/(S+R) and Σ C₂₇-C₂₉ββ/(ββ+ α α) reach equilibrium during the peak stage of oil generation (Figure 3.17; Peters et al., 2005). The ratio Ts/(Ts+Tm) increases

from 0 to 1 with increasing thermal maturity (Seifert and Moldowan, 1978; 1980). The $C_{32}S/(S+R)$ ratio, which reaches equilibrium at $\sim 0.57-0.62$ (Seifert and Moldowan, 1980), indicates that only seven samples from the Lapa Formation and eight samples from the Mocambo have reached the peak stage of oil generation; all of the other samples appear to be immature or in the early stage of oil generation. Additionally, both sterane ratios from the Vazante samples are well below equilibrium ($0.52-0.55$ and 0.7 , respectively; Seifert and Moldowan, 1986) suggesting low levels of thermal maturity. The $\beta\alpha C_{30}H/(\beta\alpha+\alpha\beta)$ and $Ts/(Ts+Tm)$ ratios on the other hand, suggests that all the Vazante samples are mature and have reached the peak stage of oil generation. These conflicting results could be due to input from non-syngenetic hydrocarbons, however, it could also be an artifact of the GCMS analysis. These ratios, especially the sterane ratios, are typically calculated from GCMS/MS or MRM-GCMS analyses, which are better able to fully separate compounds from each other.

CSIA – Comparison of the $\delta^{13}C$ isotopic compositions of the *n*-alkanes and Ph with the $\delta^{13}C$ isotopic composition of bulk organic matter ($\delta^{13}C_{org}$) from the 11 Mocambo samples analyzed show a unique relationship (Figure 3.18). The average isotopic composition of the *n*-alkanes in each sample is depleted relative to bulk organic carbon by 1.3 to 9.8‰. Additionally, Ph is isotopically depleted relative to the *n*-alkanes (by 4.2 to 7.1‰) and bulk organic carbon (by 6.2 to 9.1‰). Lipids from both autotrophs and heterotrophs are depleted relative to average biomass, therefore the depletion of *n*-alkanes and Ph relative to bulk organic carbon suggests that the extracted bitumen of these samples is related to the bulk organic matter and thus may be syngenetic. The depletion of Ph relative to the *n*-alkanes, however, is opposite of what is seen in modern biomass as

well as what is typically observed in Phanerozoic bitumens (Logan et al., 1995). This inverse signal is, however, characteristic of Proterozoic successions (Logan et al., 1995; Brocks et al., 2003; Close et al., 2011). Logan and colleagues (1995) propose that intense heterotrophic reworking of slowly sinking organic matter under anoxic conditions is the cause of the enrichment seen in *n*-alkanes relative to Pr and Ph. If true, these Mocambo samples were most likely deposited under a largely anoxic water column, which is consistent with time-series stable isotope data from the Vazante Group (Chapter 2).

3.4.6: Conclusions

Biomarker distributions and ratios calculated from the Serra do Garrote, Mocambo, and Lapa samples show evidence for redox stratification. This is based on the presence of γ as well as the juxtaposition of anoxic, reducing conditions, inferred from Pr/Ph and %C₃₅H ratios, combined with oxic conditions, inferred from the presence of steranes and C₃₁-C₃₅ extended hopanes. Insofar as these results can be interpreted in the face of possible contaminants they support the earlier findings of the Olcott et al. (2005) study published in *Science*.

However, biomarkers and biomarker ratios calculated from procedural blanks are similar to what is observed from the samples and may have resulted from contamination. Whether the biomarkers from the samples also represent contamination is uncertain. Bimodal *n*-alkane distributions suggest mixing of at least two sources of organic matter in several (n=11) of the Vazante samples. However, the identification of bimodal *n*-alkane distributions in samples analyzed by Brody (2007) suggests that the mixing, if it occurred, happened prior to sample processing. Additionally, samples with unimodal *n*-

alkane distributions do not directly contain evidence of mixing. Furthermore, source related biomarker parameters vary within each formation, as well as between formations. If there was significant cross contamination between these samples one would expect to see the same biomarker distributions in all samples. Since this is not the case it seems reasonable to suggest that if cross contamination between samples occurred, it was minor and did not significantly alter the biomarker distributions within the samples.

Table 3.4: Source related biomarker ratios from the 41 Vazante Group samples. Pr/Ph <1 is typical of anoxic conditions (Didyk et al., 1978). S/H describes the relative input from eukaryotes compared with prokaryotes. $\alpha\beta\text{C}_{29}\text{H}/\alpha\beta\text{C}_{30}\text{H}$ describes the dominant hopane in each sample. $\%\text{C}_{35}\text{H}>5\%$ indicates highly reducing conditions (Cao et al., 2009). $\% \text{C}_{27}\text{-C}_{29}$ steranes indicate the relative abundance of each sterane.

Formation or Member	Core	Depth (m)	Pr/Ph	S/H	$\alpha\beta\text{C}_{29}\text{H}/\alpha\beta\text{C}_{30}\text{H}$	$\%\text{C}_{35}\text{H}$	$\% \text{C}_{27}$ Steranes	$\% \text{C}_{28}$ Steranes	$\% \text{C}_{29}$ Steranes
Lapa	MAF-45	204.57	0.72	0.32	0.96	10.1	38	20	42
Lapa	PPF-04	257.62	0.50	0.47	1.2	5.6	51	20	29
Lapa	PPF-04	258.78	0.63	0.31	0.96	6.7	45	22	33
Lapa	PPF-04	263.75	0.62	0.38	1.1	6.5	51	20	29
Lapa	PPF-04	273.65	0.59	0.40	0.83	9.0	44	22	34
Lapa	PPF-04	277.84	0.58	0.32	0.95	6.5	50	21	29
Lapa	PPF-04	283.27	0.68	0.32	0.93	7.2	40	21	39
Lapa	B3LF-11	459.7	0.60	0.40	1.1	7.5	42	24	34
Lapa	B3LF-11	517.1	0.64	0.56	1.2	5.2	54	20	26
Lapa	B3LF-11	527.24	0.83	0.69	1.08	6.1	52	22	26
Lapa	B3LF-11	536.76	0.73	0.49	0.97	---	46	20	34
Lapa	B3LF-11	568.82	0.92	0.29	1.0	1.6	46	21	33
Lapa	B3LF-11	636.62	0.64	0.55	1.1	6.0	53	18	28
Lapa	B3LF-11	690.14	0.78	0.30	1.1	---	39	21	40
Lapa	B3LF-11	730.15	0.59	0.42	1.2	8.5	44	19	37
Mocambo	PAF-32	66.4	0.54	0.20	0.82	21.4	30	23	47
Mocambo	PAF-32	70.7	0.58	0.24	0.99	8.2	42	22	36

Formation or Member	Core	Depth (m)	Pr/Ph	S/H	$\alpha\beta\text{C}_{29}\text{H}/\alpha\beta\text{C}_{30}\text{H}$	%C ₃₅ H	% C ₂₇ Steranes	% C ₂₈ Steranes	% C ₂₉ Steranes
Mocambo	PAF-32	76.35	0.63	0.18	0.67	5.6	38	22	40
Mocambo	PAF-32	100.8	0.59	0.18	0.67	5.8	39	21	41
Mocambo	PPF-2A	216.2	0.29	0.17	0.77	10.5	41	22	36
Mocambo	PPF-2A	226.4	0.43	0.03	0.81	6.0	45	20	35
Mocambo	PPF-08	432.05	0.38	0.14	0.83	20.2	27	23	51
Mocambo	PPF-08	432.7	0.66	0.02	0.76	6.0	39	22	39
Mocambo	PPF-08	443.45	---	0.15	0.68	5.4	32	23	44
Mocambo	PPF-08	450.99	0.59	0.02	0.69	6.6	40	20	40
Mocambo	MAF-28	219.05	0.48	0.45	0.75	11.1	40	25	34
Mocambo	MAF-28	225.5	0.46	0.64	0.57	11.5	38	25	37
Mocambo	MAF-28	231.55	0.65	0.24	0.81	7.7	38	22	41
Mocambo	MAF-42.88	802.32	0.73	0.14	2.5	17.2	43	22	35
Mocambo	MAF-42.88	808.32	0.74	0.20	0.69	5.9	41	19	40
Mocambo	MAF-42.88	811.75	0.78	0.28	0.67	9.3	45	20	35
Mocambo	MAF-009	475.5	1.2	0.17	0.89	18.9	28	21	51
Mocambo	MAF-009	479	1.1	0.33	0.81	15.5	38	21	41
Mocambo	MAF-011	847.85	0.78	0.19	1.1	13.5	37	23	39
Mocambo	MAF-011	850.9	0.43	0.11	1.3	18.3	34	23	43
Garrote	B4LS-01	138.2	0.40	0.33	0.95	9.5	41	22	37
Garrote	B4LS-01	164.1	0.93	0.19	0.59	6.2	37	20	43
Garrote	B4LS-01	207.8	0.41	0.26	0.66	8.9	41	18	40
Garrote	B4LS-01	225.4	0.62	0.21	0.63	7.1	40	17	43
Garrote	B4LS-01	237.1	0.59	0.21	0.69	8.5	37	20	43

Formation or Member	Pr/Ph	S/H	$\frac{\alpha\beta C_{29}H}{\alpha\beta C_{30}H}$	%C ₃₅ H	% C ₂₇ Steranes	% C ₂₈ Steranes	% C ₂₉ Steranes
Blank 1	---	0.14	0.69	5.9	35	22	43
Blank 2	---	0.28	1.5	11.9	40	23	36
Blank 3	---	0.34	1.0	10.1	45	22	33
Blank 4	---	0.32	1.1	8.5	42	25	33

* S/H=total steranes/total hopanes, Pr/Ph=pristane/phytane, %C₃₅H=(C₃₅ hopane (R+S)/C₃₁-C₃₅ (R+S) hopanes)*100, %C₂X steranes=(C₂X steranes ($\alpha\alpha S + \beta\beta R + \alpha\alpha R + \beta\beta S$))/(C₂₇-C₂₉ steranes ($\alpha\alpha S + \beta\beta R + \alpha\alpha R + \beta\beta S$))*100.

Table 3.5: Maturity related biomarker ratios from the 41 Vazante Group samples. The maturity ratios do not agree with each other.

The Ts/(Ts+Tm) and $\beta\alpha C_{30}H/(\beta\alpha C_{30}H+\alpha\beta C_{30}H)$ hopane ratios suggest the samples are mature and in the peak stages of oil generation, whereas the $C_{32}S/(S+R)$ hopane, and S/(S+R) and $\beta\beta/(\beta\beta+\alpha\alpha)$ sterane ratios indicate immature samples.

Formation or Member	Core	Depth (m)	Ts/(Ts+Tm)	$\beta\alpha C_{30}H/(\beta\alpha C_{30}H+\alpha\beta C_{30}H)$	$C_{32}S/(S+R)$ Hopane	S/(S+R) $\Sigma C_{27-} C_{29}$ Steranes	$\beta\beta/(\beta\beta+\alpha\alpha)$ $\Sigma C_{27-} C_{29}$ Steranes
Lapa	MAF-45	204.57	0.51	0.13	0.56	0.36	0.48
Lapa	PPF-04	257.62	0.47	0.09	0.57	0.45	0.44
Lapa	PPF-04	258.78	0.53	0.10	0.59	0.45	0.43
Lapa	PPF-04	263.75	0.50	0.09	0.55	0.45	0.47
Lapa	PPF-04	273.65	0.46	0.13	0.55	0.42	0.46
Lapa	PPF-04	277.84	0.49	0.10	0.56	0.45	0.47
Lapa	PPF-04	283.27	0.46	0.10	0.54	0.43	0.47
Lapa	B3LF-11	459.7	0.48	0.09	0.56	0.40	0.43
Lapa	B3LF-11	517.1	0.46	0.09	0.59	0.48	0.49
Lapa	B3LF-11	527.24	0.45	0.10	0.59	0.46	0.46
Lapa	B3LF-11	536.76	0.52	0.11	0.51	0.42	0.45
Lapa	B3LF-11	568.82	0.52	0.10	0.95	0.46	0.42
Lapa	B3LF-11	636.62	0.45	0.09	0.57	0.42	0.46
Lapa	B3LF-11	690.14	0.53	---	0.53	0.44	0.55
Lapa	B3LF-11	730.15	0.59	0.11	0.59	0.41	0.45
Mocambo	PAF-32	66.4	0.54	0.12	0.55	0.46	0.48
Mocambo	PAF-32	70.7	0.50	0.11	0.56	0.48	0.47
Mocambo	PAF-32	76.35	0.61	0.13	0.56	0.46	0.50
Mocambo	PAF-32	100.8	0.60	0.13	0.56	0.46	0.50

Formation or Member	Core	Depth (m)	Ts/ (Ts+Tm)	$\beta\alpha C_{30}H/$ $(\beta\alpha C_{30}H+\alpha\beta C_{30}H)$	$C_{32}S/$ (S+R) Hopane	S/(S+R) ΣC_{27-} C ₂₉ Steranes	$\beta\beta/(\beta\beta+\alpha\alpha) \Sigma C_{27-}$ C ₂₉ Steranes
Mocambo	PPF-2A	216.2	0.55	0.13	0.53	0.47	0.44
Mocambo	PPF-2A	226.4	0.53	0.12	0.57	0.48	0.48
Mocambo	PPF-08	432.05	0.49	0.11	0.56	0.46	0.50
Mocambo	PPF-08	432.7	0.57	0.12	0.57	0.46	0.49
Mocambo	PPF-08	443.45	0.61	0.13	0.57	0.44	0.52
Mocambo	PPF-08	450.99	0.58	0.14	0.58	0.46	0.49
Mocambo	MAF-28	219.05	0.64	0.12	0.47	0.46	0.44
Mocambo	MAF-28	225.5	0.67	0.11	0.44	0.46	0.46
Mocambo	MAF-28	231.55	0.58	0.12	0.58	0.47	0.51
Mocambo	MAF-42.88	802.32	0.33	0.09	0.58	0.40	0.42
Mocambo	MAF-42.88	808.32	0.54	0.13	0.58	0.46	0.46
Mocambo	MAF-42.88	811.75	0.44	0.11	0.47	0.46	0.37
Mocambo	MAF-009	475.5	0.44	0.11	0.57	0.44	0.48
Mocambo	MAF-009	479	0.53	0.12	0.49	0.45	0.43
Mocambo	MAF-011	847.85	0.53	0.14	0.47	0.49	0.44
Mocambo	MAF-011	850.9	0.48	0.12	0.54	0.49	0.48
Garrote	B4LS-01	138.2	0.48	0.17	0.46	0.43	0.46
Garrote	B4LS-01	164.1	0.50	0.15	0.53	0.40	0.47
Garrote	B4LS-01	207.8	0.52	0.15	0.54	0.41	0.49
Garrote	B4LS-01	225.4	0.53	0.14	0.50	0.36	0.42
Garrote	B4LS-01	237.1	0.50	0.14	0.55	0.39	0.45
	Blank 1		0.60	0.08	0.57	0.48	0.51
	Blank 2		0.25	0.10	0.69	0.49	0.46
	Blank 3		0.47	0.09	0.57	0.43	0.53
	Blank 4		0.49	0.10	0.58	0.50	0.47

Table 3.6: Abundances of total *n*-alkanes, pristane (Pr), and phytane (Ph) from the 41 Vazante Group samples. Abundances are reported as ng/g of extracted sample.

Formation or Member	Core	Depth (m)	Mass (g)	Total <i>n</i> -Alkanes (ng/g)	Pr (ng/g)	Ph (ng/g)
Lapa	MAF-45	204.57	129.69	0.31	0.005	0.007
Lapa	PPF-04	257.62	128.01	1.34	0.014	0.028
Lapa	PPF-04	258.78	112.86	0.41	0.006	0.010
Lapa	PPF-04	263.75	149.59	1.17	0.039	0.063
Lapa	PPF-04	273.65	140.10	0.42	0.008	0.014
Lapa	PPF-04	277.84	90.20	0.57	0.009	0.015
Lapa	PPF-04	283.27	146.11	0.15	0.003	0.004
Lapa	B3LF-11	459.7	83.58	0.59	0.004	0.007
Lapa	B3LF-11	517.1	82.10	4.41	0.173	0.271
Lapa	B3LF-11	527.24	69.36	6.35	0.438	0.530
Lapa	B3LF-11	536.76	113.02	1.08	0.093	0.128
Lapa	B3LF-11	568.82	113.70	1.08	0.125	0.136
Lapa	B3LF-11	636.62	67.70	4.40	0.168	0.263
Lapa	B3LF-11	690.14	62.95	0.76	0.069	0.089
Lapa	B3LF-11	730.15	106.55	1.64	0.008	0.013
Mocambo	PAF-32	66.4	107.00	0.12	0.001	0.002
Mocambo	PAF-32	70.7	90.82	2.61	0.160	0.276
Mocambo	PAF-32	76.35	131.78	0.25	0.008	0.013
Mocambo	PAF-32	100.8	96.00	0.65	0.020	0.034
Mocambo	PPF-2A	216.2	116.60	0.32	0.001	0.004
Mocambo	PPF-2A	226.4	104.81	0.06	0.001	0.002
Mocambo	PPF-08	432.05	121.80	0.35	0.002	0.007
Mocambo	PPF-08	432.7	111.19	---	---	---
Mocambo	PPF-08	443.45	102.43	0.17	0.002	0.004
Mocambo	PPF-08	450.99	107.06	0.04	0.000	0.001
Mocambo	MAF-28	219.05	163.57	0.28	0.004	0.009
Mocambo	MAF-28	225.5	151.98	0.35	0.004	0.009
Mocambo	MAF-28	231.55	112.03	0.08	0.001	0.002
Mocambo	MAF-42.88	802.32	166.33	1.23	0.016	0.022
Mocambo	MAF-42.88	808.32	107.84	0.55	0.009	0.013
Mocambo	MAF-42.88	811.75	150.65	4.93	0.157	0.203
Mocambo	MAF-009	475.5	149.77	0.32	0.016	0.013
Mocambo	MAF-009	479	168.09	0.61	0.020	0.018
Mocambo	MAF-011	847.85	87.63	0.17	0.006	0.008
Mocambo	MAF-011	850.9	106.90	0.40	0.033	0.076

Formation or Member	Core	Depth (m)	Mass (g)	Total <i>n</i> -Alkanes (ng/g)	Pr (ng/g)	Ph (ng/g)
Garrote	B4LS-01	138.2	144.35	0.53	0.006	0.014
Garrote	B4LS-01	164.1	142.52	0.58	0.088	0.095
Garrote	B4LS-01	207.8	146.65	0.10	0.001	0.003
Garrote	B4LS-01	225.4	146.17	0.17	0.003	0.006
Garrote	B4LS-01	237.1	133.74	0.50	0.006	0.011

Table 3.7: Carbon isotopic composition of *n*-alkanes and pristane (Pr) and phytane (Ph) measured using CSIA. $\delta^{13}\text{C}$ *n*-alkane average is an average of the isotopic composition of all *n*-alkanes measured in each sample. $\delta^{13}\text{C}$ of *n*-C₁₈, Pr, and Ph is the isotopic composition of individual compounds. All values are reported relative to V-PDB. Uncertainties are typically better than $\pm 0.5\text{‰}$ (1σ).

Formation or Member	Core	Depth (m)	$\delta^{13}\text{C}$ <i>n</i> -alkane average (‰)	$\delta^{13}\text{C}$ <i>n</i> -C ₁₈ (‰)	$\delta^{13}\text{C}$ Pr (‰)	$\delta^{13}\text{C}$ Ph (‰)
Mocambo	PAF-32	70.7	-30.0	-28.8	-34.5	---
Mocambo	PAF-32	76.35	-30.5	-29.4	-37.6	---
Mocambo	PAF-32	100.8	-30.5	-28.5	-36.6	---
Mocambo	PPF-2A	226.4	-30.3	-27.9		---
Mocambo	PPF-2A	227.25	-29.1	-27.7	-34.1	---
Mocambo	PPF-08	450.99	-30.3	-28.1	---	---
Mocambo	MAF-28	225.5	-29.4	---	---	---
Mocambo	MAF-28	231.55	-30.1	-28.4	---	---
Mocambo	MAF-42.88	808.32	-30.3	-28.5	-34.5	-31.6
Mocambo	MAF-42.88	811.75	-29.5	-28.8	-34.8	---
Mocambo	MAF-009	475.5	-29.2	---	---	---

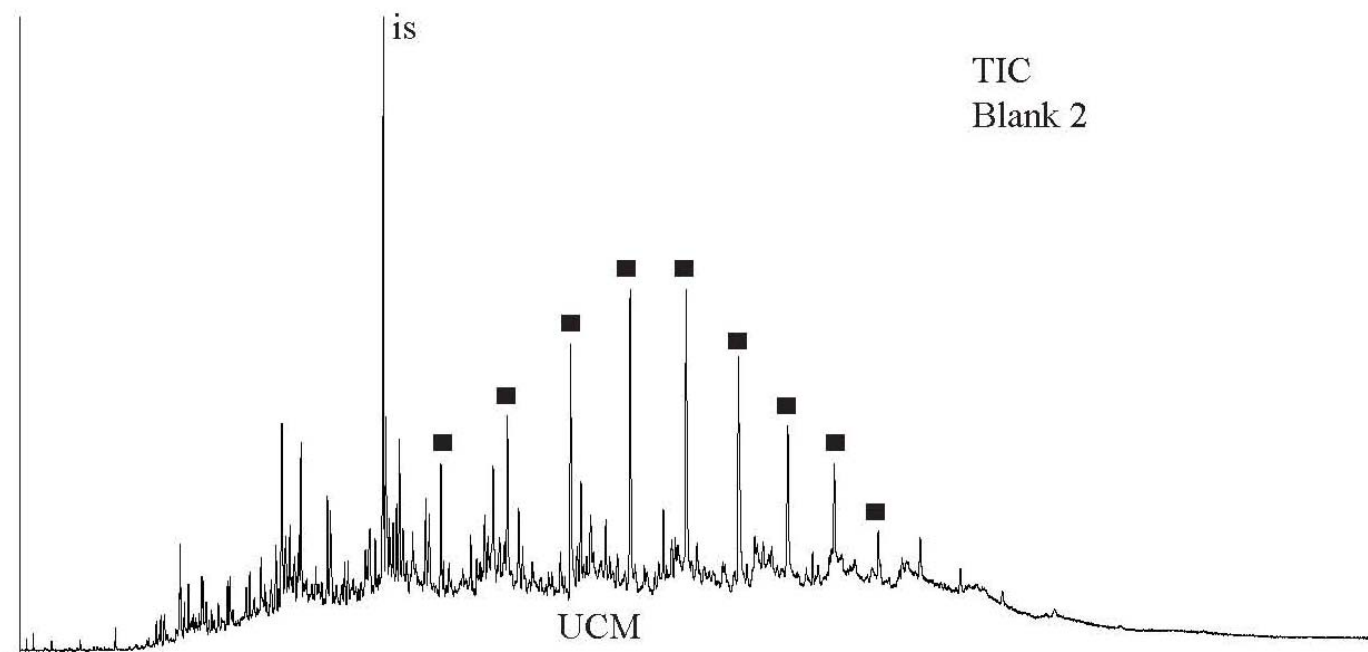


Figure 3.8: Total ion chromatogram (TIC) for Blank 2. Siloxanes (identified with black boxes) and branched alkanes (between the siloxanes) are the dominant compounds. The underlying hump is an unresolved complex mixture (UCM). The 3-methylenecosane internal standard (is) is marked. The x-axis is residence time and the y-axis is peak intensity.

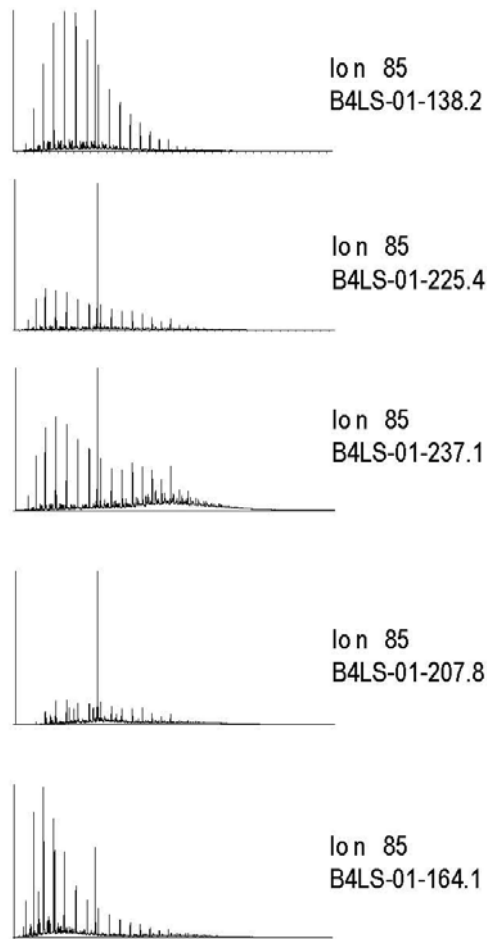


Figure 3.9: Selected ion chromatograms (m/z 85) from samples from the Serra do Garrote Formation show unimodal distributions for all samples. The large peak central in each trace is the 3-methylhenicosane internal standard (100 ng). The x-axis is residence time and the y-axis is peak intensity.

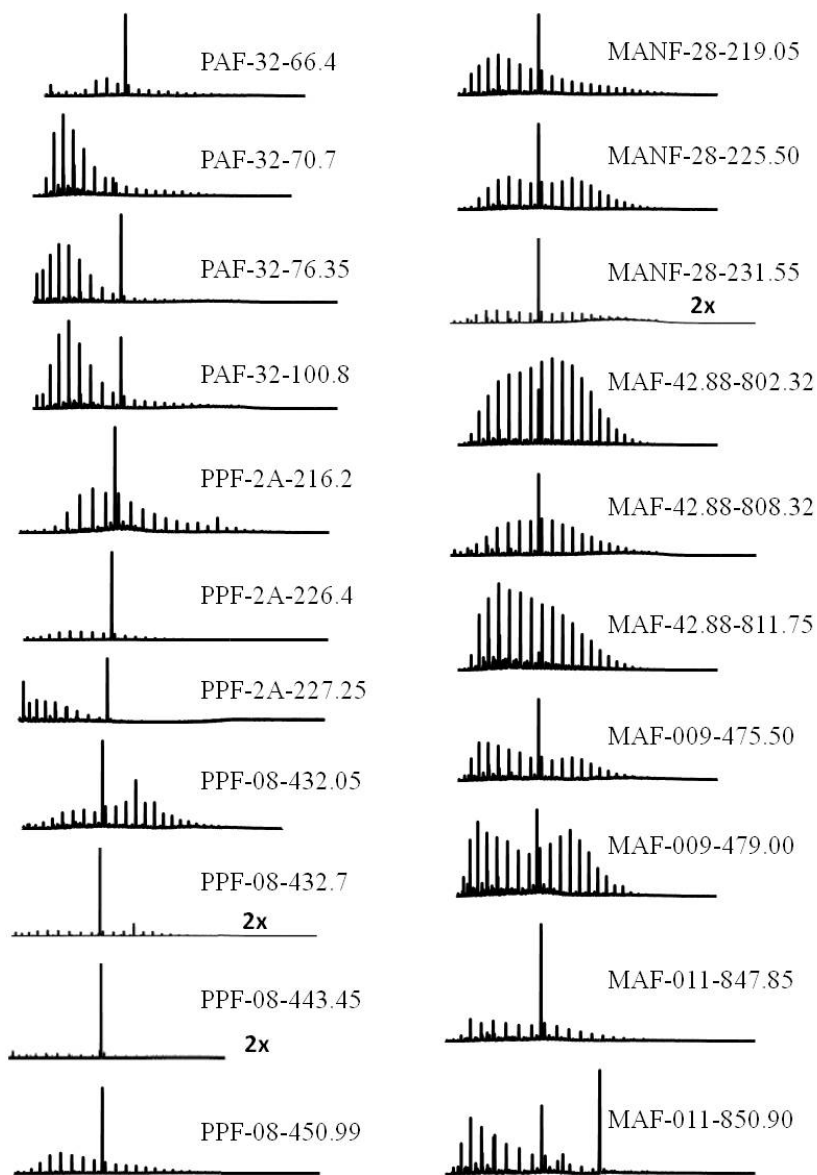


Figure 3.10: Selected ion chromatograms (m/z 85) from the Serra do Poço Verde Formation (Mocambo). The large peak central in each trace is the 3-methylhenicosane internal standard (100 ng). Samples marked with 2x are shown at two times the scale of the other samples. The x-axis is residence time and the y-axis is peak intensity.

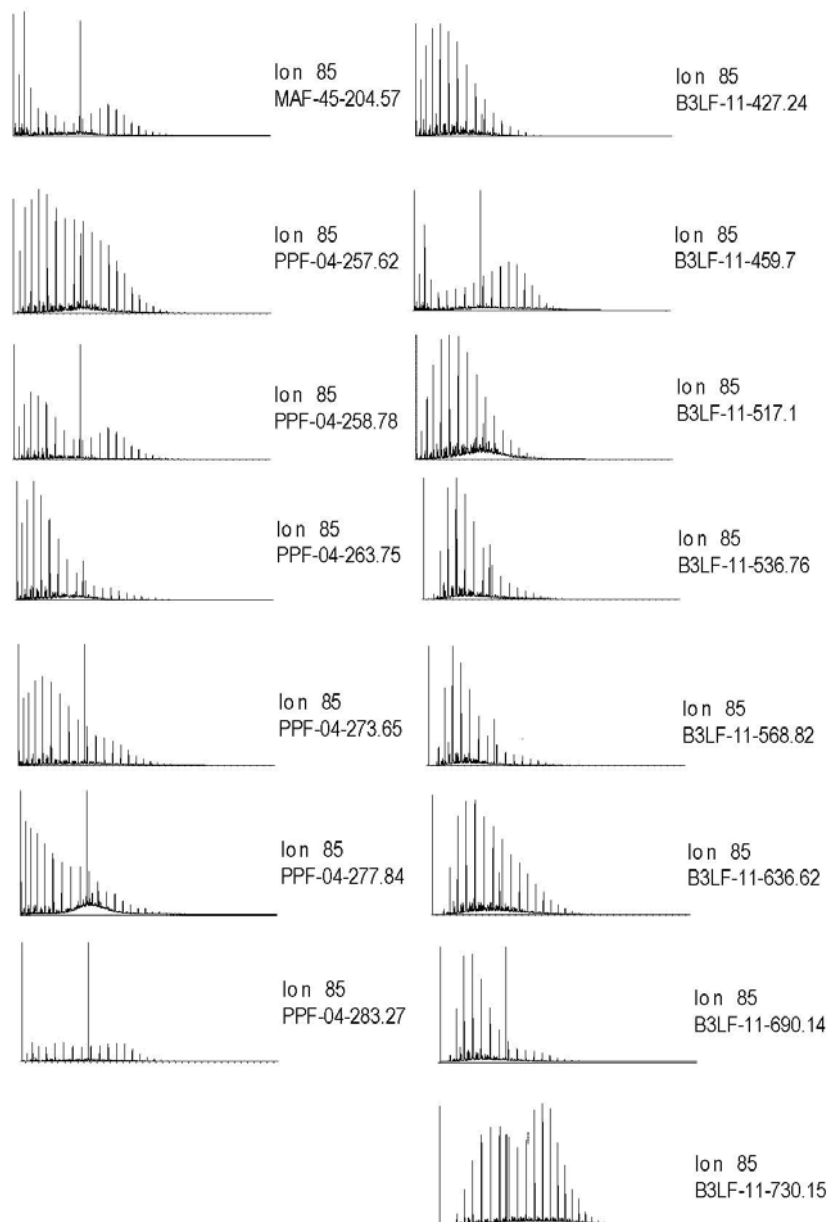


Figure 3.11: Selected ion chromatograms (m/z 85) from samples from the Lapa Formation show unimodal and bimodal n -alkane distributions. The large peak central in each trace is the 3-methylhenicosane internal standard (100 ng). The x-axis is residence time and the y-axis is peak intensity.

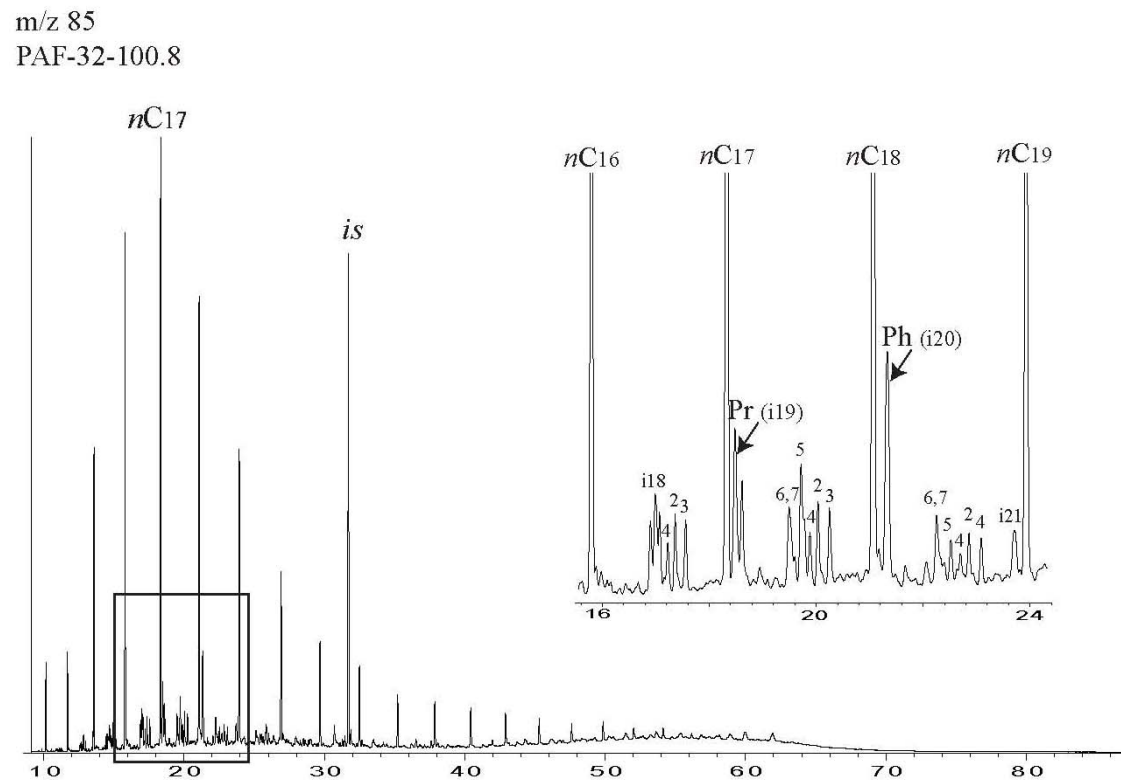


Figure 3.12: Selected ion chromatogram ($m/z=85$) for sample PAF-32-100.8. The inset shows a detailed view of where Pr, Ph, and MMAs elute in relation to the n -alkanes. Each n -alkane is identified as nC_X where X is carbon number. Isoprenoids, including Pr and Ph are identified by i_X . MMAs are identified by branching location between the n -alkanes. The numbers directly over each MMA peak represents the branching carbon. IS the 3-methylhenicosane internal standard (100 ng). The x-axis is residence time and the y-axis is peak intensity.

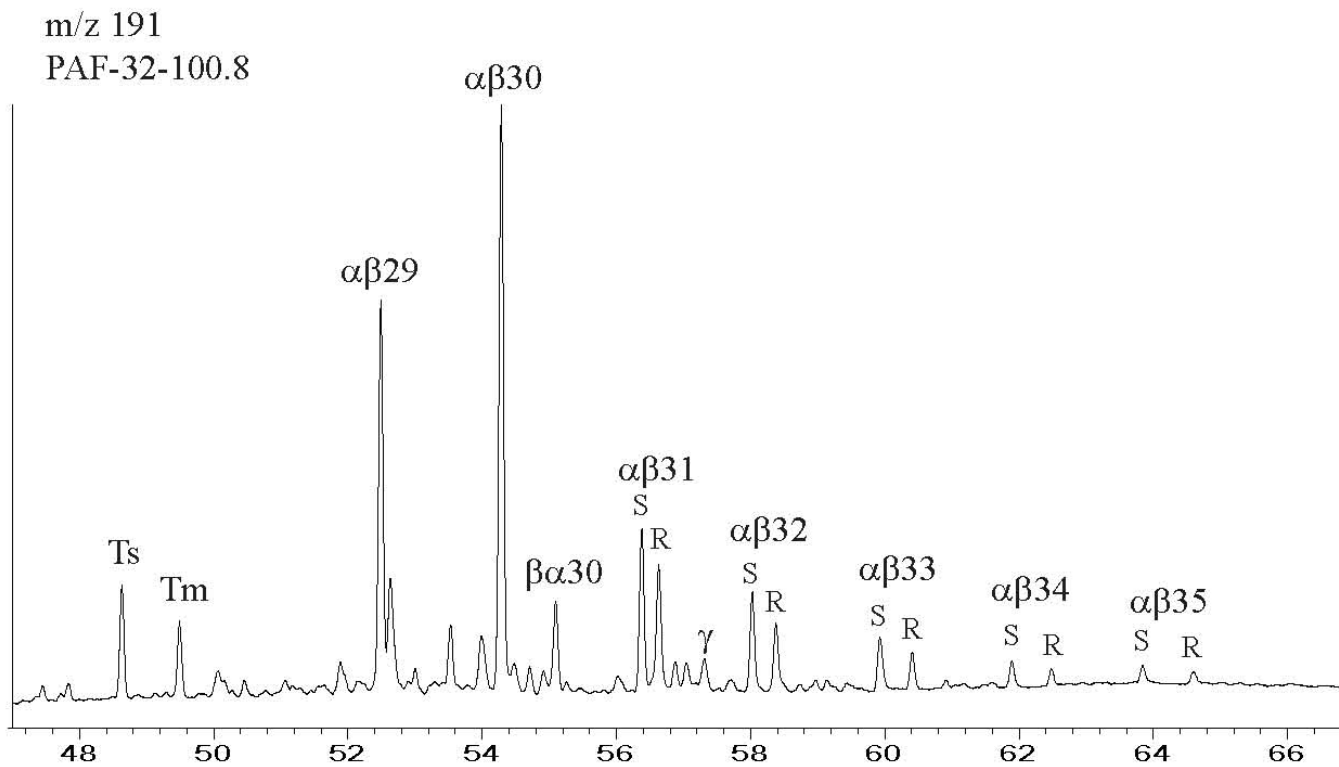


Figure 3.13: Selected ion chromatogram ($m/z=191$) for sample PAF-32-100.8 shows a detailed view of the hopanes. Ts and Tm are C_{27} hopanes and γ is gammacerane. Other hopanes are identified by carbon number. The x-axis is residence time and the y-axis is peak intensity.

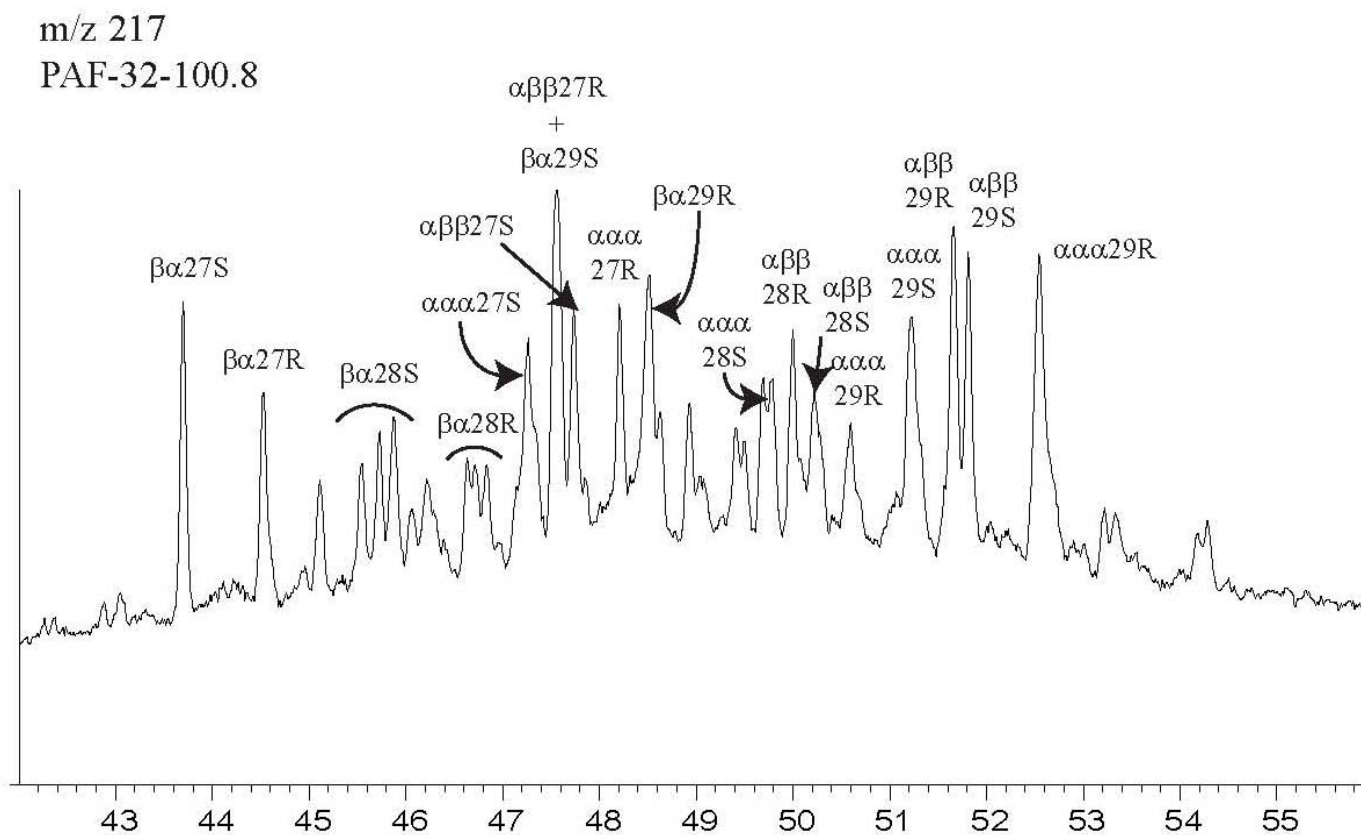


Figure 3.14: Selected ion chromatogram (m/z=217) for sample PAF-32-100.30 shows a detailed view of the steranes and diasteranes. Each compound is identified by carbon number. The x-axis is residence time and the y-axis is peak intensity.

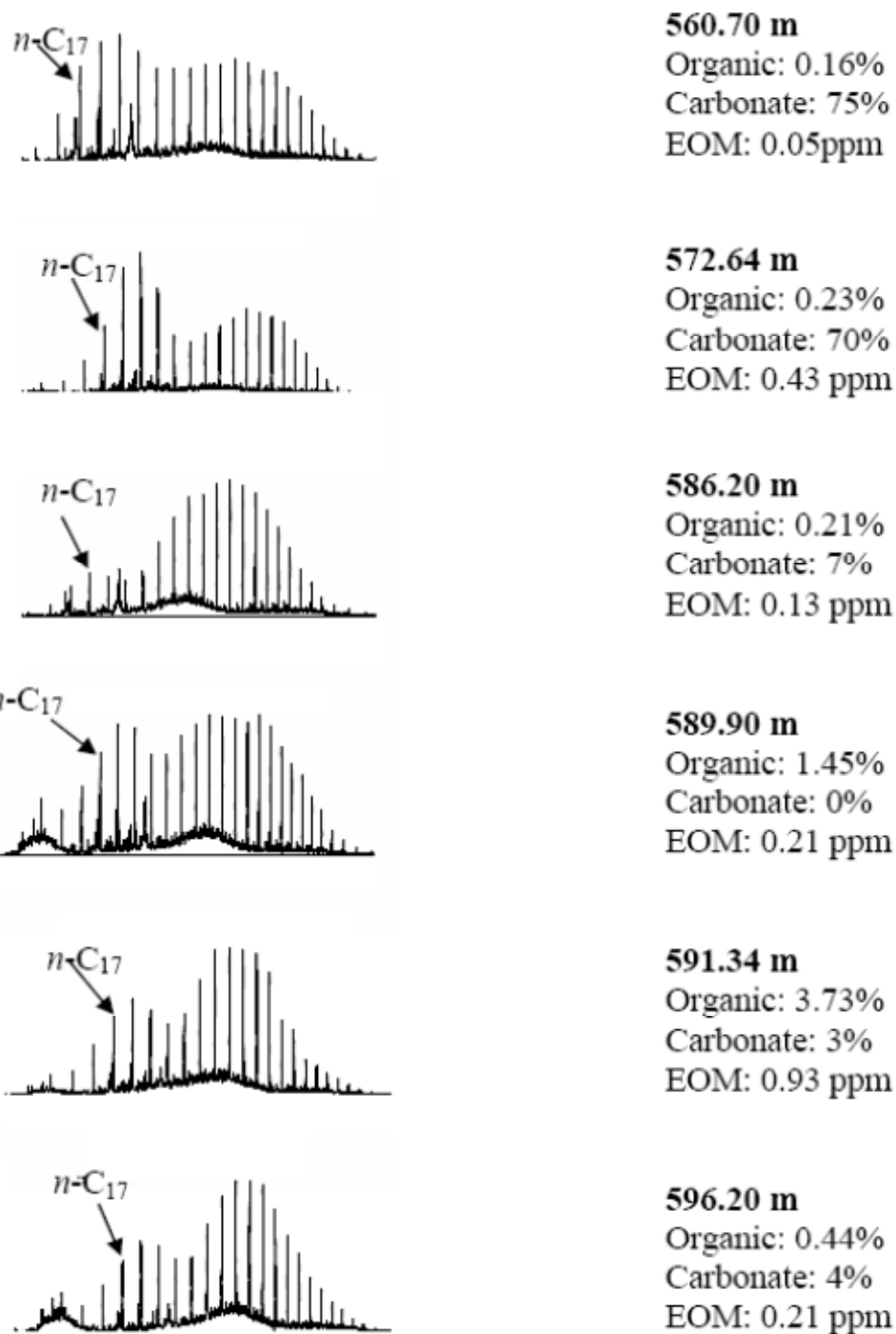


Figure 3.15: Selected ion chromatograms (m/z 85) from the Lapa Formation analyzed by Brody (2007). Bimodal n -alkane distributions were prominent in all samples. The x-axis is residence time and the y-axis is peak intensity.

Steranes

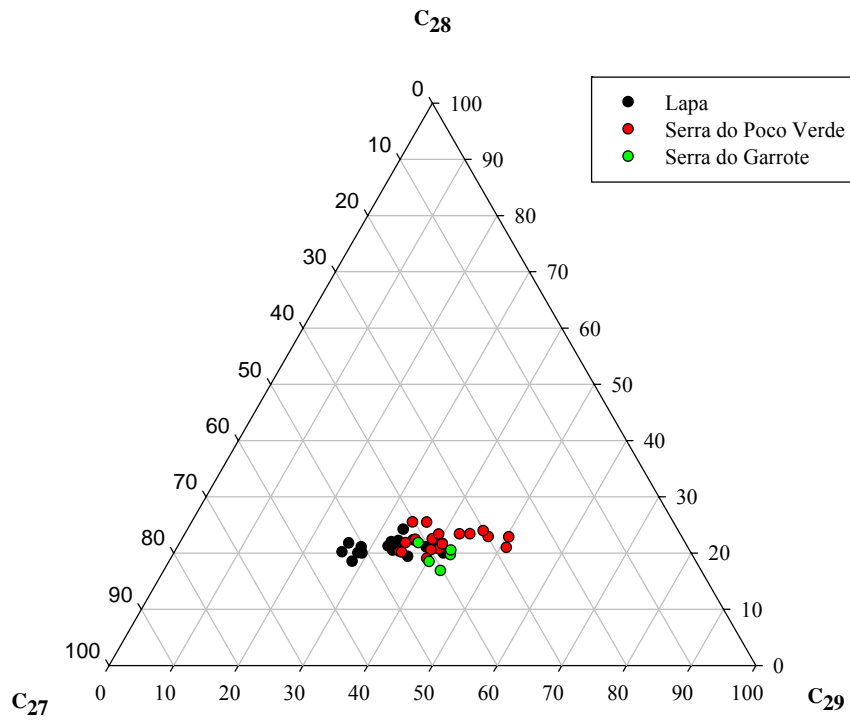


Figure 3.16: Ternary diagram of the relative abundance of the C₂₇-C₂₉ steranes for the Serra do Garrote, Serra do Poço Verde, and Lapa formation samples.

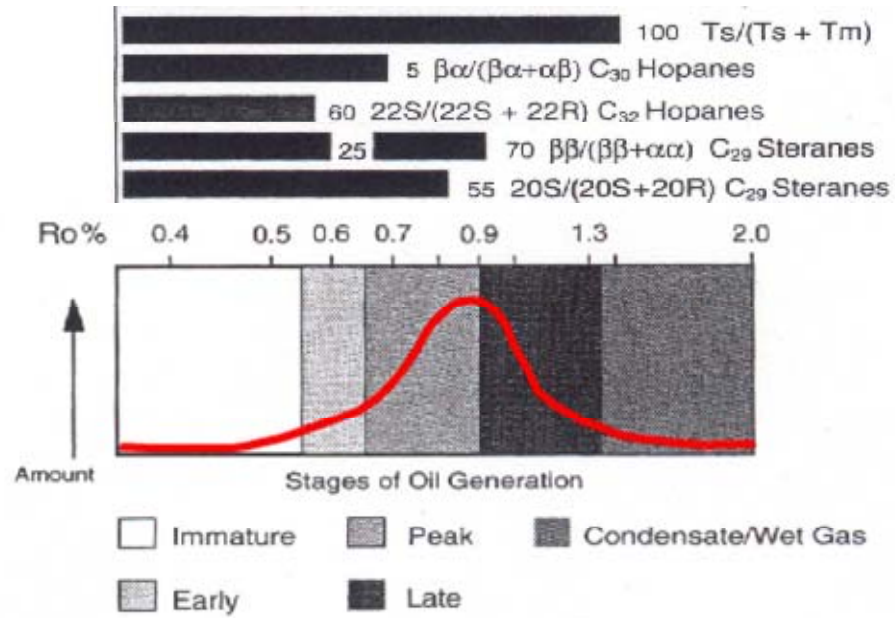


Figure 3.17: The range of maturity related biomarker ratios (black bars) relative to the stages of oil generation. The numbers at the end of each black bar are the equilibrium ratios (%) for each maturity parameter. The red line is the estimated amount of oil generated with increasing maturity (modified from Peters et al., 2005).

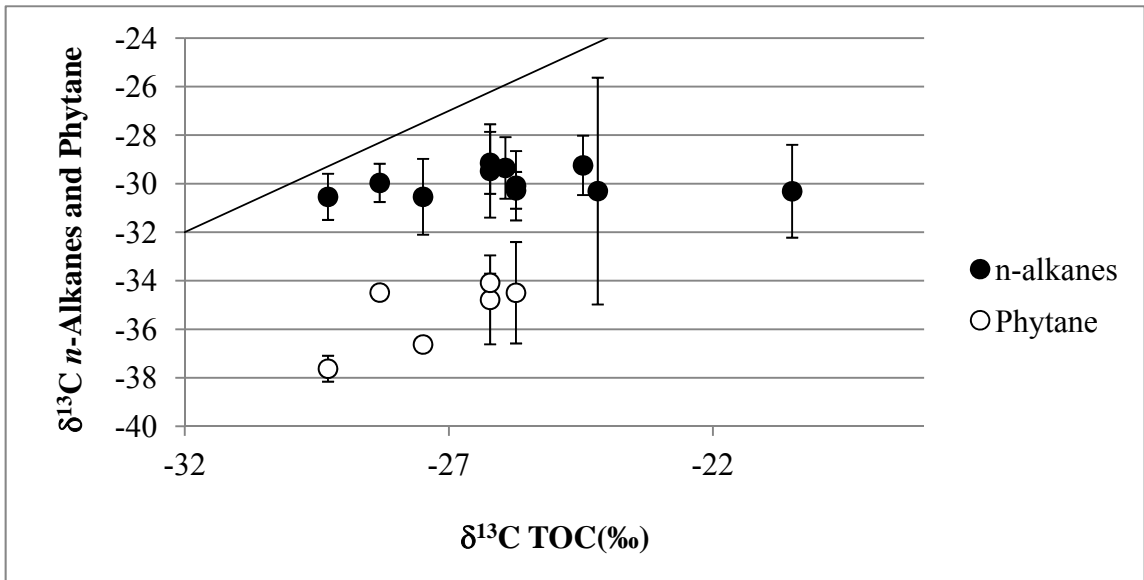


Figure 3.18: Cross plot of $\delta^{13}\text{C}$ of the Total Organic Carbon (TOC) vs. the $\delta^{13}\text{C}$ of phytane and the average $\delta^{13}\text{C}$ of the *n*-alkanes. The solid line represents a 1:1 relationship with $\delta^{13}\text{C}$ TOC. The *n*-alkanes and phytane are depleted with respect to bulk kerogen and phytane is depleted with respect to the *n*-alkanes. The depletion of *n*-alkanes and phytane relative to TOC suggests that the extracted organic matter is related to the kerogen and therefore syngenetic. The enrichment of the *n*-alkanes relative to phytane is typical of Proterozoic units and may indicate intense heterotrophic reworking of organic matter under anoxic conditions (Logan et al., 1995). Uncertainties are 1σ .

3.5: Study 3 – Biomarkers from kerogen and bulk extractions: An alternative test for syngeneity

As indicated above, biomarkers from the Serra do Garrote, Serra do Poço Verde, and Lapa formations, analyzed by GCMS, show evidence of being deposited under a redox stratified water column. However, procedural blanks processed and analyzed along with the Vazante samples also contain identifiable biomarkers. Because the biomarker distributions in the blanks resemble those of the samples, I hypothesize that they were introduced into the blanks via cross contamination. Likewise, the biomarkers within each sample could be a mixture of indigenous biomarkers and biomarkers from cross-contaminated sample material. However, based on the variations in biomarker ratios between closely-spaced samples, I hypothesize that the impact of contamination within each sample, if it occurred, was minor.

As a test of syngeneity, the kerogen fraction of a select sub-set of samples was isolated and re-extracted. This secondary, kerogen-related extract (hereafter called Bitumen 2) represents bitumen that was either not fully expelled from the kerogen, or was trapped between layers of clay minerals (Hallmann et al., 2010). This close association with the kerogen of the host rock increases the probability that Bitumen 2 is related to syngenetic organic matter. If the biomarkers from the bulk extracts discussed in Study 2 (hereafter called Bitumen 1) are syngenetic, then similar biomarker distributions should be evident in the Bitumen 2 extracts.

3.5.1: Sample selection

A set of 16 Mocambo samples from five cores were selected for Bitumen 2 analysis. These samples were chosen because the Mocambo is represented by the largest number of samples and has the greatest distribution of cores. Additionally, based on GCMS analysis of Bitumen 1, these samples were identified as being most likely to contain only syngenetic organic matter.

3.5.2: Methods

Approximately 30 g of post-extracted (Bitumen 1) powder was removed from each of the chosen samples and placed into 60 ml Teflon centrifuge tubes. The powder was treated with 6 M HCl to remove any carbonate that may have been present in the samples. HCl continued to be added to the samples until they no longer reacted; the samples were then left for an additional two hours before being centrifuged and decanted. They were subsequently rinsed 3x with ultra-pure (18 M Ω) Milli-Q water. The samples were then treated with concentrated HF in order to digest all silicate minerals. HF was slowly added to the samples and then left to react for 48 hours. During this 48 hour reaction time, the samples were periodically agitated with a Teflon stirring rod in order to ensure complete reaction and to homogenize the residue. The samples were then centrifuged, decanted, and fresh HF was added for an additional 48 hours. Once a reaction could no longer be observed the HF was removed by centrifugation and decanting and the samples were rinsed again 3x with Milli-Q water. The samples were then dried at 60°C in a drying oven. Once the samples were dry they were homogenized with a Teflon stirring rod. Hexane (40 ml) was then added to each sample, covered and sonicated for 30 minutes. The solvent was then decanted into a clean collection beaker

and the sonication step was repeated two additional times. All three extract aliquots from the same sample were combined. The samples were then covered and sonicated in a heated water bath (~60C) in Hexane for 30 minutes. The Bitumen 2 extracts were then loosely covered and allowed to dry down to ~1 ml in a fume hood. DCM-rinsed reduced Cu wires were added to each extract and allowed to react for 2-6 hours in order to remove elemental sulfur. If the Cu wires turned black, indicating precipitation of elemental sulfur, then more Cu was added. When a reaction could no longer be observed, the extract was dried down to ~70 μ l under a gentle stream of ultra pure N₂ gas and transferred to autosample vials fitted with 100 μ l glass inserts. 3-methylheneicosane (100 ng), d₄-C₂₉ $\alpha\alpha\alpha$ (20R)-ethylcholestane (25 ng), and *p*-terphenyl-d₁₄ (100 ng) were added to the samples as internal standards.

Metastable Reaction Monitoring Gas Chromatography Mass Spectrometry (MRM-GCMS) was performed on the Bitumen 2 extracts as well as their Bitumen 1 counterparts. MRM-GCMS analysis monitors key precursor-product ion transitions that are characteristic of individual hopanes and steranes. This resulted in better separation of these compounds than what can be obtained using GCMS only. Additionally, better separation of compounds, as well as the addition of a d₄-C₂₉ $\alpha\alpha\alpha$ (20R)-ethylcholestane internal standard, makes quantification of individual biomarkers possible.

MRM-GCMS analyses were performed using an Agilent 6890N gas chromatograph coupled to a Micromass Autospec-Ultima mass spectrometer housed in Dr. Roger Summons laboratory at the Massachusetts Institution of Technology (MIT). The samples were injected in splitless mode with He as the carrier gas. The GC oven was programmed to hold at 60°C for 2 minutes, heat to 150°C at 10°/min and then heat from

150° to 315°C at 3°C/min with a final hold time of 24 minutes resulting in a total run time of 96 minutes per sample. The GC was fitted with a 60 m DB-1ms fused silica capillary column. The source was operated in EI-mode with an ionization energy of 70 eV. The resulting chromatograms were processed using MassLynx v4.0 software; peak areas were integrated using this automated software program and then manually adjusted if required. Analytical and peak integration uncertainties are summarized in Appendix A (Tables A-1 and A-2). Compounds were identified based on comparison with a standard oil (AGSO Standard Oil) and quantified by comparing peak areas with the d₄-C₂₉ααα(20R)-ethylcholestane internal standard.

3.5.3: Results

A total of 9 Bitumen 1 extracts (8 samples and one procedural blank) and eight Bitumen 2 extracts were analyzed using MRM-GCMS. Hopanes, including γ and all C₂₇-C₃₅ regular and rearranged hopanes, were present in both the Bitumen 1 and Bitumen 2 extracts, as well as methylated hopanes. Steranes and diasteranes in the C₂₇-C₃₀ range, including regular and rearranged forms, are also present in the Bitumen 1 and Bitumen 2 extracts. The concentration of hopanes and steranes however, are up to 30x greater in the Bitumen 1 extracts than those from Bitumen 2 (Table 3.8).

3.5.4: Discussion

A comparison of biomarker ratios calculated from the Bitumen 1 and 2 extracts, analyzed by MRM-GCMS, was used to evaluate the genetic relationship between the sources of these two fractions. Biomarker ratios calculated from the Bitumen 2 extracts

in general did not correlate with ratios calculated from the Bitumen 1 extract (Table 3.9; Figure 3.19). However, the best tool for correlating extracts is to compare where Bitumen 1 and 2 plot on a sterane ternary diagram (Figure 3.20). Extracts with a close genetic relationship should plot close together on the ternary diagram whereas samples with different organic matter sources will plot separately (cf. Grantham et al., 1988).

The first point of note is that all of the Bitumen 1 samples, including the procedural blank, plot closely together on the sterane ternary diagram. This suggests that the Bitumen 1 extracts have a common source. The Bitumen 1 samples plotted here are all from the Mocambo; therefore a common source of the organic matter could reflect a common depositional source. However, since these samples were taken from locations across the basin, one would expect to see some variation related to the depositional environment. Therefore, either the biological and environmental conditions were uniformly distributed across the Mocambo basin or the Bitumen 1 extracts represent a ubiquitous infiltration of non-syngenetic organic matter.

The Bitumen 2 samples do not plot as closely together and are slightly shifted towards the C₂₇ and C₂₈ steranes relative to the Bitumen 1 samples. This suggests a different organic matter source for Bitumen 1 and 2. If true, this may indicate that Bitumen 1 contains a non-syngenetic component. It is however, also possible that both Bitumen 1 and 2 contain a common non-syngenetic component and that the offset may simply reflect a difference in the quantity of the non-syngenetic organic matter incorporated in the kerogen vs. the free bitumen. If this is the case, then it could have resulted either from cross contamination or permeation of non-syngenetic hydrocarbons through the rock before sampling.

3.5.5: *Conclusions*

Differences in biomarker ratios and the relative abundance of the C₂₇-C₂₉ steranes calculated from Bitumen 1 and 2 suggest that the two extracts are not closely related. Bitumen 2, which is associated with the kerogen of the samples, is more likely to represent syngenetic organic matter. Therefore, the differences seen in the biomarker ratios from Bitumen 1 compared with Bitumen 2 may be the result of contamination. If true then the ubiquitous nature of the biomarkers in Bitumen 1 suggests that the infiltration of non-syngenetic organic matter was widespread. This could have occurred prior to sampling if migrating hydrocarbon fluids infiltrated the rocks. However, the similarity of the biomarker ratios calculated from the procedural blank with the Bitumen 1 ratios suggests that it is more likely the result of laboratory contaminants.

Table 3.8: Abundances of total hopanes and total steranes from Bitumen 1 and Bitumen 2 extracts. The totals represent the sum of all regular hopanes and steranes. Abundances are reported as ng/g of extracted sample.

Formation or Member	Core	Depth (m)	Bitumen 1			Bitumen 2		
			Mass (g)	Total Steranes (ng/g)	Total Hopanes (ng/g)	Mass (g)	Total Steranes (ng/g)	Total Hopanes (ng/g)
Mocambo	PAF-32	76.35	131.78	0.164	1.13	21.36	0.083	0.272
Mocambo	PAF-32	100.8	96.00	0.180	1.07	14.27	0.219	0.569
Mocambo	PPF-2A	226.4	104.81	0.135	0.511	20.71	0.139	0.281
Mocambo	PPF-2A	227.25	104.66	0.250	0.709	21.45	0.193	0.272
Mocambo	PPF-08	432.7	111.19	0.098	0.488	22.68	0.414	0.675
Mocambo	PPF-08	443.45	102.43	0.075	0.423	23.88	0.058	0.161
Mocambo	PPF-08	450.99	107.06	0.395	2.16	16.58	0.193	0.464
Mocambo	MAF-28	231.55	112.03	0.793	2.80	27.32	0.154	0.373
Mocambo	MAF-42.88	808.32	107.84	0.456	2.33	20.98	0.127	0.374
Blank 1			116.47	0.645	3.68	---	---	---

Table 3.9: Source and maturity related biomarker ratios for Bitumen 1 and Bitumen 2.

	Formation or Member	Core	Depth (m)	S/H	$\frac{\alpha\beta C_{29}H}{\alpha\beta C_{30}H}$	%C ₃₅ H	Ts/ (Ts+Tm)	$\frac{\beta\alpha C_{30}H}{\beta\alpha C_{30}H + \alpha\beta C_{30}H}$	C ₃₂ S/(S+R) Hopane	S/(S+R) $\Sigma C_{27-C_{29}}$ Steranes	$\frac{\beta\beta}{(\beta\beta + \alpha\alpha)}$ $\Sigma C_{27-C_{29}}$ Steranes
Bitumen 1	Mocambo	PAF-32	76.35	0.15	0.73	2.14	0.66	0.09	0.59	0.47	0.54
	Mocambo	PAF-32	100.8	0.17	0.75	1.70	0.63	0.09	0.59	0.55	0.50
	Mocambo	PPF-2A	226.4	0.26	0.95	1.75	0.57	0.08	0.60	0.56	0.48
	Mocambo	PPF-2A	227.25	0.35	1.04	9.04	0.55	0.09	0.72	0.56	0.52
	Mocambo	PPF-08	432.7	0.28	0.88	2.18	0.63	0.08	0.60	0.57	0.54
	Mocambo	PPF-08	443.45	0.20	0.83	1.85	0.62	0.08	0.59	0.56	0.51
	Mocambo	PPF-08	450.99	0.18	0.76	1.73	0.67	0.09	0.58	0.55	0.52
	Mocambo	MAF-28	231.55	0.18	0.83	1.70	0.64	0.09	0.58	0.53	0.49
	Mocambo	MAF-42.88	808.32	0.20	0.74	1.72	0.59	0.08	0.59	0.54	0.44
		Blank 2			0.18	0.76	1.70	0.67	0.10	0.56	0.54
Bitumen 2	Mocambo	PAF-32	76.35	0.30	0.91	3.86	0.62	0.07	0.60	0.54	0.56
	Mocambo	PAF-32	100.8	0.37	0.86	4.88	0.57	0.11	0.59	0.56	0.53
	Mocambo	PPF-2A	226.4	0.48	1.69	4.33	0.62	0.16	0.58	0.55	0.52
	Mocambo	PPF-2A	227.25	0.69	1.42	4.40	0.61	0.15	0.59	0.55	0.57
	Mocambo	PPF-08	432.7	0.39	1.06	8.79	0.59	0.13	0.54	0.54	0.51
	Mocambo	PPF-08	443.45	0.59	1.12	5.55	0.57	0.16	0.56	0.59	0.58
	Mocambo	PPF-08	450.99	0.35	1.01	5.57	0.59	0.18	0.60	0.54	0.54
	Mocambo	MAF-28	231.55	0.41	0.91	4.69	0.63	0.12	0.51	0.56	0.56
	Mocambo	MAF-42.88	808.32	0.33	0.86	5.07	0.58	0.13	0.53	0.54	0.49

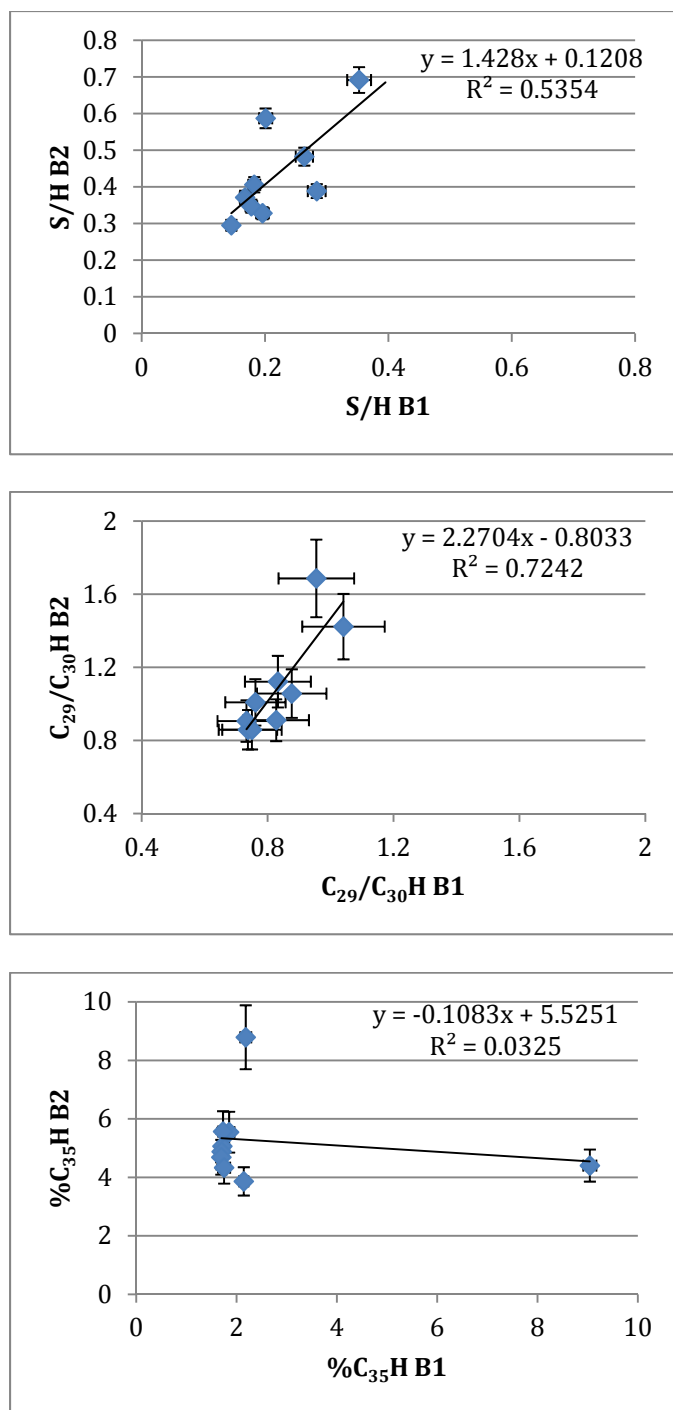


Figure 3.19: Cross-plots of source-related biomarker ratios calculated from the Bitumen 1(B1) and Bitumen 2 (B2) extracts.

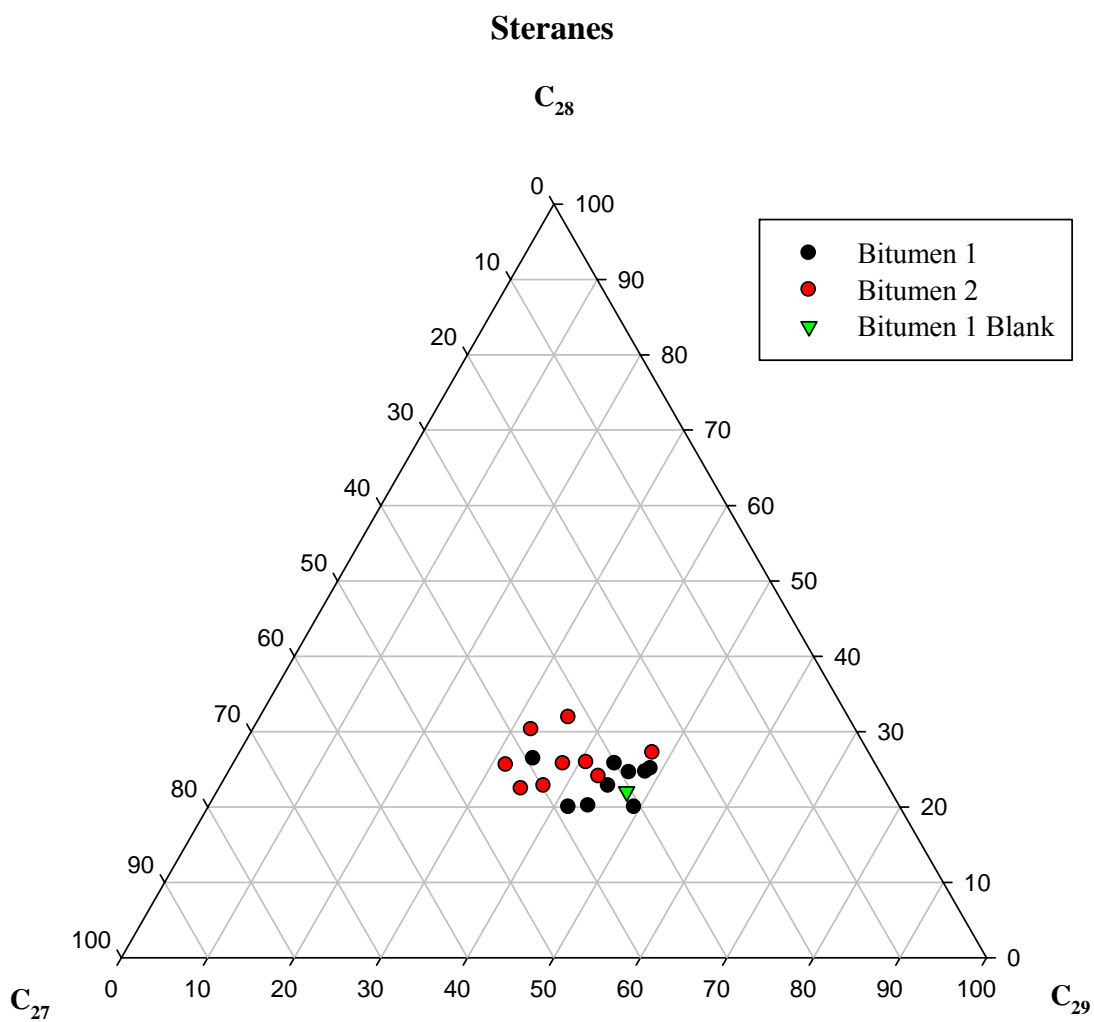


Figure 3.20: Ternary diagram of the C_{27} - C_{29} steranes from Bitumen 1 and Bitumen 2.

3.6: Study 4 – A Re-Evaluation of Biomarkers from the Vazante Group

Indigenous biomarkers isolated from Proterozoic sedimentary successions offer a unique opportunity to identify the specific organisms and environmental conditions that existed in an otherwise poorly understood time period. However, in order for biomarkers to provide information about Proterozoic life and environment they must be syngenetic. Biomarkers from the 41 Vazante samples analyzed in this study, however, appear to contain some fraction of non-syngenetic organic matter. This is based on the presence of biomarkers in the procedural blanks as well as differences in the biomarker composition of Bitumen 1 and Bitumen 2. Hence, any biological and environmental interpretations based on these results must be viewed with suspicion.

Therefore, in order to understand how life and environment co-evolved through the changing environmental conditions of the Vazante Group, a new biomarker study that does not contain evidence of laboratory contamination is necessary. In order to achieve this, a sub-set of archived core material from the Serra do Garrote, Serra do Poço Verde and Lapa formations were processed and extracted in the Summons laboratory at MIT. The Summons laboratory is specially designed for biomarker work and therefore offers the best opportunity to obtain ‘clean’ sample extracts. If the biomarkers extracted in this focused study of the Vazante Group are indeed syngenetic, then biomarkers from samples deposited before and after the Vazante glaciations will not only help us to understand the nature of life and environment in a possibly Mesoproterozoic succession, but they will also provide a test to see how early life reacted and adapted to a strongly changing environment.

3.6.1: Sample selection

Fourteen samples from the Serra do Garrote, Serra do Poço Verde, and Lapa formations were chosen to be included in this focused study (Table 3.1). These samples were chosen from archived core material initially collected for biomarker analysis. However, because each sample included in the initial biomarker study required 100-200 g of core material, few samples had enough material left over for a second biomarker analysis. Therefore, only half the samples included in this study were previously analyzed. The remaining seven samples consist of material that was originally deemed less suitable for biomarker analysis based on low TOC composition (<0.5 %) and no measurable ROCK EVAL peaks.

Samples from this focused study of the Vazante Group however, still represent a basin-wide distribution of cores and all three formations. The Serra do Garrote Formation is represented by three samples from core B3LF-11. The Serra do Poço Verde Formation is represented by eight samples from five cores. While most of these samples were taken from the Mocambo shale (n=6), two samples, both from core MAF-011, represent the Retiro Member of the Serra do Poço Verde Formation. Unlike the other shale samples analyzed thus far, these samples are composed of stromatolitic carbonate. Additionally, core MAF-011 is from the western region of the Vazante Basin, which experienced higher temperatures than the other cores located in the eastern portion of the basin. The Lapa Formation is represented by three samples from two cores (B3LF-11 and MAF-45). It is important to note that while the Lapa sample B3LF-11-517.1 was analyzed in the earlier biomarker study and found to contain biomarkers and a unimodal *n*-alkane distribution, re-examination of the lithology identified this sample as being significantly recrystallized.

3.6.2: *Methods*

Fourteen samples and two procedural blanks were prepared for biomarker analysis using methods designed to eliminate any potential sources of contamination (described in Hallmann, 2010). Approximately 75-100 g of each core sample were prepared for biomarker extraction. Additionally, two procedural blanks were processed along with the samples. The blank material consisted of ~50 g of annealed sand rather than Si gel, which may contain trace oils (Roger Summons, pers. comm.). The samples were first rinsed with deionized water, then the outer ¼ cm of each sample was ground off using a Struers grinding apparatus in order to remove surface contaminants. The samples were then chipped into ½ cm pieces using a stainless steel mortar and pestle that was extensively cleaned with soap and water, DCM and annealed sand prior to use. The chipped samples were then sequentially cleaned by sonication in methanol (MeOH) three times for ~10 minutes each; this step was then repeated with DCM. The solvents were discarded between each rinse and fresh solvent was used each time.

Once the sample chips were sufficiently cleaned and dried they were powdered using a shatterbox equipped with a stainless steel puck and mill located in the Summons laboratory at MIT. The puck and mill were specially designed so that they could be completely submerged in solvent during the cleaning process. These were extensively cleaned prior to each use with soap and water, MeOH and annealed sand. The sample powders were then separated into 25 g aliquots and loaded into 60 ml glass vials for organic matter extraction. Twenty ml of DCM:MeOH (9:1) were added to each 60 ml vial. The vials were sonicated for 30 minutes and then centrifuged before the solvent

was removed with a glass pipette. This extraction process was repeated three times and the solvent for each sample was combined and dried down to ~1 ml under a stream of high purity N₂ gas. Reduced Cu granules were then added to remove elemental S.

Typically, the samples would then be separated into saturate, aromatic and polar fractions using column chromatography. However, in order to avoid contact with Si gel, these samples were not fractionated. Instead the bulk extracts were transferred to autosample vials fitted with 100 µl glass inserts and concentrated to 50 µl for analysis. 3-methylheneicosane (100 ng), d₄-C₂₉ααα(20R)-ethylcholestane (25 ng), and *p*-terphenyl-d₁₄ (100 ng) were added to the samples as internal standards.

Full scan and SIM analyses of alkanes, isoprenoids, and aromatics were conducted using the GCMS housed in Dr. George Cody's laboratory at CIW. GCMS was operated under the same run conditions described in Study 1. Alkanes, isoprenoids, and aromatics were quantified by comparing peak areas with the 3-methylheneicosane and *p*-terphenyl-d₁₄ internal standards. MRM-GCMS analyses of hopanes and steranes were conducted in Dr. Roger Summons laboratory at MIT. MRM-GCMS was operated under the same run conditions described in Study 3. Hopanes and Steranes were identified based on comparison with a standard oil (AGSO Standard Oil) and quantified by comparing peak areas with the d₄-C₂₉ααα(20R)-ethylcholestane internal standard.

3.6.3: Results and Interpretations

Typically compound peaks identified by MRM-GCMS were typically at least 20x greater than the background signal with the exception of three samples (B3LF-11-517.1, MAF-011-844.1 and 845.45) that contained compound peaks that were less than 5x greater than background. Biomarkers from these three samples therefore are not distinct

enough from background and will not be included in the discussion of results. The remaining 11 samples contain a suite of paleobiologically and paleoenvironmentally informative biomarkers including alkanes, Pr and Ph, MMAs, hopanes, steranes, and aromatic hydrocarbons.

Procedural blanks – Two procedural blanks were processed along with the samples in this focused biomarker study. One blank contained no biomarker compounds; the other blank however contained traces of hopanes and steranes. A small amount of hopanes and steranes in a procedural blank is acceptable as long as they are present in far lower abundances than the samples (Summons, Pers. Comm.). In general, peak areas of the hopanes and steranes in the blank were 5-50x smaller than found in the samples. This is an acceptable range supporting the assumption that laboratory contamination in these samples was not significant (Waldbauer et al., 2009).

Additionally, samples from core MAF-011 can also be treated as procedural blanks. The low TOC (0.46-0.64 % TOC) and high metamorphic grade (amphibolite-granulite facies; Dardenne, 1978; Fuck et al., 1994) of these samples should preclude the presence of biomarkers. Therefore, the lack of measurable biomarkers in these samples suggests that if laboratory contamination was introduced, it was below detection levels.

Alkanes and Isoprenoids – Normal alkanes, branched alkanes, and Pr and Ph, measured on $m/z=85$ selected ion mass chromatograms, were present in these Vazante samples. The total abundance of these compounds, however, was low; *n*-alkanes for example range from 0.00 to 0.39 ng/g extracted rock (Table 3.10). These are on average 6x lower than the *n*-alkanes reported in Study 2. Additionally, MMAs which were abundant in the alkane traces from Study 2 are only detected in the five samples from this

study that have the highest *n*-alkane concentrations (MAF-42.88-811.75, 818, PPF-2A-227.25, B3LF-11-138.2, 164.2).

Unlike what was reported in Study 2, *n*-alkanes from these samples display only unimodal distributions which center on the C₁₆ or C₁₇ *n*-alkane and range in carbon length from C₁₄ to C₂₃. The dominance of low molecular weight *n*-alkanes is consistent with the unimodally distributed *n*-alkanes in Study 2, as well as what was reported by Olcott et al. (2005). Pr/Ph ratios calculated from the Serra do Garrote, Serra do Poço Verde, and Lapa formations range from 0.42-1.1 (Table 3.11) indicating anoxic to sub-oxic conditions (Didyk et al., 1978).

Hopanes – Hopanes, measured from MRM M⁺→191 mass chromatograms, are present in all samples (Figure 3.21). However, the concentration of total hopanes/g of extracted sample is low (0.000-0.083 ng/g). The highest abundances of total hopanes are from core MAF-42.88, which is the same core analyzed in the Olcott et al. (2005) study. Despite low concentrations, both regular and rearranged hopanes in the C₂₇-C₃₀ range are present in all samples from this study. Conversely, not all of the extended hopanes (C₃₁-C₃₅) were detected in all of the samples; one Serra do Garrote (B3LF-11-207.8), two Serra do Poço Verde (MAF-009-476.85 and MAF-45-239.12), and one Lapa sample (MAF-45-197.1) did not contain the C₃₄ and C₃₅ extended hopanes. This may suggest oxic to sub-oxic conditions because, as mentioned previously, the C₃₄ and C₃₅ extended hopanes are not formed if oxygen is present (Demaison et al., 1983). Additionally, in samples that do contain the full range of C₃₁-C₃₅ extended hopanes, the %C₃₅H ratio is low (1.8-3.3; Table 3.11). Unlike the %C₃₅H values calculated in Study 2, these do not indicate highly reducing conditions.

Additionally, 28,30-dinorhopane, a C₂₈ hopane, was identified in the Vazante Group samples. 28,30-Dinorhopane (28,30-DNH) is thought to originate from chemoautotrophic bacteria, possibly H₂S oxidizers, that live at the oxic/anoxic interface (Schoell et al., 1992). This is based on CSIA analyses in which 28,30-DNH is typically depleted relative to bitumen by up to 9‰. In order to achieve a 9‰ depletion relative to bitumen, the organism responsible for 28,30-DNH biosynthesis must have utilized ¹³C-depleted substrates. Methanotrophs typically show greater ¹³C depletions (as low as -110‰; Whiticar, 1999) and are therefore probably not the source of 28,30-DNH. Sulfur-oxidizing bacteria however, which live at an oxic/anoxic interface in the water column or sediments, can be a source of the ¹³C depleted 28,30-DNH hopanes. As such, an abundance of 28,30-DNH (relative to αβC₃₀H) is typical of anoxic, and often sulfidic, environments (Mello et al., 1989; Schoell et al., 1992).

Methylated hopanes, which consist of 2α-methylhopanes (2αMeH) and 3β-methylhopanes (3βMeH), were also identified in the Vazante samples based on MRM M⁺→205 mass chromatograms (Figure 3.22). 2αMeH is typically described as a biomarker of oxygenic cyanobacteria because, until recently, they were the only organisms known to produce the precursor compounds, 2-methylbacteriohopanepolyols (2-MeBHPs) in abundance (Summons et al., 1999). New work however, has shown that some anoxygenic phototrophic bacteria can also produce high quantities of 2-MeBHPs (Rashby et al., 2007). However, 2-MeBHPs have yet to be identified in abundance in any non-phototrophic bacteria. 3βMeH are known primarily from aerobic methanotrophic bacteria, although they have also been isolated from acetotrophic archaea (Zundel and Rohmer, 1985). Carbon isotopic analysis of the 3βMeHs in the Vazante samples could

differentiate between the potential biomarker sources; however, the abundances of these compounds are too low for CSIA analyses. In either case, the presence of 3 β MeHs suggests that bacterial methane cycling was occurring at the time that the Vazante Group shales were accumulating.

Steranes – Like the hopanes, steranes, measured on MRM $M^+ \rightarrow 217$ mass chromatograms, are present in the Vazante samples but in low concentrations (0.000-0.021 ng/g). Again, the samples from core MAF-42.88 have the highest total sterane concentrations. In spite of the low concentrations, all regular and rearranged forms of the C₂₆-C₃₀ steranes and diasteranes are present in the Vazante samples. The C₂₇-C₂₉ steranes dominate each sample. When plotted on a ternary diagram (Figure 3.23) the samples plot closely together and in the same location as samples from the Olcott study. They also overlap with the Bitumen 2 steranes from Study 3 (Figure 3.24).

C₃₀ steranes, which represent 2.1-5.7% of the total C₂₇-C₃₀ steranes in the Vazante samples, are likely products of chrystophytes, a common photosynthesizing marine algae (Raederstorff and Rohmer, 1984). Therefore, the presence of C₃₀ steranes is an important indicator of marine organic matter input. 24-Isopropylcholestane (24-IPC), a C₃₀ sterane indicative of demosponges (Bergquist et al., 1980) was not detected in any of the samples. 24-IPC was however, identified during the course of the Olcott study (Olcott, 2006). Given the absence of 24-IPC in our samples as well as probable euxinic depositional conditions for the Mocambo shale (Olcott et al., 2005), we suggest that the 24-IPC identified in the Olcott study was either misidentified or a contaminant.

Aromatics – Aromatic hydrocarbons detected in the Vazante samples consist mainly of low molecular weight polycyclic aromatic hydrocarbons (PAHs). Aryl

isoprenoids, measured on the $m/z=133$ selected ion chromatogram, are present in two of the Serra do Garrote (B3LF-11-138.2 and 164.2) and four of the Mocambo samples (PPF-2A-227.25, MAF-42.88-811.75, 818, and MAF-009-494.75; Figure 3.25). Aryl isoprenoids are derivatives of the pigment isorenieratene, which is specific to Chlorobiaceae, a green sulfur bacteria (Summons and Powell, 1987). Chlorobiaceae split H_2S (rather than H_2O) using Photosystem I to obtain hydrogen and electrons during anoxygenic photosynthesis and are therefore restricted to environments where H_2S extends into the photic zone.

Additionally, naphthalenes, including the methyl-, dimethyl-, and ethyl- derivatives, measured on $m/z=142$, 156, and 170 selection ion chromatograms, were detected in six samples. While methylated naphthalenes are ubiquitous in sedimentary samples, they are sensitive to thermal alteration and therefore are commonly used as thermal maturation indicators. Methyl- and dimethylnaphthalene ratios (MNR and DNR) calculated from the samples range from 1.1-2.0 and 2.2-4.7, respectively.

3.6.4: Discussion: Syngeneity

Interpretations of biomarkers as evidence for the presence of organisms or metabolisms are only pertinent when they are shown to be syngenetic to the host rock. Since biomarkers from the previous study (Study 2) were thought to be contaminants based on the presence of biomarker compounds in the procedural blanks and a lack of consistency between Bitumen 1 and Bitumen 2 extracts (Study 3), an assessment of the syngeneity of these new Vazante samples is of utmost importance.

If there is non-syngenetic bitumen in the samples from this focused study of the Vazante, it does not appear to be from laboratory contamination. This is based on the low procedural blanks achieved in this study as well as the lack of measurable biomarkers in samples from core MAF-011. Additionally, biomarkers from the Serra do Poço Verde samples analyzed in this study are consistent with the results from Olcott et al. (2005) from the same horizon. Relative abundances of the C₂₇-C₂₉ regular steranes from this study plotted on a ternary diagram along with the steranes from the Olcott study, show that despite being processed in separate laboratories the steranes still display similar distributions (Figure 3.23).

Determining if non-syngenetic bitumen was introduced to the rock prior to sampling is a more difficult task. Two lines of evidence have been examined in order to test the syngeneity of the extracted biomarkers. First, all of the compounds identified in the samples are consistent with Precambrian organic matter; compounds restricted to Phanerozoic organic matter are not present in the Vazante samples. Secondly, the thermal maturity ratios calculated from extracted biomarkers (Table 3.12) are consistent with each other and with the low metamorphic grade of the eastern Vazante Basin (temperatures <130°C; Azmy et al., 2001). The hopane rearrangement ratios (C₃₂S/(S+R) and $\beta\alpha C_{30}H/(\beta\alpha C_{30}H + \alpha\beta C_{30}H)$) and the sterane S/(S+R) ratio have reached equilibrium meaning that the samples have entered the peak stage of oil generation, a process that typically occurs at temperatures between 50 and 150°C (Tissot and Welte, 1984). Additionally, the $\beta\beta/(\beta\beta + \alpha\alpha)$ sterane ratio is below equilibrium for all samples indicating that although the samples have entered the peak stage of oil generation, they have not surpassed it. This is further supported by the MNR and DNR ratios, which

when greater than 0.9, indicate mature, oil-generating samples (Radke et al., 1982). In sum, it seems reasonable that the biomarkers analyzed in this focused study of the Vazante Group are syngenetic.

Since it seems likely that the biomarkers analyzed in this study are syngenetic to the depositional age and environment of the Vazante Group, we can use these to evaluate the co-evolution of life and environment in response to rapidly changing environmental conditions.

3.6.5: Discussion: Environmental and Biological Conditions of the Vazante Group

Comparison of biomarkers from Serra do Garrote, Serra do Poço Verde, and Lapa samples will help us to understand the impact that Vazante glaciations had on early life and ocean chemistry. The Serra do Garrote Formation represents the slow accumulation of sediments that were deposited before the commencement of the Vazante ice ages. Therefore, interpretations of biomarkers from the Serra do Garrote Formation characterize the biological conditions that were present during the environmentally stable period before glaciations. The Serra do Poço Verde and Lapa formations on the other hand, represent sedimentation at the end of two discrete glacial episodes. Interpretations of biomarkers from these units therefore characterize biological and environmental conditions in the wake of rapidly changing environmental conditions.

Biologically informative biomarkers, which were present in all samples from this focused study, point to a microbial community that consisted of phototrophic bacteria ($2\alpha\text{MeH}$), chemoautotrophic bacteria ($28,30\text{-DNH}$), eukaryotic algae (C_{30} steranes), and aerobic or microaerophilic proteobacteria ($3\beta\text{MeH}$). Aryl isoprenoids however, which are diagnostic of green sulfur bacteria, were present only in samples from the Serra do

Garrote and Serra do Poço Verde formations; they were absent in samples from the Lapa Formation. This is consistent with previous biomarker studies of the Vazante Group. Olcott et al. (2005) identified aryl isoprenoids in three Serra do Poço Verde (Mocambo) samples (depths 805, 810, and 812 m) from core MAF-42.88. This is the same core and depth interval found to contain aryl isoprenoids in this study. Additionally, Brody (2007) reported finding no aryl isoprenoids in five Lapa samples analyzed from an adjacent core (MAF-134.86). Therefore, the presence of aryl isoprenoids in the Serra do Poço Verde Formation and lack of aryl isoprenoids in the Lapa Formation is supported by two independent studies. Additionally, no previous biomarker work has focused on samples from the Serra do Garrote Formation, therefore the aryl isoprenoids discovered in samples from this unit and presented here are novel.

The implications of the aryl isoprenoids identified in only the lower two shale units is that euxinic conditions extending into the photic zone were prevalent before and in the immediate aftermath of the Serra do Poço Verde glaciation but that water column H₂S either receded or collapsed prior to the deposition of the Lapa Formation. The loss of euxinic conditions in the photic zone could readily be caused by increased oxygenation of the surface water. This could shift the boundary between oxic and euxinic water out of the photic zone until it settled deeper in the water column. If this were the case, one would expect to see increased oxygenation reflected in other redox sensitive biomarker parameters. However, Pr/Ph and %C₃₅H from the Lapa samples are consistent with those from both the Serra do Garrote and Serra do Poço Verde samples. Another possibility for the absence of photic zone euxinia in the Lapa is that the water column was no longer rich in H₂S. The local accumulation of iron-formation associated with the Lapa ice age

supports this explanation. This is because any Fe^{2+} introduced into a H_2S rich environment would immediately precipitate out as highly insoluble pyrite ($\text{Fe}^{2+} + \text{H}_2\text{S} \rightarrow \text{FeS}_2$). Thus, in order for Fe to accumulate as oxide cements and local iron-formation H_2S in the water column had to be absent (Canfield, 1998).

3.6.6: *Conclusions*

Taken together, the biomarker distributions present in the Vazante samples depict a redox stratified environmental setting that supported a diverse microbial community including phototrophic bacteria, chemoautotrophic bacteria, eukaryotic algae, and aerobic or microaerophilic proteobacteria. Green sulfur bacteria were also present, but only in the Serra do Garrote and Serra do Poço Verde water columns. This is corroborated by other biomarker studies which also identified aryl isoprenoids in the Serra do Poço Verde Formation (Olcott et al., 2005) but not in the Lapa Formation (Brody, 2007). The presence of green sulfur bacteria in sediments deposited before and immediately after the Serra do Poço Verde glaciation suggest that euxinic conditions extending into the photic zone may have been prevalent throughout much of the Vazante deposition. However, photic zone euxinic conditions appear not to be present when the Lapa Formation was deposited.

Table 3.10: Abundances of total *n*-alkanes, pristane (Pr), phytane (Ph), total steranes and total hopanes from this focused analysis of Vazante Group. Total hopanes and total steranes are the sum of all regular hopanes and steranes. Abundances are reported as ng/g of extracted sample.

Formation or Member	Core	Depth (m)	Mass (g)	Total <i>n</i> -Alkanes (ng/g)	Pr (ng/g)	Ph (ng/g)	Total Steranes (ng/g)	Total Hopanes (ng/g)
Lapa	MAF-45	191.1	105.0	0.07	0.002	0.005	0.023	0.093
Lapa	MAF-45	197.1	102.1	0.39	0.004	0.009	0.005	0.011
Mocambo	MAF-42.88	811.75	76.79	0.34	0.073	0.088	0.173	0.619
Mocambo	MAF-42.88	818	101.5	0.00	0.001	0.001	2.10	8.46
Mocambo	MAF-009	474.75	102.0	---	0.014	0.035	0.007	0.015
Mocambo	MAF-009	476.85	103.8	0.03	0.001	0.003	0.003	0.004
Mocambo	PPF-2A	227.25	73.68	0.13	0.003	0.003	0.007	0.025
Mocambo	MAF-45	239.12	76.16	0.04	0.000	0.000	0.005	0.010
Garrote	B4LS01	138.2	73.38	0.06	0.005	0.008	0.009	0.027
Garrote	B4S01	164.2	102.3	0.09	0.024	0.034	0.042	0.258
Garrote	B4LS01	207.8	78.35	0.05	0.001	0.002	0.004	0.007

Table 3.11: Source related biomarker ratios from the Vazante Group. S/H describes the relative input from eukaryotes compared with prokaryotes. Pr/Ph <1 is typical of anoxic conditions (Didyk et al., 1978). %C₃₅H<5% indicates less reducing conditions (Cao et al., 2009). % 28,30-DNH>0.5 is typical of reducing environments (Seifert et al. 1978; Grantham et al., 1980; Schoell et al., 1992), %C₃₀ steranes are indicative of marine algae (Raederstorff and Rohmer, 1984).

Formation or Member	Core	Depth (m)	S/H	Pr/Ph	%C ₃₅ H	% 28,30-DNH	% C ₃₀ Steranes
Lapa	MAF-45	191.1	0.32	0.44	3.0	6.1	3.6
Lapa	MAF-45	197.1	0.40	0.50	---	9.4	7.2
Mocambo	MAF-42.88	811.75	0.31	0.83	3.4	6.1	6.0
Mocambo	MAF-42.88	818	0.29	1.1	2.2	7.4	2.5
Mocambo	MAF-009	474.75	0.47	0.84	3.0	4.7	4.7
Mocambo	MAF-009	476.85	0.64	0.53	---	12	7.9
Mocambo	PPF-2A	227.25	0.32	0.42	2.2	4.5	3.2
Mocambo	MAF-45	239.12	0.38	0.46	---	6.7	4.7
Garrote	B4LS01	138.2	0.37	0.64	1.8	4.5	2.8
Garrote	B4S01	164.2	0.19	0.71	2.9	2.7	5.0
Garrote	B4LS01	207.8	0.53	0.61	---	8.5	5.9

* S/H=total steranes/total hopanes, Pr/Ph=pristane/phytane, %C₃₅H=(C₃₅ hopane (R+S)/C₃₁-C₃₅ (R+S) hopanes)*100, %28,30-DNH=(28,30-DNH/(28,30-DNH+αβC₃₀H))*100, %C₃₀ steranes=(C₃₀ steranes (ααS+ββR+ααR+ββS)/C₂₇-C₃₀ steranes (ααS+ββR+ααR+ββS))*100.

Table 3.12: Maturity related biomarker ratios from this focused study of the Vazante Group. Ts/(Ts+Tm) increased from 0-1 through the immature-overmature range. The maturity related ratios are in agreement with each other and suggest that the Vazante Group samples are mature and are in the peak stages of oil generation.

Formation or Member	Core	Depth (m)	Ts/(Ts+Tm)	C ₃₂ S/(S+R) hopane	$\beta\alpha C_{30}H / \beta\alpha C_{30}H + \alpha\beta C_{30}H$	S/(S+R) $\Sigma C_{27-C_{29}}$ Steranes	$\beta\beta / (\beta\beta + \alpha\alpha) \Sigma C_{27-C_{29}}$ Steranes	MNR	DNR
Lapa	MAF-45	191.1	0.54	0.66	0.05	0.60	0.62	---	---
Lapa	MAF-45	197.1	0.43	0.72	0.08	0.52	0.66	1.7	4.7
Mocambo	MAF-42.88	811.75	0.32	0.69	0.07	0.60	0.56	1.6	3.5
Mocambo	MAF-42.88	818	0.32	0.63	0.07	0.65	0.56	---	---
Mocambo	MAF-009	474.75	0.40	0.63	0.09	0.58	0.55	---	---
Mocambo	MAF-009	476.85	0.46	0.52	0.07	0.52	0.47	---	---
Mocambo	PPF-2A	227.25	0.42	0.65	0.06	0.57	0.66	1.4	2.6
Mocambo	MAF-45	239.12	0.40	0.72	0.08	0.51	0.63	2.0	4.2
Garrote	B4LS01	138.2	0.38	0.61	0.09	0.56	0.64	---	---
Garrote	B4S01	164.2	0.42	0.65	0.09	0.59	0.70	1.1	2.2
Garrote	B4LS01	207.8	0.50	0.60	0.11	0.51	0.59	---	---

* MNR=2-methylnaphthalene/1-methylnaphthalene, DNR=(1,6-dimethylnaphthalene+2,7-dimethylnaphthalene)/1,5-dimethylnaphthalene.

2A_227_25 + 25 ng D4

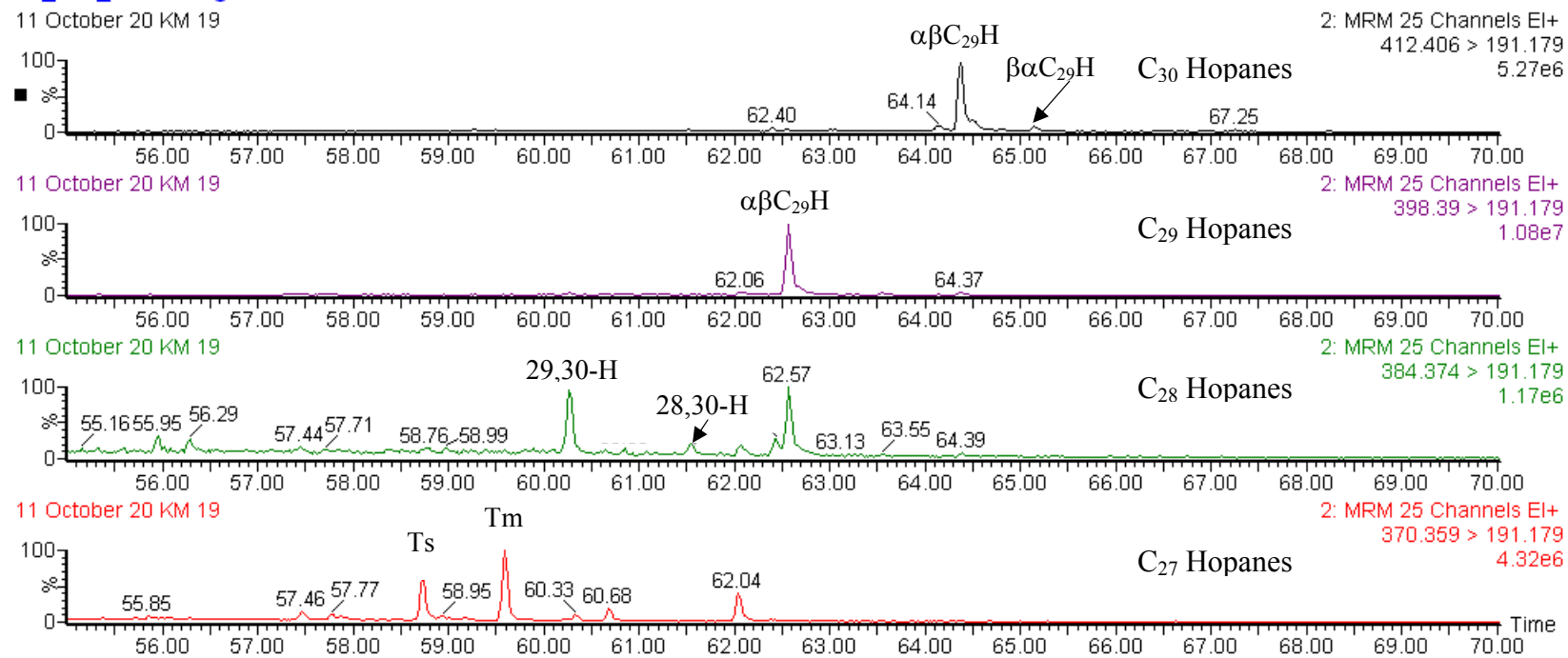
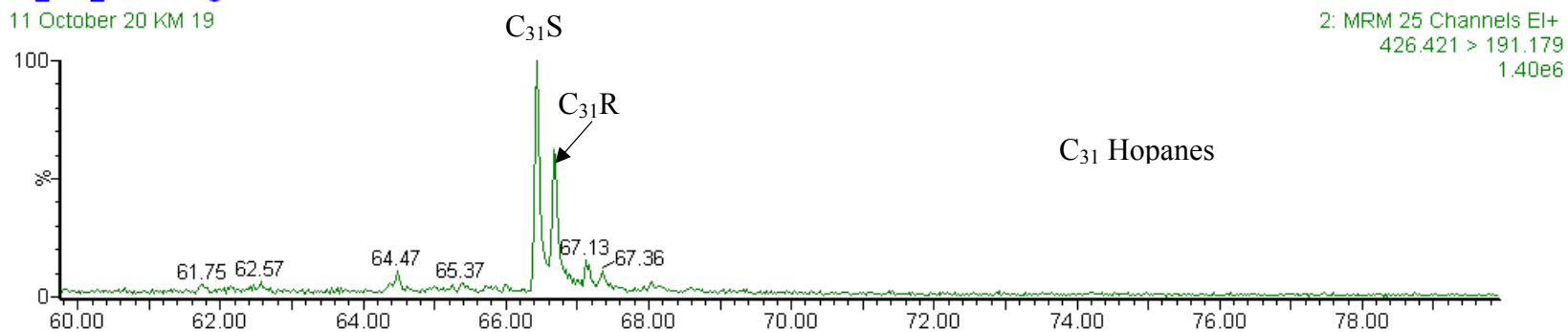


Figure 3.21: $\text{M}^+ \rightarrow 191$ transitions from MRM-GCMS analysis of a sample PPF-2A-227.25. The x-axis is residence time and the y-axis is peak intensity.

2A_227_25 + 25 ng D4

11 October 20 KM 19



11 October 20 KM 19

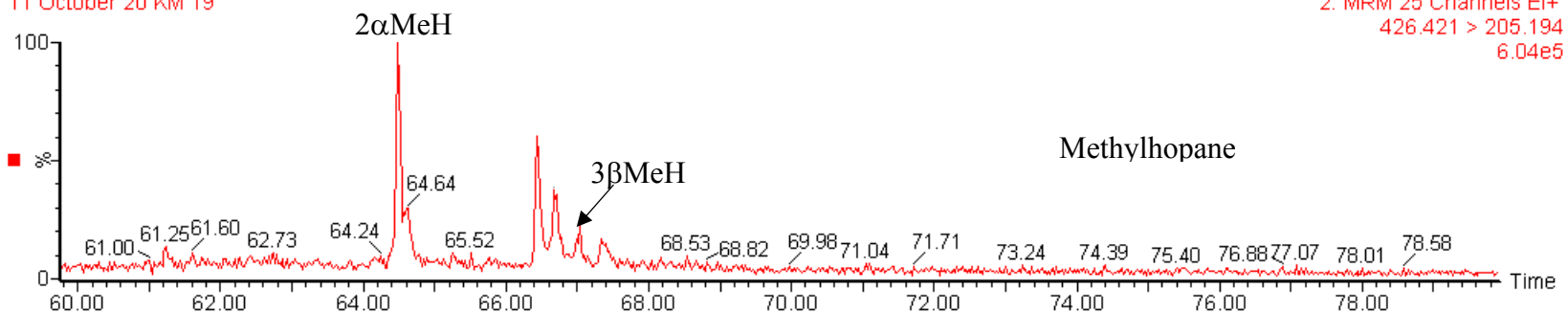


Figure 3.22: $M^+ \rightarrow 205$ transitions from MRM-GCMS analysis of a sample PPF-2A-227.25 showing the methylhopanes and where they elute in relation to the C_{31} extended hopanes ($M^+ \rightarrow 191$). $2\alpha\text{MeH}$ is 2α -methylhopane and $3\beta\text{MeH}$ is 3β -methylhopane. The x-axis is residence time and the y-axis is peak intensity.

Steranes

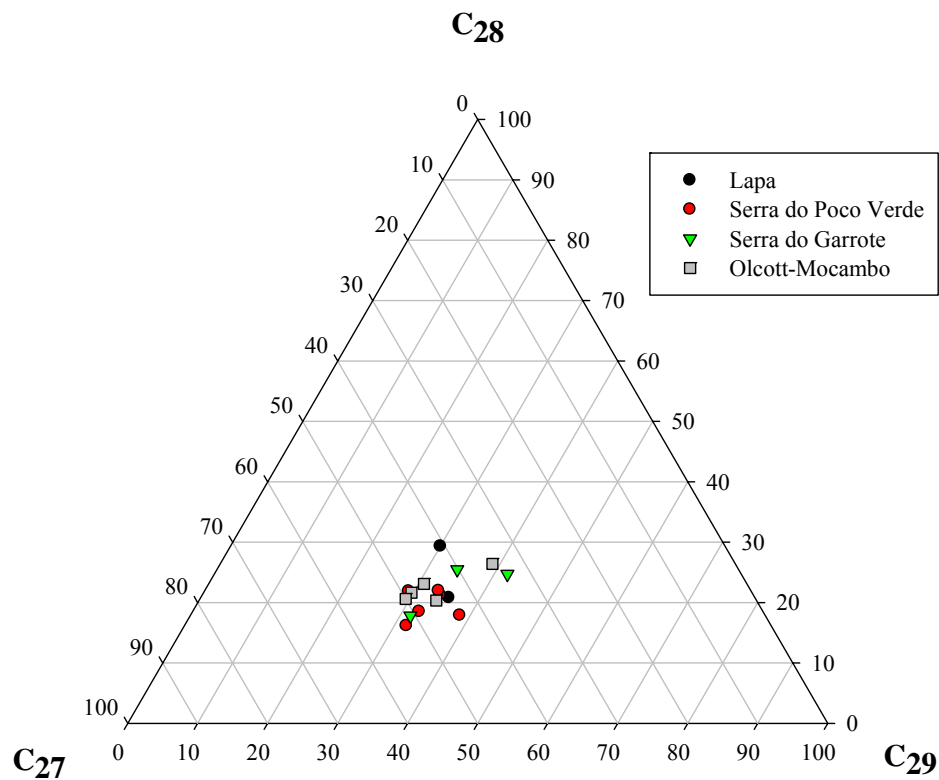


Figure 3.23: Ternary diagram of the C₂₇-C₂₉ steranes from this focused study of the Vazante Group along with values reported by Olcott (2006).

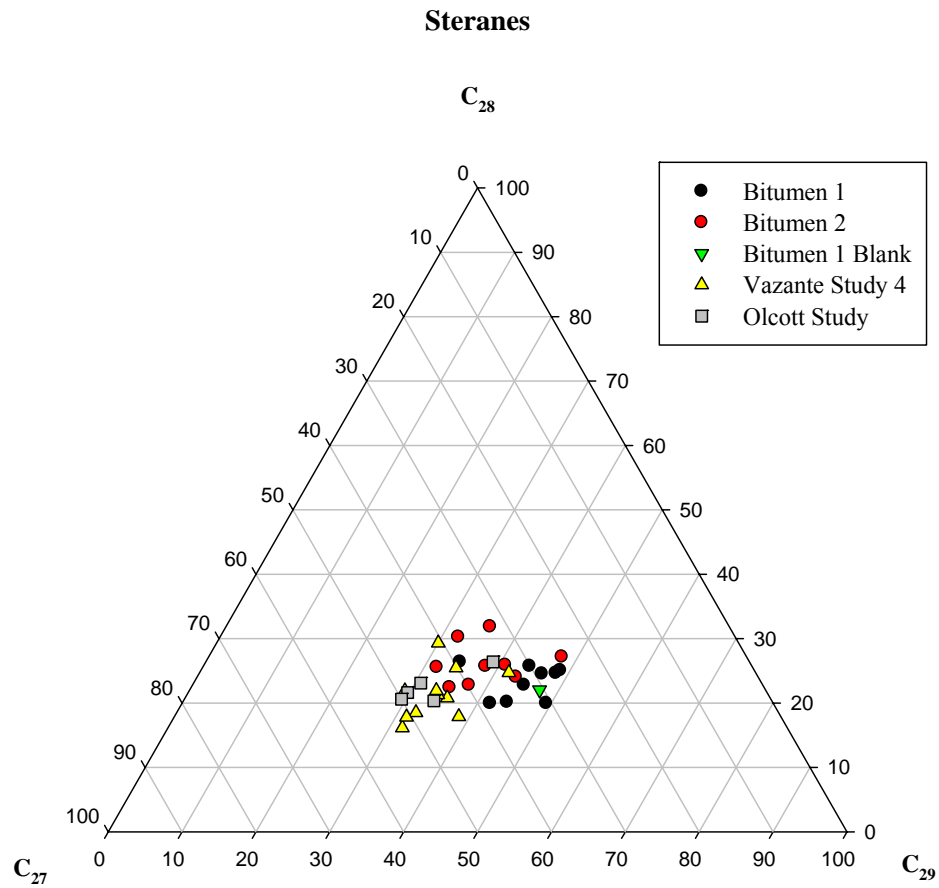


Figure 3.24: Ternary diagram of the C_{27} - C_{29} steranes from this focused study of the Vazante Group along with Bitumen 1 and 2 results from Study 3 and values reported by Olcott (2006).

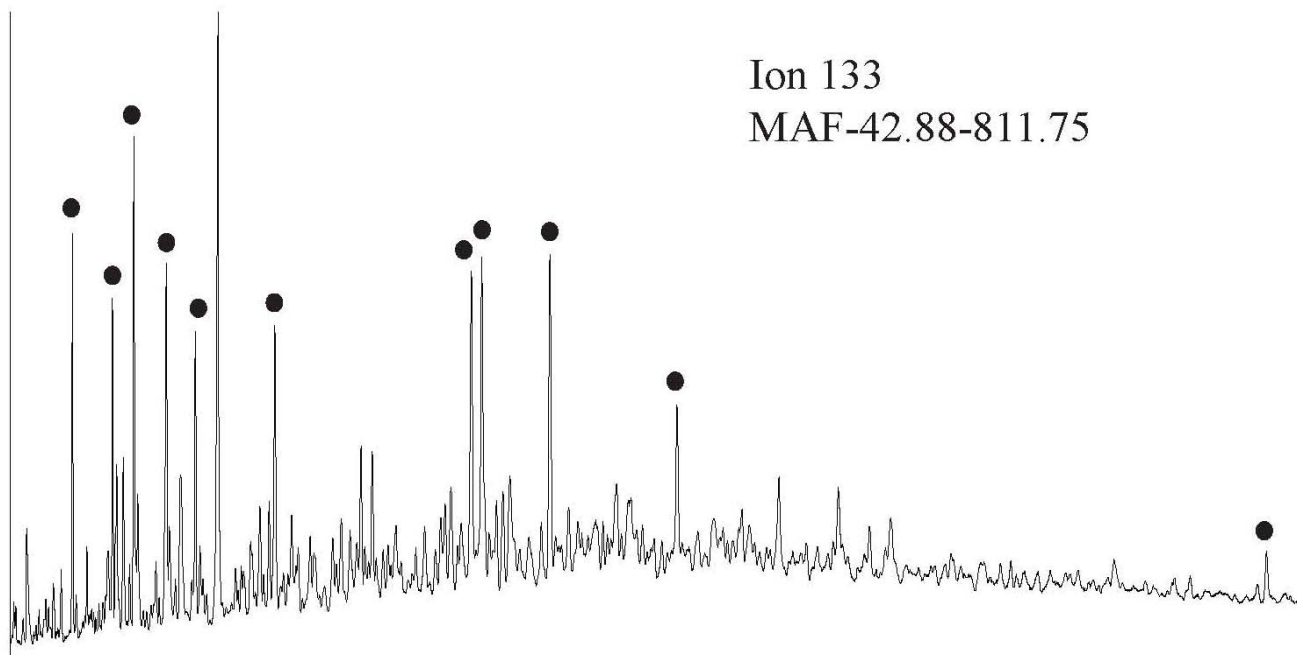


Figure 3.25: Selected ion chromatogram (m/z 133) from sample MAF-42.88-811.75. Aryl isoprenoids are indicated by ●. The x-axis is residence time and the y-axis is peak intensity.

Chapter 4: Speculations on Mesoproterozoic (?) biological, environmental, and climatic change

The various studies in this dissertation provide time-series isotopic and biomarker constraints that may be combined to evaluate biological diversity and environmental complexity in the marine environment associated with evidence for two discrete ice ages in the Mesoproterozoic (?) upper Vazante Group of south-central Brazil.

4.1: Review of Geologic Interpretations

The association of diamictite with thick, well-preserved carbonate and organic-rich shale intersected in unmineralized exploratory drill cores throughout the Vazante Basin sparked initial interest in this integrated project. Previous studies interpret the Mocambo diamictite, within the Serra do Poço Verde Formation, as possibly being related to a Neoproterozoic global glaciations (aka Snowball Earth; Azmy et al., 2001; 2006; Olcott et al., 2005) although radiometric age constraints were lacking. Because the dropstone-laden Macombo shale was sandwiched between carbonate diamictite and contained glendonite (a cold water carbonate precipitate), it had been interpreted as syn-glacial in origin, and hence biomarker distributions within the unit were used to infer active photosynthesis during the ice age (Olcott et al., 2005), which was a conclusion at odds with the end member hard Snowball hypothesis (Hoffman et al., 1998; Hoffman and

Schrag, 2002). However, detailed investigations of several cores suggested that the overlying carbonate diamictite lies unconformably above the Mocambo shale and likely represent glacial deposits of the younger Lapa ice age (Figure 1.5)

Additionally, coupled Re-Os and detrital zircon U-Pb ages (Geboy, 2006; Azmy et al., 2008; Rodrigues et al., 2008) suggest discordant ages for the lower and upper Vazante Group, both of which contain lithological evidence for glaciation. These studies indicate that the lower Vazante Group is likely Neoproterozoic in age whereas the upper Vazante Group is older, representing late Mesoproterozoic deposition (ca. 1.3 to 1.0 Ga). A reverse fault, which is evident in field outcrop localities of the Lagamar Formation (Figure 1.6), provides a possible explanation for the superposition of older Mesoproterozoic strata on top of a younger Neoproterozoic succession.

In sum, the results of this study allow me to speculate that the Serra do Poço Verde diamictite and overlying Mocambo shale (as well as the Morro do Calcário diamictite and overlying Lapa shale) represent sedimentation during two discrete post-glacial transgressions in the Mesoproterozoic, a time previously thought to be ice-free. Given this possibility, the coupled isotopic and biomarker study presented here is compared against similar results from three units, including the Neoproterozoic Doushantuo Formation of South China and the Mesoproterozoic Roper and Atar groups of northern Australia and west Africa, respectively.

4.2: Geobiology of the Serra do Poço Verde Formation

Taking only our most confident results into consideration, biomarkers from the organic-rich Mocambo shale, in concert with isotopic analysis of associated carbonates

and shale, broadly corroborate the results of the Olcott et al. (2005) study. These authors found the same consortium of microorganisms identified in our study, including eukaryotic algae, microaerophilic bacteria, and oxygenic and anoxygenic photosynthesizers. These microorganisms, now identified throughout the basin, would only have co-existed if the water column exhibited a strong, but shallow, chemocline with oxic surface water overlaying euxinic water. Euxinic conditions must have existed in the photic zone in order to support anoxygenic photosynthesis; a process that requires sunlight and a source of H₂S.

The existence of a stratified, euxinic water column is supported by time-series sulfur isotope trends documented in this study (see Chapter 2) as well as sulfur isotopic and iron speciation measurements conducted by Geboy et al. (in prep; Figure 4.1). Iron speciation is the measurement of biogeochemically highly reactive iron (FeHR) relative to total iron (FeT). In modern oxic environments a value of FeHR/FeT <0.38 is expected, but in anoxic environments the ratio is believed to be >0.38. Additionally, the proportion of sulfide bound sulfur (FeS) relative to FeHR is typically >0.8 in euxinic basins (Raiswell and Canfield, 1998). The results shown in Figure 4.1 illustrate the transition from anoxic to progressively euxinic conditions through the Mocambo interval, which then shift to oscillating oxic/anoxic conditions above the shale in core MAF-42.88. Notably, the transition to euxinic conditions is accompanied by a positive shift in the $\delta^{34}\text{S}_{\text{py}}$, which is similar to a time-series sulfur isotope trend through the Mocambo shale in core MAF-45 (see also Figure 2.2). This may be the result of intense BSR on a limited sulfate pool, which would progressively distill the lighter ³²S and lead to the enrichment of ³⁴S in shallow marine sulfate and therefore to coeval sedimentary sulfides. Thus, the

strong up-section ^{34}S enrichment relative to seawater compositions inferred from CAS studies (Azmy et al., 2001) provides evidence that sulfate was limited in the depositional environment (Habicht and Canfield, 1997; Canfield, 2001; Habicht et al., 2002).

4.3: Time-series Comparison of the Vazante Shales

Time-series biomarker and isotopic data from the three shale intervals of the upper Vazante Group capture a transition from a stratified/euxinic ocean (represented by the Serra do Garrote and Mocambo shales) to a still stratified but no longer euxinic water column (represented by the Lapa shale). While biomarker ratios from the Serra do Garrote, Serra do Poço Verde, and Lapa formations are comparable (Table 3.10) and the suite of microorganisms identified are similar, only the Serra do Garrote and Serra do Poço Verde show biomarker evidence for anoxygenic photosynthesis performed by green sulfur bacteria. Thus, euxinic conditions, which necessarily must have existed shallow in the water column so that H_2S splitting anoxygenic photosynthesizers would have access to sunlight, were present before and in the immediate aftermath of the Serra do Poço Verde glaciation but then receded prior to the end of the Lapa glaciation.

The variability (or lack thereof) in time-series isotopic analyses in conjunction with measurements of the fractionation between oxidized and reduced carbon and sulfur pools may inform us about the relative sizes of various reservoirs in these ancient oceans. Notably, the pre-glacial Serra do Garrote Formation is characterized by an invariant $\delta^{13}\text{C}_{\text{org}}$ trend up-section (Figure 2.2). In this unit the $\delta^{13}\text{C}_{\text{org}}$ signatures all hover around -30‰ over ca. 80 m of section, suggesting the presence of a large DOC pool that potentially buffered the oceanic carbon cycle (Rothman et al., 2003; McFadden et al.,

2008; Swanson-Hysell et al., 2010). Based on a few outcrop samples of carbonates near this stratigraphic horizon (Azmy et al., 2001; ca. +3.2‰), the magnitude of carbon isotope fractionation for the Serra do Garrote is estimated at ~33‰. Invariance in the organic carbon trends is also characteristic of the post-glacial Serra do Poço Verde shale in core MAF-45 (Figure 2.2) and in core MAF-42.88 (Figure 4.1), with values near -30 and -26‰, respectively. Similar stratigraphic invariance in organic carbon records is noted in the Neoproterozoic Doushantuo Formation in South China, which displays a remarkably stable $\delta^{13}\text{C}_{\text{org}}$ signature (ca. -30‰) over ~80 m of section (McFadden et al., 2008), and in the Mesoproterozoic Roper Group in northern Australia, which hovers around -33‰ over ~100 m of strata (Johnston et al., 2008).

In contrast, a strong positive up-section shift in the $\delta^{13}\text{C}_{\text{org}}$ characterizes core samples from the Lapa Formation. The 3 to 5‰ shifts observed in the Lapa cores (MAF-45 and B3LF-11) correspond to negative anomalies in the $\delta^{13}\text{C}_{\text{carb}}$ record from the Lapa Formation (Figure 2.3; Brody, 2007; Azmy et al., 2001; 2006). I speculate that progressive oxidation of the DOC pool (thus decreasing its size relative to the DIC pool) in the post-glacial Lapa environment was the cause of the carbon isotope excursion. This might result from carbon limitation (i.e. where both ^{12}C and ^{13}C are fixed with less discrimination between the two during photosynthesis) so that the fractionation between oxidized and reduced reservoirs is less than expected.

While the $\delta^{13}\text{C}_{\text{org}}$ signature differs only slightly between the three formations, the $\delta^{34}\text{S}_{\text{py}}$ signature exhibits signs of major rearrangements in the sulfur cycle. The $\delta^{34}\text{S}_{\text{py}}$ values from all three formations are enriched relative to sulfides forming from expected seawater sulfate and measured CAS (reported by Azmy et al., 2001). This decreased

fractionation between sedimentary sulfides and seawater sulfate most likely represents BSR acting on a limited sulfate pool (i.e. the rate of sulfate consumption is \geq the rate of sulfate supply; Zaback et al., 1993). The stable signal in the Serra do Garrote Formation suggests stasis in the sulfur cycle prior to glaciations. A negative shift in the $\delta^{34}\text{S}_{\text{py}}$ in the Lapa Formation (core MAF-45; Figure 2.1) however, could reflect re-oxidation of bacterially reduced (and therefore isotopically light) H_2S . Additionally, the presence of an inverse fractionation in the Lapa signal from core B3LF-11 could reflect the decoupling of the surface- and deep-water sulfur pools in a stratified water column. This could occur if the CAS value for the Lapa Formation (ca. +22‰; Azmy et al., 2001) is representative of surface water (i.e. an open system) and the $\delta^{34}\text{S}_{\text{py}}$ was derived from closed-system bottom-water (e.g. sediment pore space isolated from sulfate input) where BSR on a limited sulfate source lead to increasingly heavy sulfate and therefore sulfide (Shen et al., 2010). If the water column remained largely anoxic but the H_2S boundary was pushed into the sediments then this would allow for the accumulation of ferrous iron (forming iron oxide cements and localized iron-formation associated with the Lapa) at least along the coastal rim of the Vazante Basin. The lack of biomarker evidence for anoxygenic photosynthesis in the Lapa Formation as well as geologic evidence for the build up of ferrous iron supports this view.

The conclusion that prior to the Lapa glaciation the ocean water was stratified and euxinic has implications for the timing of key biological events, such as the radiation and diversification of eukaryotes, as H_2S -rich water would be a hindrance for most aerobic life. This is evident in our biomarker study as sterane/hopane ratios in all samples are low, indicating a bacterially dominated microbial community. It is also consistent with

the fossil record of eukaryotic diversification, which suggests that the rapid rise of eukaryotes occurred in shallow, near-shore environments (Butterfield, 2000; Javaux et al., 2001) where euxinic conditions are less likely to occur.

4.4: Life and Environment in the Mesoproterozoic

The transition from a H₂S-rich stratified ocean to a stratified ocean with H₂S restricted to the sediment or deep water as recorded in the biomarkers and carbon and sulfur isotopic signatures from the upper Vazante Group is significant, especially if this represents Mesoproterozoic deposition. The traditional view of the Mesoproterozoic is that it represents a period of biogeochemical stasis in which the oceans were at least mildly oxygenated (Holland, 1984, 2003). This is based on the relative stability of the ¹³C_{carb} isotopic signatures from the known Mesoproterozoic stratigraphic units (Brasier and Lindsay, 1998) as well as a billion year hiatus in the accumulation of banded iron formation (BIF) starting at ca. 1.8 Ga (Holland et al., 1984, 2003, 2005; Hoffman et al., 1998). However, the consensus now is that rather than being oxygenated, the oceans were dominantly euxinic during the Mesoproterozoic (Canfield, 1998). The presence of H₂S, rather than O₂, would have titrated any available ferrous iron out of the water column, thus potentially leading to the billion-year gap in the BIF record.

Much evidence for this “sulfur-ocean” comes from sulfur isotopic and biomarker studies of the late Paleo-Mesoproterozoic McArthur Basin, Australia (Canfield, 1996; Shen, 2002; Brocks, 2005; Johnston, 2008; among others). One study of note identified abundant aryl isoprenoids and the biomarkers they derive from (chlorobactane and isorenieratane) in the 1.64 Ga Roper Group in the McArthur Basin, suggesting euxinic

conditions in the photic zone during the early Mesoproterozoic (Brocks, 2005). In contrast, a recent study identified biomarkers indicative of anoxic conditions as well as aryl isoprenoids in the late Mesoproterozoic Tourist Formation in the Atar Group, Martinique (Blumenberg, in press). The Atar Group is bracketed by unconformities, which have been interpreted to have a glacial origin based on the presence of erradics and laterally extensive glacial diamictites and cap dolostones (Trompette, 1973; Deynoux, 2006). Additionally, based on new Re-Os ages (Rooney, 2010) this unit may have been deposited concurrently with the upper Vazante Group. The marriage of geochronological and biomarker data from these two widely separated basins therefore provide support for the Mesoproterozoic age of the Vazante Group. Thus, if the biomarkers analyzed in this study are syngenetic and if the upper Vazante Group is late Mesoproterozoic in age (1.3-1.0 Ga), then the presence of euxinic conditions, as indicated by aryl isoprenoids, sulfur isotopic analysis, and iron speciation, in the pre- and post- Serra do Poço Verde shales suggests an extended interval of H₂S-rich oceanic conditions spanning the entire Mesoproterozoic.

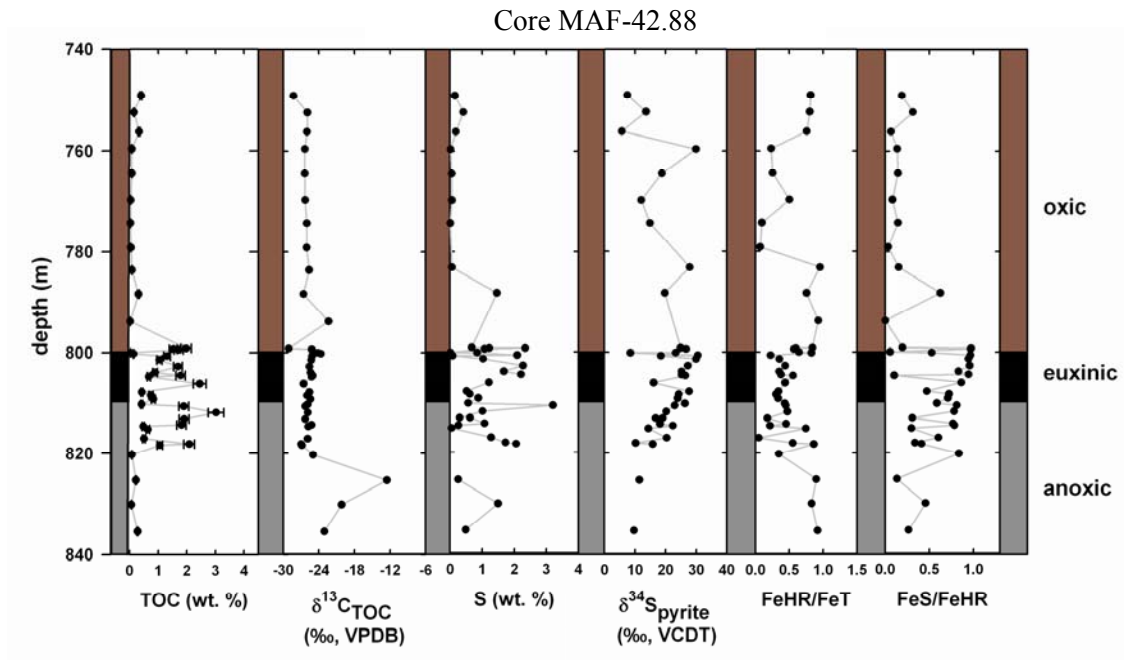


Figure 4.1: Time series elemental and stable isotope compositions of the Serra do Poço Verde Formation shale. Iron speciation data illustrates the susceptibility of iron to be mobilized during early diagenesis under oxic, anoxic or euxinic conditions. FeHR is biogeochemically highly reactive iron, FeT is total iron, and FeS is highly reactive iron bound in sulfide species. $\text{FeHR}/\text{FeT} > 0.38$ are indicative of anoxic conditions; where this is coupled with $\text{FeS}/\text{FeHR} > 0.8$ it is indicative of euxinic conditions (Raiswell and Canfield, 1998). Modified from Geboy et al. (in prep.).

Appendix A: Precision of Biomarker Measurements

Table A-1: Typical analytical uncertainties for SIM-GC-MS and MRM-GC-MS

analyses shown as % error (1σ).

Compound	GC-MS SIM	MRM-GC-MS
<i>n</i> -Alkanes	2% (1σ)	---
Hopanes	2% (1σ)	5% (1σ)
Steranes	6% (1σ)	3% (1σ)

Table A-2: Typical peak area integration uncertainties for SIM-GC-MS and MRM-GC-MS analyses shown as % error (1σ). The uncertainties for Study 4 are based on the final focused study of the archived core material from the Vazante Group.

Compound	SIM-GC-MS		MRM-GC-MS		
	ASE Extract	Sonication Extract	Bitumen 1	Bitumen 2	Study 4
<i>n</i> -Alkanes	0.5% (1σ)	0.8% (1σ)	---	---	---
Hopanes	0.7% (1σ)	1.5% (1σ)	0.3% (1σ)	7.5% (1σ)	5% (1σ)
Steranes	1.6% (1σ)	2% (1σ)	0% (1σ)	0.5% (1σ)	0% (1σ)

Bibliography

- Azmy, K., Kaufman, A.J., Misi, A., Oliveira, T.F. "Isotope stratigraphy of the Lapa Formation, Sao Francisco Basin, Brazil: implications for Late Neoproterozoic glacial events in South America." *Precambrian Research*, 2006: 231.
- Azmy, K., Kendall, B., Creaser, R.A., Heaman, L., Oliveira, T.F. "Global correlation of the Vazante Group, Sao Francisco Basin, Brazil: Re-Os and U-Pb radiometric age constraints." *Precambrian Research*, 2008: 160.
- Azmy, K., Viexer, J., Misi, A., de Oliveira, T.F., Sanches, A.L., Dardenne, M.A. "Dolomitization and isotope stratigraphy of the Vazante Formation, Sao Francisco Basin, Brazil." *Precambrian Research*, 2001: 303-329.
- Babinski, M., Monteiro, L.V.S., Fetter, A.H., Bettencourt, J.S., Oliveira, T.F. "Isotope geochemistry of the mafic dikes from the Vazante nonsulfide zinc deposit, Brazil." *Journal of South American Earth Sciences*, 2005: 293-304.
- Babinski, M., Vieira, L.C., Trindade, R.I.F. "Direct dating of the Sete Lagoas cap carbonate (Bambui Group, Brazil) and implications for the Neoproterozoic glacial events." *Terra Nova*, 2007: 401-406.
- Bergquist, P.R., Hofheinz, W., Oesterhelt, G. "Sterol composition and classification of the Demospongiae." *Biogeochemical Systematics and Ecology*, 1980: 423-435.
- Blumenberg, M., Thiel, V., Riegel, W., Kah, L.C., Reitner, J. "Biomarkers of black shales formed by microbial mats, Late Mesoproterozoic (1.1 Ga) Taoudeni Basin, Mauritania." *Precambrian Research*, in press.
- Bourbonniere, R.A. Meyers, P.A. "Sedimentary geolipid records of historical changes in the watersheds and productivities of Lakes Ontario and Erie." *Limnology and Oceanography*, 1996: 352-359.
- Bowring, S.A., Grotzinger, J.P., Condon, D.J., Ramezani, J., Newall, M.J., Allen, P.A. "Geochronologic constraints on the chronostratigraphic framework of the Neoproterozoic Huqf Supergroup, Sultanate of Oman." *American Journal of Science*, 2007: 1097.
- Brasier, M.D., Green, O., Shields, G. "Ediacarian sponge spicule clusters from southwestern Mongolia and the origins of the Cambrian fauna." *Geology*, 1997: 303-306.
- Brasier, M.D., Lindsay, J.F. "A billion years of environmental stability and the emergence of eukaryotes: New data from northern Australia." *Geology*, 1998: 555-558.
- Bridigare, R.R., Fluegge, A., Freeman, K.H., Hanson, K.L., Hayes, J.M., Hollander, D., Jasper, J.P., King, L.L., Laws, E.A., Milder, J., Millero, F.J., Fancost, R., Popp, B.N., Steinberg, P.A. "Consistent fractionation of C-13 in nature and in the

- laboratory: Growth-rate effects in some haptophyte algae.” *Global Biogeochemical Cycles*, 1997: 279-292.
- Brocks, J.J., Buick, R., Logan, G.A., Summons, R.E. “Composition and syngeneity of molecular fossils from the 2.78 to 2.45 billion-year-old Mount Bruce Supergroup, Pilbara Craton, Western Australia.” *Geochimica et Cosmochimica Acta*, 2003: 4289-4319.
- Brocks, J.J., Logan, G.A., Buick, R., Summons, R.E. “Archean molecular fossils and the early rise of eukaryotes.” *Science*, 1999: 1033-1036.
- Brocks, J.J., Love, G.D., Summons, R.E., Knoll, A.H., Logan, G.A., Bowden, S.A. “Biomarker evidence for green and purple sulphur bacteria in a stratified Palaeoproterozoic sea.” *Nature*, 2005: 866-870.
- Brocks, J.J., Summons, R.E. “Sedimentary hydrocarbons, biomarkers for early life.” In *Treaties on Geochemistry Biogeochemistry*, edited by W.H. Schlesinger, 63-115. Oxford: Elsevier-Pergamon, 2004.
- Brody, K. “Isotope and organic geochemistry of a unique Proterozoic, postglacial succession: The Lapa Formation, Vazante Group, Brazil.” *Master of Science Thesis*, 2007.
- Brody, K.B., Kaufman, A.J., Eigenbrode, J.L., Cody, G.D. “Biomarker geochemistry of a post-glacial Neoproterozoic succession in Brazil.” *Geological Society of America Annual Meeting (Abstract)*, 2004: 7-10.
- Butterfield, N.J. “Bangiomorpha pubescens n. gen., n. sp.: implications for the evolution of sex, multicellularity, and the Mesoproterozoic/Neoproterozoic radiation of eukaryotes.” *Paleobiology*, 2000: 386-404.
- Campos-Neto, M.C. “Litoestratigrafia, relacoes estratigraficas e evolucao paleogeografica dos grupos Canastra e Paranao (regiao Vazante-Lagamar, MG).” *Rev. Brazil Geocien.*, 1984: 81-91.
- Canfield, D.E. “A new model for Proterozoic ocean chemistry.” *Nature*, 1998: 450-453.
- Canfield, D.E. “Isotope fractionation by natural populations of sulfate-reducing bacteria.” *Geochimica et Cosmochimica Acta*, 2001: 1117-1124.
- Canfield, D.E., Poulton, S.W., Narbonne, G.M. “Late-Neoproterozoic deep-ocean oxygenation and the rise of animal life.” *Science*, 2007: 92-95.
- Canfield, D.E., Teske, A. “Late Proterozoic rise in atmospheric oxygen concentration inferred from phylogenetic and sulphur-isotope studies.” *Nature*, 1996: 127-132.
- Cao, C., Love, G.D., Hays, L.E., Wang, W., Shen, S., Summons, R.E. “Biogeochemical evidence for euxinic oceans and ecological disturbance presaging the end-Permian mass extinction event.” *Earth and Planetary Science Letters*, 2009.
- Close, H.G., Bovee, R., Pearson, A. “Inverse carbon isotope patterns of lipids and kerogen record heterogeneous primary biomass.” *Geobiology*, 2011: 1-11.
- Cloud, P.E. “A working model of the primitive Earth.” *American Journal of Science*, 1972: 537-548.

- Cloud, P.E., Dardenne, M.A. "Proterozoic age of the Bambui Group in Brazil." *Geological Society of America Bulletin*, 1973: 1673-1676.
- Coale, K.H., Fitzwater, S.E., Gordon, T.M., Johnson, K.S., Barber, R.T. "Control of community growth and export production by upwelled iron in the equatorial Pacific Ocean." *Nature*, 1996: 621-624.
- Cody, G. *Carnegie Institution of Washington Geophysical Laboratory*, 2012.
- D'Agrella-Filho, M.S., Pacca, I.G., Renne, P.R., Trindade, R.I.F., Teixeira, W., Raposo, M.I.B., Onstott, T.C. "Paleomagnetism and $40\text{Ar}/39\text{Ar}$ ages of mafic dikes from Salvador (Brazil): new constraints on the Sao Francisco craton APW path between 1080 and 1010 Ma." *Precambrian Research*, 2004: 55-77.
- D'Agrella-Filho, M.S., Pacca, I.G., Renne, R.P., Onstott, T.C., Teixeira, W. "Paleomagnetism of middle Proterozoic (1.01-1.08 Ga) mafic dykes in southeastern Bahia State Sao Francisco Craton, Brazil." *Earth and Planetary Science Letters*, 1990: 332-348.
- Dardenne, M.A. "Lithostratigraphic dedimentary sequences of the Vazante Group." In *IGCP 450 Proterozoic sediment-hosted base metal deposits of western Gondwana (abstr.)*, 48-50. Belo Horizonte, 2001.
- Dardenne, M.A. "Sentese sobre a estratigrafiado Grupo Bambui no Brasil Central." *Trigesimo Congresso Brasileiro de Geologia 2*. 1978. 597-610.
- Demaison, G., Holck, A.J.J., Jones, R.W., Moore, G.T. "Predictive source bed stratigraphy; a guide to regional petroleum occurrence." *Proceedings of the 11th World Petroleum Congress*. London: John Wiley & Sons, 1983. 1-13.
- Derry, L.A., Kaufman, A.J., Jacobsen, S.B. "Sedimentary cycling and environmental-change in the Late Proterozoic-Evidence from stable and radiogenic isotopes." *Geochimica et Cosmochimica Acta*, 1992: 1317-1329.
- Deynoux, M., Affaton, P., Trompette, R., Villeneuve, M. "Pan-African tectonic evolution and glacial events registered in Neoproterozoic to Cambrian cratonic and foreland basins of West Africa." *Journal of African Earth Sciences*, 2006: 397-426.
- Didyk, B.M., Simoneit, B.R.T., Brassell, S.C., Eglinton, G. "Organic geochemical indicators of paleoenvironmental conditions of sedimentation." *Nature*, 1978: 216-222.
- Dowham, W., Bogdanov, M. In *Biochemistry of Lipids, Lipoproteins and Membranes*, edited by D.E. Vance and J.E. Bance, 1. New York: Elsevier, 2002.
- Eglinton, G., Scott, P.M., Besky, T., Burlingame, A.L., Calvin, M. "Hydrocarbons of biological origin from a one-billion-year-old sediment." *Science*, 1964: 263-264.
- Eigenbrode, J.L. "Fossil lipids for life-detection: a case study from the early earth record." *Space Science Reviews*, 2008: 161-185.
- Emrich, K., Vogel, J.C. "Carbon isotope fractionation during precipitation of calcium carbonate." *Earth and Planetary Science Letters*, 1970: 363-.

- Eyles, N. "Glacio-epochs and the supercontinent cycle after ~3.0 Ga: Tectonic boundary conditions for glaciation." *Palaeogeography, Palaeoclimatology, Palaeoecology*, 2008: 89-129.
- Fowler, M.G., Douglas, A.G. "Saturated hydrocarbon biomarkers in oils of Late Precambrian age from Eastern Siberia." *Organic Geochemistry*, 1987: 201-213.
- Frank, T.D., Kah, L.C., Lyons, T.W. "Changes in organic matter production and accumulation as a mechanism for isotopic evolution in the Mesoproterozoic ocean." *Geology*, 2003: 397-420.
- Fuck, R.A., Pimentel, M.M., Silva, L.J.H.D.R. "Compartimentacao Tectonica na porcao oriental da Provincia Tocantins." *SBG, Congresso Brasileiro de Geologia, Balneario de Camboriu*, 1994: 215-216.
- Geboy, N.J. "Rhenium-Osmium age determinations of glaciogenic shales from the Mesoproterozoic Vazante Formation, Brazil." *Master of Science Thesis*, 2006.
- Geboy, N.J., Kaufman, A.J., Walker, R.J., Miller, K.E., Brody, K.B., Sievers, N., Misi, A., de Oliveira, T.F., Azmy, K., Kendall, B., Poulton, S. "Evidence for Mesoproterozoic Ice Ages in Brazil." in prep.
- Grantham, P.J., Lijmbach, G.W.M., Postuma, J. "Origin of crude oils in Oman." *Journal of Petroleum Geology*, 1988: 61-80.
- Grantham, P.J., Postuma, J., DeGroot, K. "Variation and significance of the C27 and C28 triterpane content of a North Sea core and various North Sea crude oils." In *Advances in Organic Geochemistry 1979*, edited by A.G., Maxwell, J.R. Douglas, 29-38. Oxford: Pergamon Press, 1980.
- Grotzinger, J.P., Watters, W.A., Knoll, A.H. "Calcified metazoans in thrombolite-stromatolite reefs of the terminal Proterozoic Nama Group, Namibia." *Paleobiology*, 2000: 334-359.
- Habicht, K.S., Canfield, D.E. "Sulfur isotope fractionation during bacterial sulfate reduction in organic-rich sediments." *Geochimica et Cosmochimica Acta*, 1997: 5351-5361.
- Habicht, K.S., Grade, M., Thamdrup, B., Berg, P., Canfield, D.E. "Calibration of sulfate levels in the Archean ocean." *Science*, 2002: 2372-2374.
- Hallmann, C., Kelly, A.E., Gupta, S.N., Summons, R.E. "Reconstructing deep-time biology with molecular fossils." 2010.
- Harrison, A.G., Thode, H.G. "Mechanisms of the bacterial reduction of sulfate from isotope fractionation studies ." *Transactions of the Faraday Society*, 1958: 84-92.
- Hayes, J.M., Freeman, K.H., Popp, B.N., Hoham, C.H. "Compound-specific isotopic analyses: A novel tool for reconstruction of ancient biogeochemical processes." *Advances in Organic Geochemistry*, 1989: 1115-1128.
- Hayes, J.M., Freeman, K.H., Popp, B.N., Hoham, C.H. "Compound-specific isotopic analyses: a novel tool for reconstruction of ancient biogeochemical processes." *Organic Geochemistry*, 1990: 1115-1128.

- Hayes, J.M., Strauss, H., Kaufman, A.J. "The abundance of C-13 in marine organic matter and isotopic fractionation in the global biogeochemical cycle of carbon during the past 800 Ma." *Chemical Geology*, 1999: 103-125.
- Hoering, T.C. "The conversion of polar organic molecules in rock extracts to saturated hydrocarbons." *Carnegie Institution of Washington Yearbook*, 1980: 251-258.
- Hoffman, P.F., Kaufman, A.J., Halverson, G.P., Schrag, D.P. "A Neoproterozoic Snowball Earth." *Science*, 1998: 1342-1346.
- Hoffman, P.F., Schrag, D.P. "The snowball Earth hypothesis: testing the limits of global change." *Terra Nova*, 2002: 129-155.
- Holland, H.D. "Sedimentary Mineral Deposits and the Evolution of Earth's Near-Surface Environments." *Economic Geology*, 2005: 1498-1509.
- . *The chemical evolution of the atmosphere and oceans*. Princeton, N.J.: Princeton University Press, 1984.
- Holland, H.D. "The geologic history of seawater." *Treatis on Geochemistry*, 2003: 583-625.
- Hollander, D.J., McKenzie, J.A. "CO₂ control on the carbon-isotope fractionation during aqueous photosynthesis: A paleo-CO₂ barometer." *Geology*, 1991: 929-932.
- James, N.P., Narbonne, G.M., Dalrymple, R.W., Kyser, T.K. "Glendonites in Neoproterozoic low-latitude, interglacial, sedimentary rocks, northwest Canada; insights into the Cryogenian ocean and Precambrian cold-water carbonates." *Geology*, 2005: 9-12.
- Javaux, E.J., Knoll, A.H., Walter, M.R. "Morphological and ecological complexity in early eukaryotic ecosystems." *Nature*, 2001: 66-69.
- Johnston, D.T., Farquhar, J., Summons, R.E., Shen, Y., Kaufman, A.J., Masterson, A.L., Canfield, D.E. "Sulfur isotope biogeochemistry of the Proterozoic McArthur Basin." *Geochimica et Cosmochimica Acta*, 2008: 4278-4290.
- Jones, G.E., Starkey, R.J. "Fractionation of stable isotopes of sulfur by micro-organisms and their role in deposition of native sulfur." *Journal of Applied Microbiology*, 1957: 111-115.
- Kah, L.C., Lyons, T.W., Chesley, J.T. "Geochemistry of a 1.2 Ga carbonate-evaporite succession, northern Baffin and Bylot Islands: implications for Mesoproterozoic marine evolution." *Precambrian Research*, 2001: 203-234.
- Kah, L.C., Sherman, A.G., Narbonne, G.M., Knoll, A.H., Kaufman, A.J. "d¹³C isotope stratigraphy of the Mesoproterozoic Bylot Supergroup, northern Baffin Island: Implications for regional lithostratigraphic correlations." *Canadian Journal of Earth Sciences*, 1999: 313-332.
- Kaplan, I.R., Rittenberg, S.C. "Microbiological fractionation of sulphur isotopes." *Journal of General Microbiology*, 1964: 195-212.

- Kaufman, A.J., Knoll, A.H., Narbonne, G.M. "Isotopes, ice ages, and terminal Proterozoic Earth history." *Proceedings of the National Academy of Sciences*, 1997: 6600-6605.
- Kerr, R.G., Baker, B.J. "Marine Sterols." *Natural Product Reports*, 1991: 465-497.
- Kissen, Y.V. "Catagenesis of light acyclic isoprenoids in petroleum." *Organic Geochemistry*, 1993: 1077-1090.
- Klomp, U.C. "The chemical structure of a pronounced series of iso-alkanes in South Oman crudes." *Organic Geochemistry*, 1986: 807-814.
- Knauth, L.P., Kennedy, M.J. "The late Precambrian greening of the Earth." *Nature*, 2009: 1-5.
- Knoll, A.H., Hayes, J.M., Kaufman, A.J., Swett, K., Lamvert, I.B. "Secular variation in carbon isotope ratios from upper Proterozoic successions of Svalbard and east Greenland." *Nature*, 1986: 832-838.
- Knoll, A.H., Javaux, E.J., Hewitt, D., Cohen, P. "Eukaryotic organisms in Proterozoic oceans." *Philosophical Transactions of the Royal Society B*, 2006: 1023-1039.
- Knoll, A.H., Walter, M.R. "Latest Proterozoic stratigraphy and Earth history." *Nature*, 1992: 673-678.
- Knoll, A.H., Walter, M.R., Narbonne, G.M., Cristie-Blick, N. "Three "first places" for Eciacaran Period." *Episodes*, 2004: 222.
- Konings, W., Albers, S.-V., Koning, S., Driessen, A. *Antonie Van Leeuwenhoek*, 2002: 61.
- Logan, G.A., Hayes, J.M., Hieshima, G.B., Summons, R.E. "Terminal Proterozoic reorganization of biogeochemical cycles." *Nature*, 1995: 53-56.
- Logan, G.A., Summons, R.E., Hayes, J.M. "An isotopic biogeochemical study of Neoproterozoic and Early Cambrian sediments from the Centralian Superbasin, Australia." *Geochimica et Cosmochimica Acta*, 1997: 5391-5409.
- Lorant, F., Behar, F. "Late generating of methane from mature kerogens." *Energy & Fuels*, 2002: 412-427.
- Love, G.D., Grosjean, E., Stalvies, C., Fike, D.A., Grotzinger, J.P., Bradley, A.S., Kelly, A.E., Bhatia, M., Meredith, W., Snape, C.E., Bowring, S.A., Condon, D.J., Summons, R.E. "Fossil steroids record the appearance of Demospongiae during the Cryogenian period." *Nature*, 2009: 718-721.
- McFadden, K.A., Huang, J., Chu, X., Jiang, G., Kaufman, A.J., Zhou, C., Yuan, X., Xiao, S. "Pulsed oxidation and biological evolution in the Ediacaran Douchantuo Formation." *PNAS*, 2008: 3197-3202.
- Mello, M.R., Koutsoukos, E.A.M., Hart, M.B., Brassell, S.C., Maxwell, J.R. "Late Cretaceous anoxic events in the Brazilian continental-margin." *Organic Geochemistry*, 1989: 529-542.

- Misi, A., Kaufman, A.J., Veizer, J., Powis, K., Azmy, K., Boggiani, P.C., Caucher, C., Teixeira, J.B.G., Sanches, A.L., Iyer, S.S. "Chemostratigraphic correlation of Neoproterozoic successions in South America." *Chemical Geology*, 2007: 161-185.
- Moldowan, J.M., Jacobson, S.R. "Chemical signals for early evolution of major taxa: Biosignatures and taxon-specific biomarkers." *International Geology Review*, 2000: 805-812.
- Moldowan, J.M., Seifert, W.K., Gallegos, E.J. "Relationship between petroleum composition and depositional environment of petroleum source rocks." *American Association of Petroleum Geologists Bulletin*, 1985: 1255-1268.
- Moldowan, J.M., Sundararaman, P., Schoell, M. "Sensitivity of biomarkers properties to depositional environment and/or source input in the Lower Toarcian of S.W. Germany." *Organic Geochemistry*, 1986: 915-926.
- Muller, W.E.G. "Review: How was metazoan threshold crossed? They hypothetical Urmetazoa." *Comparative Biochemistry and Physiology Part A*, 2001: 433-.
- Olcott, A.N. "Signs of photosynthesis on a Neoproterozoic Snowball Earth." *Doctor of Philosophy Dissertation*, 2006.
- Olcott, A.N., Sessions, A.L., Corsetti, F.A., Kaufman, A.J., de Oliviera, T.F. "Biomarker evidence for photosynthesis during Neoproterozoic glaciation." *Science*, 2005: 471-474.
- Ourisson, G., Albrecht, P., Rohmer, M. "Palaeochemistry and biochemistry of a group of natural products." *Pure and Applied Chemistry*, 1979: 709-729.
- Peters, K.E., Moldowan, J.M. "Effects of source, thermal maturity, and biodegradation of the distribution and isomerization of homohopanes in petroleum." *Organic Geochemistry*, 1991: 47-61.
- Peters, K.E., Walters, C.C., Moldowan, J.M. *The Biomarker Guide: Biomarkers and Isotopes in Petroleum Systems and Earth History*. Vol. 2. Cambridge: Cambridge University Press, 2005.
- Popp, B.N., Laws, E.A., Bidigare, R.R., Dore, J.E., Hanson, K.L., Wakeham, S.G. "Effect of phytoplankton cell geometry of carbon isotopic fractionation." *Geochimica et Cosmochimica Acta*, 1998: 69-77.
- Popp, B.N., Laws, E.A., Bidigare, R.R., Dore, J.E., Hanson, K.L., Wakeham, S.G. "Effect of phytoplankton cell geometry on carbon isotopic fractionation." *Geochimica et Cosmochimica Acta*, 1998: 69-77.
- Popp, B.N., Parekh, P., Tilbrook, B., Bidigar, R.R., Laws, E.A. "Organic carbon d13C variations in sedimentary rocks as chemostratigraphic and paleoenvironmental tools." *Palaeogeography, Palaeoclimatology, Palaeonecology*, 1997: 119-132.
- Powell, T.G., McKirdy, D.M. "Relationship between ratio of pristane to phytane, crude oil composition and geological environment in Australia." *Nature*, 1973: 37-39.
- Radke, M., Willsch, H., Leythaeuser, D. "Aromatic components of coal: relation of distribution pattern to rank." *Geochimica et Cosmochimica Acta*, 1982: 1831-1848.

- Raederstorff, D., Rohmer, M. "Sterols of the unicellular algae *nematochryopsis-rosceffensis* and *chrystola-lamellosa* - isolation of (24E)-24-normal-propylidenecholesterol and 24-n-propylcholesterol." *Phytochemistry*, 1984: 2835-2838.
- Raiswell, R., Canfield, D.E. "Sources of iron for pyrite formation in marine sediments." *American Journal of Science*, 1998: 219-245.
- Rashby, S.E., Sessions, A.L., Summons, R.E., Newman, D.K. "Biosynthesis of 2-methylbacteriohopanepolyols by an anoxygenic phototroph." *PNAS*, 2007: 15099-15104.
- Rashby, S.E., Sessions, A.L., Summons, R.E., Newman, D.K. "Biosynthesis of 2-methylbacteriohopanepolyols by an anoxygenic phototroph." *PNAS*, 2007: 15099-15104.
- Rasmussen, B., Fletcher, I.R., Brocks, J.J., Kilburn, M.R. "Reassessing the first appearance of eukaryotes and cyanobacteria." *Nature*, 2008: 1101-1104.
- Rodrigues, J.B., Pimentel, M.M., Buhn, B., Dardenne, M.A., Alvarenga, C.J.S. "Provenance of Vazante Group-Preliminary Data." *VI South American Symposium on Isotope Geology*, 2008.
- Rodrigues, J.B., Pimentel, M.M., Buhn, B., Dardenne, M.A., Alvarenga, C.J.S., Armstrong, R.A. "Provenance of the Vazante Group (new Sm-Nd and U-Pb (LAM-ICPMS and SHRIMP) isotopic data and implications for the tectonic evolution of the Brasilia Belt." 2008.
- Rooney, A.D., Selby, D., Houxay, J.P., Renne, P.R. "Re-Os geochronology of a Mesoproterozoic sedimentary succession, Taoudeni basin, Mauritania: Implications for basin-wide correlations and Re-Os organic-rich sediments systematics." *Earth and Planetary Science Letters*, 2010: 486-496.
- Rothman, D.H., Hayes, J.M., Summons, R.E. "Dynamics of the Neoproterozoic carbon cycle." *PNAS*, 2003: 8124-8129.
- Schoell, M., Hwang, R.J., Carlson, R.M.K., Welton, J.E. "Carbon isotopic composition of individual biomarkers in gilsonites (Utah)." *Organic Geochemistry*, 1994: 673-683.
- Schoell, M., McCaffrey, M.A., Fago, F.J., Moldowan, J.M. "Carbon isotopic compositions of 28,30-bisnorhopanes and other biological markers in a Monterey crude oil." *Geochimica et Cosmochimica Acta*, 1992: 1391-1399.
- Schoell, M., Teschner, M., Wehner, H., Durdad, B., Oudin, J.L. "Maturity related biomarker and stable isotope variations and their application to oil/source rock correlation in the Mahakam Delta, Kalimantan." In *Advances in Organic Geochemistry 1981*, edited by M., Albrecht, C., Cornford, C., et al., Bjoroy, 156-163. New York: John Wiley & Sons, 1983.
- Schopf, J.W., Sovietov, Y.K. "Microfossils in Conophyton from Soviet-Union and their bearing on Precambrian biostratigraphy." *Science*, 1976: 143-146.

- Schutze, J., Krasko, A., Custodio, M.R., Efremova, S.M., Muller, I.M., Muller, W.E.G. "Evolutionary relationships of Metazoa within the eukaryotes based on molecular data from Proifera." *Proceedings of the Royal Society of London B*, 1999: 63.
- Seifert, W.K., Moldowan, J.M. "Applications of steranes, terpanes and monoaromatics to the maturation, migration and source of crude oils." *Geochimica et Cosmochimica Acta*, 1978: 77-95.
- Seifert, W.K., Moldowan, J.M. "The effect of thermal stress on source-rock quality as measured by hopane stereochemistry." *Physics and Chemistry of the Earth*, 1980: 229-237.
- Seifert, W.K., Moldowan, J.M. "Use of biological markers in petroleum exploration." In *Methods in Geochemistry and Geophysics*, edited by R.B. Johns, 261-290. Amsterdam: Elsevier, 1986.
- Seifert, W.K., Moldowan, J.M., Smith, G.W., Whitehead, E.V. "First proof of a C28-pentacyclic triterpane in petroleum." *Nature*, 1978: 436-437.
- Shen, B., Xiao, S., Zhou, C., Kaufman, A.J., Yuan, X. "Carbon and sulfur isotope chemostratigraphy of the Neoproterozoic QuANJI Group of the Chaidam Basin, NW China: Basin stratification in the aftermath of an Ediacaran glaciation postdating the Shuram event?" *Precambrian Research*, 2010: 241-252.
- Shen, Y., Canfield, D.E., Knoll, A.H. "Middle Proterozoic Ocean Chemistry: Evidence from the McArthur Basin, Northern Australia." *American Journal of Science*, 2002.
- Sherman, L.S., Waldbauer, J.R., Summons, R.E. "Improved methods for isolating and validating indigenous biomarkers in Precambrian rocks." *Organic Geochemistry*, 2007: 1987-2000.
- Shiea, J., Brassell, S.C., Ward, D.M. "Mid-chain branched mono- and dimethyl alkanes in hot spring cyanobacterial mats: a direct biogenic source for branched alkanes in ancient sediments?" *Organic Geochemistry*, 1990: 223-231.
- Sinninghe Damste, J.S., Kenig, F., Koopmans, M.P., Koster, J., Schouten, S., Hayes, J.M., De Leeuw, J.W. "Evidence for gammacerane as an indicator of water-column stratification." *Geochimica et Cosmochimica Acta*, 1995: 1895-1900.
- Skorokhod, A., Gamulin, V., Gundacker, D., Kavsan, V., Muller, I.M., Muller, W.E.G. "Origin of insulin receptor-like Tyrosine Kinases in marine sponges." *Biological Bulletin*, 1999: 198.
- Strauss, H. "The sulfur isotopic record of Precambrian sulfates: New data and a critical evaluation of the existing record." *Precambrian Research*, 1993: 225-246.
- Summons, R.E. *Massachusetts Institute of Technology*, 2011.
- Summons, R.E. "Branched alkanes from ancient and modern sediments: isomer discrimination by GC/MS with multiple reaction monitoring." *Organic Geochemistry*, 1987: 281-289.
- Summons, R.E., Jahnke, L.L. "Hopanes and hopanes methylated ring A: correlation of the hopanoids from extant methylotrophic bacteria with their fossil analogues." In

- Biological Markers in Sediments and Petroleum*, edited by J.M., Albrecht, P., Philip, R.P. Moldowan, 182-200. Englewood Cliffs, N.J.: Prentice-Hall, 1992.
- Summons, R.E., Jahnke, L.L., Hope, J.M., Logan, G.A. "2-Methylhopanoids as biomarkers for cyanobacterial oxygenic photosynthesis." *Nature*, 1999: 554-557.
- Summons, R.E., Powell, T.G. "Identification of aryl isoprenoids in a source rock and crude oils: biological markers for the green sulfur bacteria." *Geochimica et Cosmochimica Acta*, 1987: 557-566.
- Swanson-Hysell, N.J., Rose, C.V., Calmet, C.C., Halverson, G.P., Hurtgen, M.T., Maloof, A.C. "Cryogenian glaciation and the onset of carbon-isotope decoupling." *Science*, 2010: 608-611.
- Ten Haven, H.L., de Leeuw, J.W., Rullkotter, J., Sinninghe Damste, J.S. "Restricted utility of the pristane/phytane ratio as a palaeoenvironmental indicator." *Nature*, 1987: 641-643.
- Ten Haven, H.L., Rohmer, M., Rullkotter, J., Bissere, P. "Tetrahymanol, the most likely precursor of gammacerane, occurs ubiquitously in marine sediments." *Geochimica et Cosmochimica Acta*, 1989: 3073-3079.
- Thompson, K.F.M. "Fractionated aromatic petroleums and the generation of gas condensates." *Organic Geochemistry*, 1987: 573-590.
- Thompson, K.F.M. "Gas-condensate migration and oil fractionation in deltaic systems." *Marine Petroleum Geology*, 1988: 237-246.
- Tissot, B.P., Welte, D.H. *Petroleum Formation and Occurrence*. New York: Springer-Verlag, 1984.
- Tohver, E., van der Pluijm, B.A., Scandolara, J.E., Essen, E.J. "Late Mesoproterozoic deformation of SW Amazonia (Rodonia, Brazil): geochronological and structural evidence for collision with Southern Laurentia." *Journal of Geology*, 2005: 309-323.
- Tomanek, A. *Silicones and Industry: a compendium for practical use, instruction and reference*. Munich: Wacker-Chemie, 1990.
- Trompette, R. *Travaux des Laboratoires des Sciences de la Terre St-Jerome*. Marseille: B-7, 1973.
- Venkatesan, M.I. "Tetrahymanol: its widespread occurrence and geochemical significance." *Geochimica et Cosmochimica Acta*, 1989: 3095-3101.
- Vorob'eva, L.I. *Applied Biochemistry and Microbiology*, 2004: 217.
- Waldbauer, J.R., Newman, D.K., Summons, R.E. "Microaerobic steriod biosynthesis and the molecular fossil record of Archean Life." *PNAS*, 2011.
- Waldbauer, J.R., Sherman, L.S., Sumner, D.Y., Summons, R.E. "Late Archean molecular fossils from the Transvaal Supergroup record the antiquity of microbial diversity and aerobiosis." *Precambrian Research*, 2009: 28-47.

- Walker, J.C.G., Klein, C., Schidlowski, M., Schopf, J.W., Stevenson, E.J., Walter, M.R. "Environmental evolution of the Archean-Early Proterozoic Earth." In *Earth's earliest biosphere: its origin and evolution*, 260-290. 1983.
- Whiticar, M.J. "Carbon and hydrogen isotope systematics of bacterial formation and oxidation of methane." *Chemical Geology*, 1999: 291-314.
- Xiao, S., Zhang, Y., Knoll, A. "Three-dimensional preservation of algae and animal embryos in a Neoproterozoic phosphorite." *Nature*, 1998: 553-558.
- Zhang, J.Z., Millero, F.J. "The chemistry of the anoxic waters in the Cariaco Trench." *Deep-Sea Research*, 1993: 1023-1041.
- Zundel, M., Rohmer, M. "Prokaryotic triterpenoids 1. 3 β -methylhopanoids from *Acetobacter* species and *Methylococcus capsulatus*." *European Journal of Biogeochemistry*, 1985: 23-27.